University of Alberta

COKE YIELD AND TRANSPORT PROCESSES IN AGGLOMERATES OF BITUMEN AND SOLIDS

by

Mohamed Ali Hassan Ali

A thesis submitted to the Faculty of Graduate Studies and Research
in partial fulfillment of the requirements for the degree of

Doctor of Philosophy in Chemical Engineering

The Department of Chemical and Materials Engineering

Fall 2010
Edmonton, Alberta

Examining Committee

Murray R. Gray, Department of Chemical and Materials Engineering.

William C. McCaffrey, Department of Chemical and Materials Engineering.

Amos Ben-Zvi, Department of Chemical and Materials Engineering.

Brian Fleck, Department of Mechanical Engineering.

Nader Mahinpey, Department of Chemical and Petroleum Engineering, University of Calgary.

Jennifer McMillan, Syncrude Canada Ltd.

Abstract

Agglomerate formation is a common phenomenon that can cause operating problems in the fluid coking reactor. When agglomerates form they provide longer diffusion paths of the reaction products through the liquid layers and liquid bridges within the agglomerate, which leads to higher mass transfer resistance, trapping of the reaction products and increasing the undesired coke formation reactions. Surviving agglomerates in the reactor can also cause fouling of the reactor interior and defluidization of the bed. The ultimate coke yield was determined for agglomerates of Athabasca vacuum residue and solid particles by heating on Curie-point alloy strips in an induction furnace at 503 °C and 530 ^{o}C and in a fluidized bed reactor at 500 ^{o}C until all toluene-soluble material was converted. Coke yields from agglomerates were compared to the results from reacting thin films of vacuum residue. The average coke yield from the agglomerates was 23%, while the coke yield from thin films of 20 μm thickness was 11%, which supports the role of mass transfer in coke formation reactions. The ultimate coke yield was insensitive to vacuum residue concentration, agglomerate size, reaction temperature and agglomerate disintegration.

The temperature profile within agglomerates was measured by implanting a thermocouple at the agglomerate center, and a heat transfer model was used to describe the temperature variation with time. The effective thermal diffusivity of the agglomerates was 0.20 x 10^{-6} m^2/s. Control experiments on reactions in thin

liquid films confirmed that heating rates in the range of 14.8 to 148 K/s had no effect on the ultimate yield of coke.

Acknowledgement

I would like to thank my supervisor, Dr. Murray Gray, for giving me such opportunity to work under his supervision and for his guidance, understanding and support. I really learned a lot from him in both the technical and personal levels.

A lot of thanks go to my lab assistants; Manavdeep Riakhi, Amy Congdon, Megan Courtney, Tara Poholko and Lisa Boddez, who offered great help in conducting some of the experiments.

Many thanks to Dr. Sarah Weber, Dr. Ramin Radmanesh and Dr. Edward Chan and the Syncrude Research team for their valuable discussions, suggestions, and help.

The financial support from NSERC and Syncrude Canada Ltd is greatly acknowledged.

I also would like the thank my colleagues in the heavy oil upgrading group and the Department of Chemical and Materials Engineering for their support, discussions, suggestions and feedbacks.

Finally, to my family, nothing could ever show how grateful and thankful I am to have you in my life. You are giving me such a motive to complete everything I am doing and you give a lot of meaning to anything I am doing. Your support always makes me pass the hard times and give me scope and vision to whatever I do.

Table of Contents

List of Tables

List of Figures

Nomenclature

A^{+}	Reactant asphaltenes
A^{*}	Asphaltene cores
A^{*}_{max}	Maximum asphaltene cores that can be held in solution
A^{*}_{ex}	Excess asphaltene cores beyond that can be held in solution
A^{*A}	Cores that can accept enough hydrogen
A^{*NA}	Cores that cannot accept hydrogen
A_0	Initial concentration of the organic materials that can decompose
a	Stoichometric coefficients
Bi_h	Heat transfer Biot number $Bi_h = \frac{hd}{\lambda}$
C_P	Product concentration
C_P^{*}	Critical product concentration for bubble formation
C_R	Residue concentration
C_G	gas concentration
c	Stoichometric Coefficient
D	Diffusivity
D^{*}_{GK}	Knudson diffusivity of the gas
d	diameter
e	coefficient of restitution

h	Heat transfer coefficient
k_p	Rate constant for trapping of the products in the liquid phase
k_B	Rate constant for transport of the products to gas-phase
L	Thickness
L_0	Height of the asperities at the surface of the granule
m	Stoichometric coefficient
n	Stoichometric coefficient
r	Particle radius
Re_p	Reynolds number of the particulate phase $\frac{\rho_f U_p d_p}{\mu}$;
St_{vD}	Viscous Stock's number $St_{vD} = \frac{4\rho_D u_0 d}{9\mu}$
St^*_{vD}	Critical viscous stock's number $St^*_{vD} = \left(1+\frac{1}{e}\right)\ln\frac{L}{L_0}$
t	Time
T	Temperature
U	Gas velocity, m/s
U_{mf}	Minimum fluidization velocity, m/s
$2u_0$	Relative velocity
x	Distance

Greek letters

α_{eff}	Effective thermal diffusivity of the agglomerate, W/m^{2}s
α_m	Mean thermal diffusivity, W/m^{2}s
ε	Porosity of the agglomerate
ε_{mf}	voidage of the particulate phase at minimum fluidization
$(\rho C_p)_{fluid}$	Heat capacity of the fluid phase, J/m^3.K
$(\rho C_p)_{solid}$	Heat capacity of the solid phase, J/m^3.K
σ	Heat capacity ratio
λ_f	Thermal conductivity of the fluidizing gas, W/m.K
λ_e	Effective thermal conductivity of the particulate phase, W/m.K
ρ_D	Granule density, m^3/kg
ρ_f	Density of the fluidizing gas, m^3/kg
κ`	Ratio between the forward and retrograde reactions considering bubble formation.
κ	Ratio between the forward and retrograde reactions without bubble formation
μ	Viscosity, Pa.s
Φ_t	Film thickness parameter; is the
τ_c	Contact time between the fluidized particle and heat transfer surface

Abbreviations and Acronyms

MCR	Micro Carbon Residue
RCR	Ramsbottom Carbon Residue
CCR	Conradson Carbon Residue
TI	Toluene Insolubles
V	Volatiles
I	Reaction Intermediate
VR	Vacuum Residue
AVR	Athabasca Vacuum Residue
D	Distillate
C	Coke
TGA	Thermogravimetric Analysis
SSR	Sum or Squared Residuals

1 INTRODUCTION

1.1 Alberta Oil Sands

Alberta contains the second largest oil reserve in the world. The majority of this reserve is in the form of oil sands in the three major areas in northern Alberta: Athabasca, Cold Lake and Peace River. The oil sands areas in Alberta are estimated at 140,200 km^2 with about 602 km^2 currently producing oil sands by surface mining (Department of Energy, Government of Alberta, 2010). The Government of Alberta calculates that about 28 billion cubic meters (173 billion barrels) of crude bitumen are economically recoverable from Alberta oil at current prices using current technology; this is equivalent to about 10% of the estimated 1,700 billion barrels of bitumen in place. (Barbajosa, 2005; Department of Energy, Government of Alberta, 2010). In 2008 Alberta oil production was more than 1.8 million barrel per day, 1.3 million barrels of which were from oil sands. This rate is expected to rise to 3 million barrels by 2018. (Department of Energy, Government of Alberta, 2010). There are 91 active oil sands projects in Alberta, of these only four are mining projects, and the remaining are using different in-situ production methods (Government of Alberta, 2009).

Figure 1.1 compares Alberta's oil reserve to the world's largest oil reserves in 2008.

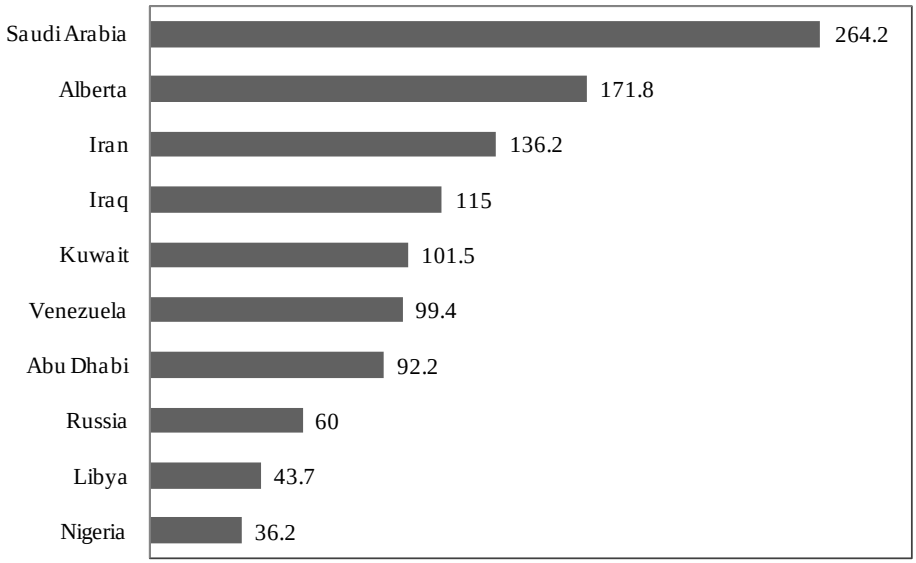

Figure 1.1: World's largest oil reserves in billion barrels in 2008. (Numbers from *ERCB 2009 ST-98 Report "Alberta's Energy Reserves 2008 and Supply/Demand Outlook 2009-2018" and Oil & Gas Journal "Worldwide Look at Reserves and Production. Special Report" December 22, 2008, Vol 108 Issue 48*)

1.2 Bitumen Upgrading

Bitumen from oil sand is very heavy (API<10^o), and it must be processed in upgraders in order to produce synthetic crude oil of higher value that can be processed to produce gasoline, heating oil, gas oils and petroleum gases. For instance, Athabasca bitumen has API of 8^o and 5% sulfur content and it contains more than 50% residue, while the synthetic crude produced from Syncrude (Syncrude sweet blend) has an API of 32^o and its sulfur content does not exceed 0.2% by weight. Commercial upgrading usually consists of two steps, primary and secondary upgrading. In primary upgrading the heavy oil is processed to remove the heavy fractions along with some of the heteroatoms and heavy metals. Primary upgrading may include processes such as vacuum distillation, coking, visbreaking and hydroconversion. The product of primary upgrading is further processed in the secondary upgrading step to remove impurities such as sulfur and nitrogen to produce light sweet blending stocks to produce synthetic oil, using processes like hydrotreating and hydrocracking.

The selection of upgrading technologies and processes depends mainly on the type of the major products. After suitable technologies are selected for upgrading, secondary considerations are taken into account including (Gray and Masliyah, 2004):

1. Capital cost: due to the high cost associated with mining, extraction and upgrading steps, it is required to select the minimum configuration upgrading steps with the minimum capital cost.

2. Bitumen-light crude price spread: the choice to whether upgrade the bitumen or blend it with the condensate for direct sale is based on the price difference from conventional crude oil. A spread of at least $5 per barrel is required for profitable operation. Larger price spreads make upgrading more attractive.

3. Coke production: processes that produces coke as a byproduct has a potential problem as it is usually required to recover the product value or the heating value of the coke. Marketing or using coke product in combustion is a problem due to the high sulfur content in coke. Syncrude and Suncor use coking as their primary upgrading technology. Both companies stockpile the excess coke indefinitely, given their access to mining operations.

4. Production of high boiling residuum or pitch: like coke, production of high boiling liquid can cause a problem if they contain high amount of sulfur and it cannot be used without further treatment. Pitch from the cracking processes can be used in manufacturing asphalt, while the pitches from thermal or catalytic hydrocracking has higher softening temperature and lack of ductility that is required for asphalt applications.

5. Available technology: well-proven technology is usually selected in order to minimize the risk associated with new process technologies.

6. Cost of hydrogen, natural gas and catalysts: the cost of these inputs determines the product and technology selection. Hydrogen-addition technologies, such as LC-Finning and H-Oil, give higher volume of products compared to feed. Oil sales are based on volumetric bases, therefore, the increase of volume can be attractive, but the cost of natural gas to produce hydrogen can be offsetting.

Table 1.1 compares the main primary upgrading processes as applied to Athabasca bitumen, from the perspective of Suncore.

Table 1.1: Comparison of Primary Upgrading Processes (Table from Gray and Masliyah, 2004)

Technology	**Capital Cost**	**Operating Complexity**	**Operating Pressure**	**Operating Cost**	**Volume Yield on 525°C+**	**Units in Operation Worldwide**
Delayed Coking	Low	Medium	350 kPa	Low	80%	137
Visbreaking	Low	Low	350 kPa	Low	60%	186
Fluid Coking	Medium	Medium	350 kPa	Low	86%	8
Felxicoking	Medium	Medium	350 kPa	Low	85%	5
LC-Finning	high	High	14-21 MPa	Very High	100%	8

In current upgraders, coking is the most common choice for primary upgrading. Coking is more appealing due to the lack of catalysts that can handle the high solid and water content in mined bitumen without the high cost of catalyst consumption. The most commonly used coking processes are delayed coking and fluid coking. The delayed coking process is usually attractive when there is no market for fuel oils. Delayed coking process has long reaction times in the liquid phase, compared to fluid coking. The condensation reactions that lead to production of high aromatic content coke product also tend to retain sulfur, nitrogen and metals. Unlike the semi-batch delayed coking process, fluid coking is a continuous operation that uses shorter reaction times in the liquid phase and also uses higher temperature. The short residence times of the cracking products in the liquid phase improves the products yield in fluid coking compared to delayed coking. More detailed discussion on the different coking processes is given in the following chapter.

1.3 Research Objectives

In fluid coking, the thermal cracking of heavy oil feed stocks occurs on the surface of fluidized coke particle in the fluid coking reactor usually at 510-550^{o}C. Forming thin liquid layer on the surface of coke particles is very important in order to ensure maximum heat transfer from the hot coke particle to the reacting liquid film and to minimize the trapping of the reaction products within the liquid due to mass transfer resistance.

Different studies on cold systems (House et al., 2004, McMillan et al., 2005, McDougal et al., 2005, House et al., 2008 and Weber et al., 2008), pilot

studies and solid products analysis (Gray 2002) indicated that liquid feeds tend to form agglomerates with the solid particles. Evidence from industrial reactors also shows that during the coking process the solid coke particles and the heavy oil feed tend to form solid-liquid agglomerates. These agglomerates then survive and travel within the reactor to cause operational problems such as fouling of the reactor internals and potentially defluidization of the fluidized bed. Also, when the reacting liquid is trapped in the agglomerates it tends to undergo undesired condensation and polymerization reactions that increases the coke yield and hence decreases the yield of the desired distillable products.

The objectives of this research are

- To determine the effect of different variables on the yield of coke from AVR-solid agglomerates, such as agglomerates size, liquid concentration, reaction temperature and heating rate.
- To study the behavior of the AVR-solid agglomerates and measure their temperature profile under controlled conditions.

1.4 Research Approach

To achieve the objectives of the research, two different types of reactors were used to conduct the experiments on the AVR-solids agglomerates; induction furnace reactor and fluidized bed reactor.

In the induction furnace reactor the AVR-coke agglomerates were reacted under controlled conditions by placing the agglomerates between two Curie-point alloys and placing them in an induction coil to heat up the Curie-point alloys to

their Curie-point temperature rapidly. The induction furnace experiments were done under 100% survival conditions, i.e. the agglomerates stayed intact through the experiments without disintegration. The coke yield in the agglomerates were measured based on the amount of coke formed after the reaction relative to the amount of AVR in the unreacted agglomerate. The induction furnace reactor was also used to determine the coke yield in reacting AVR thin films by spraying the AVR directly on the Curie-point strips and running the AVR-covered strips in the induction coil. The results from the agglomerates and the thin films reaction were compared to determine the effect of agglomeration on coke yield. Agglomerates of different thicknesses and diffetent AVR concentration were also tested to study the effect of the different agglomerates varaiables on coke yield. Also, the temperature profile within the agglomerates was measured during the heating time and a mathematical model was made to describe the change of temperature with time.

In the fluidized bed reactor, AVR-silica agglomerates were reacted in a fluidized bed of silica. Silica was used instead of coke in making the agglomerates and as fluidization solids in order to be able to determine the amount of coke formed after the reaction by burning the fluidized bed content and determine the coke formed by absorbing the CO_2 in alkaline solution. Due to fluidization, the survival conditions of the fluidized bed experiments were less than 100%, that gave the chance to study the effect of agglomerates disintegration on the coke yield by comparing the fluidized bed results to the induction furnace results. Similar to the induction furnace experiments, agglomerates with different sizes

and different AVR content were reacted to study the effect of these variables on the coke yield.

1.5 Thesis Outline

In the next chapter, the background literature on the upgrading of heavy oil generally and fluid coking particularly is reviewed. The background literature also covers the coking kinetics and formation of agglomerates. Chapter 3 deals with the materials and experimental methods used in the study. The results from the experimental work are then presented in chapter 4 and the experimental results then discussed in chapter 5. Finally, chapter 6 includes the conclusions.

2 LITERATURE REVIEW

2.1 Heavy Oil and Bitumen

Oil sands are unconsolidated sand deposits that are impregnated with high molar mass, highly viscous petroleum fluid. Bitumen production from oil sands is achieved either by in-situ operations for the deposits located deeper than 75 m below the ground, or by surface mining for shallower deposits. In 2007, the oil production from Alberta oil sands was estimated at 1.25 million barrels (Government of Alberta, 2009). Compared to conventional crude oil, bitumen properties are less favorable due to low API gravity, high content of vacuum residue, sulfur, nitrogen, metals and high viscosity. Table 2.1 shows a comparison of some properties of Athabasca bitumen and crude oil. (Speight, 2007)

Bitumen and heavy oil are differentiated according to their properties according the following definitions:

Bitumen : $API^{o}<10$, $\rho>1000$ kg/m^3, $\mu>10^5$ mPa.s at 15^{o}C

Heavy Oil: $10<API^{o}<26$, $\rho<1000$ kg/m^3, $\mu 10^2$-10^5 mPa.s at 15^{o}C

Table 2.1: Properties of Athabasca bitumen and Crude oil (Speight, 2007)

Property	**Athabasca Bitumen**	**Crude Oil**
Specific gravity	1.03	0.85–0.90
Viscosity (cp)		
38°C-100°F	750,000	<200
100°C-212°F	11,300	
Pour point (°F)	>50	ca. -20
Elemental analysis (wt.%)		
Carbon	83.0	86.0
Hydrogen	10.6	13.5
Nitrogen	0.5	0.2
Oxygen	0.9	<0.5
Sulfur	4.9	<2.0
Ash	0.8	0.0
Nickel (ppm)	250	<10.0
Vanadium (ppm)	100	<10.0
Fractional composition (wt.%)		
Asphaltenes (pentane)	17.0	<10.0
Resins	34.0	<20.0
Aromatics	34.0	>30.0
Saturates	15.0	>30.0
Carbon residue (wt.%)		
(Conradson carbon residue)	14.0	<10.0

2.2 Thermal Cracking and Coking Processes

The residue fraction ($524^{o}C+$ fraction) of bitumen and heavy oil needs to be processed in upgraders, and converted into distillable products. Bitumen from oil sands is upgraded to produce high quality synthetic oil comparable to the conventional light sweet crude, to produce pipelineable liquids with little or no diluents, or to produce cracked products with no vacuum residue. The choice of upgrading technology depends on the properties of feed material and the targeted markets. Upgrading processes either involve disproportionation of the feed into light ends, liquid products and solid byproduct (coke) as in coking processes, or catalytic hydrogen addition, such as LC-Finning or H-Oil processes. Thermal cracking processes are usually followed by hydroprocessing of the cracked products, either at the upgrader site or at a downstream refinery, to increase their quality and remove heteroatoms, such as nitrogen and sulfur. The industrial thermal cracking and coking processes are reviewed in this section.

The severity of thermal cracking processes determines the conversion and the products characteristics. Table 2.2 shows the severity of the different cracking processes and the corresponding conversions

Table 2.2: Severity of Thermal Cracking Processes (from Gray and Masliyah, 2004)

Severity	Process	Time, s	Temperature, ^{o}C	Conversion
Mild	Visbreaking	90	425-500	Low
High	Delayed coking	(semi batch)	435-480	High
	Hydroconversion	3600	420-440	Med-high
	Fluid coking	25	510-540	High
Extreme	Steam cracking	<0.5	>800	High

The mild and high severity processes are the most commonly used in residue and heavy oil upgrading. Steam cracking is used to convert gases and light distillate to olefins in the vapor phase (Mattar and Hatch, 2001), with extremely short residence times. Such extreme conditions have been suggested for liquid feedstocks such as vacumm residue, but such "ultrapyrolysis" processes have been limited to the pilot scale (Hulet et al., 2005).

Thermal cracking processes, such as coking, are used to convert the high boiling point materials into low boiling point materials by breaking the bonds in the large molecules to produce gases and distillable liquids. Among bitumen upgrading processes, coking is a major technology for the thermal conversion of heavy hydrocarbons into distillate products. Coking processes are also efficient in rejecting the minerals and solids to the coke phase. Some organic nitrogen also is rejected into the coke phase. The efficiency in rejecting sulfur is low compared to nitrogen, although the sulfur content is higher compared to the nitrogen content of

the feed materials. Table 2.3 shows the representative compositions of Athabasca feed and the corresponding compositions of delayed and fluid coke.

Table 2.3: Representative compositions of Athabasca feed and delayed and fluid coke (Data from Gray, 1994 and Chung et al., 1996)

Component	Feed	Delayed coke	Fluid coke
Carbon, wt%	84.22	83.54	83.47
Hydrogen, wt%	10.23	4.43	1.77
Sulfur, wt%	5.1	6.72	6.52
Nitrogen, wt%	0.45	1.60	2.03
H/C	1.46	0.64	0.25

2.2.1 Delayed Coking

Delayed coking is a semi-batch process that is the most widely used method for conversion of vacuum residues from bitumen, heavy oil, and conventional petroleum. The process unit consists of at least two coking vessels and a coker fractionator (Figure 2.1). In the process represented in figure 2.1, the feed is injected at the bottom of the fractionator where it is preheated and any light fractions are allowed to vaporize. The feed, along with the bottom product from the fractionator, is heated to about 500^{o}C in a heater then introduced to the bottom of the coking vessel (coke drum). The gases and distillates are withdrawn from the top of the coking drum and quenched by colder oil in the coker fractionator. The coke is deposited in the coke drum, beginning at the bottom,

until the drum is full. When one of the coking drums becomes full, the feed is switched to the other coking drum and the coke is removed from the first drum. A typical cycle of delayed coker usually takes 48 hours. The common operating problems in delayed coking include foaming in the drum, shot coke formation, coke deposition in heater tube and fouling of the fractionator. Shot coke can be a safety hazard during the quenching of the coke with water, it can break open and propelled by steam when water hit the hot center. Shot coke formation can be suppressed by ensuring that gas oil components are present to act as a solvent, therefore, high pressure, more recycle and lower temperature help the suppress shot coke.

2.2.1.1 Eureka Process

The Eureka process was invented by Kureha Chemical and Chiyoda of Japan (Aiba et al., 1981). The process is similar to the delayed coking process. Instead of coke as a byproduct, Eureka gives a high density liquid pitch. Steam is used to strip the volatile liquid product and extend the coking induction period. The same concept of a semi-batch process, using two alternating reactors, is applied in the process. While one of the drums is being filled with the reacting pitch the other drum is getting emptied. The pitch from the process is conveyed and cooled to solidify then flaked, or it can be used as boiler fuel. Compared to delayed coking, Eureka gives lower yield of gases and higher yield of liquids and lower yield of pitch (Wiehe, 2008, Speight, 2007).

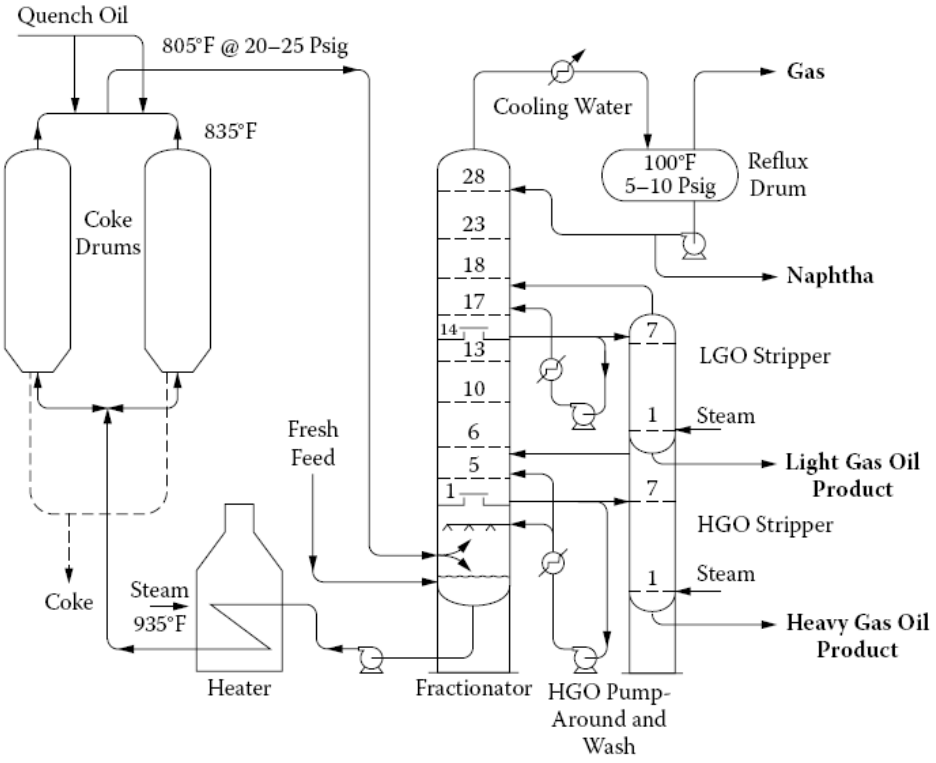

Figure 2.1: Schematic flow diagram of delayed coking process (PROCESS CHEMISTRY OF PETROLEUM MACROMOLECULES by I. A. Wiehe. Copyright 2008 by TAYLOR & FRANCIS GROUP LLC - BOOKS. Reproduced with permission of TAYLOR & FRANCIS GROUP LLC - BOOKS in the format Dissertation via Copyright Clearance Center)

2.2.2 Fluid Coking

Fluid coking is a continuous process that was developed by Exxon in the 1950's (Voorhies and Martin, 1953). In fluid coking (Figure 2.2), the heavy feed of bitumen is sprayed through steam-assisted atomizing nozzles into a fluidized bed of hot coke particles. Coking occurs on the surface of these particles at temperature of 510-550^{o}C, where the liquid reacts and thermally cracks to give gas oil, naphtha, LPG, dry gases (C1, C2) and coke byproduct. The cracked vapors rise to the top of the reactor, pass through cyclones to remove entrained particles of coke, and enter the scrubber in the top portion of the vessel. There the vapors are quenched by contact with condensed liquid of fresh feed. After stripping the coke with steam to remove liquids at the bottom of the reactor, the coke passes to the burner where a portion of the coke is burned to supply the heat to the reactor. The yields of the products are determined by the feed properties, the temperature of the bed and the residence time of the vapors in the reactor. The residence time of vapor-phase products is smaller compared to delayed coking, which reduces polymerization and coking reactions. Also, the excellent heat transfer in the fluid bed allows the reactor to operate at higher temperature, giving more cracking of volatiles from the coke. The higher operating temperature of fluid coking results in higher yield of liquid products but with lower quality compared to delayed coking. These factors generally give a lower yield of coke from fluid bed operation than from delayed coking, and the yield of gas oil and olefins is increased. (Gray, 1994). Fluid coking produces ca. 1.2 CCR (Conradson Carbon Residue; an experimental method presented by Conradson, 1912, to

determine the carbonaceous residue formed after thermal destruction of a sample) of which about 20% is burned in the heater, while delayed coking produces about 1.4-1.6 CCR coke (Wiehe, 2008).

2.2.3 Flexi Coking

Flexi coking is another continuous coking process and is considered a direct descendent from the fluid coking process. Flexi coking process has a similar configuration as fluid coking, with the addition of a gasifier in which the excess coke is gasified to produce fuel gas (Figure 2.3). Coke is gasified using steam and air at temperatures of 830-1000^{o}C. The heater in flexi coking is placed between the gasifier and the reactor and used to transfer heat between the two vessels.

The common problems in fluid coking and flexi coking are the fouling of reactor internals, over cracking of liquid products, fractionator fouling, defluidization of the bed or “bogging” that happens due to agglomeration of coke particles, and fouling in the burner if too much hydrocarbons is carried over with coke.

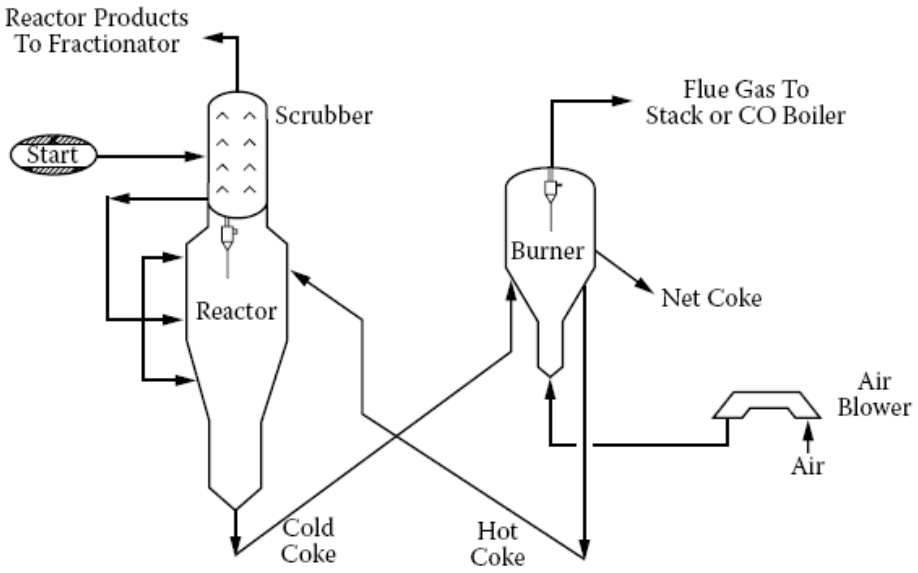

Figure 2.2: Schematic flow diagram of fluid coking (PROCESS CHEMISTRY OF PETROLEUM MACROMOLECULES by I. A. Wiehe. Copyright 2008 by TAYLOR & FRANCIS GROUP LLC - BOOKS. Reproduced with permission of TAYLOR & FRANCIS GROUP LLC - BOOKS in the format Dissertation via Copyright Clearance Center)

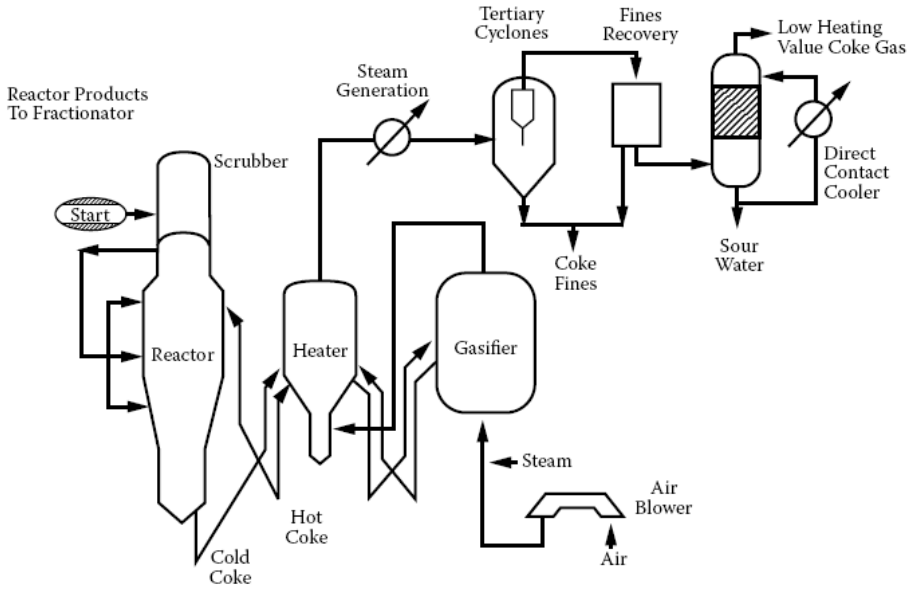

Figure 2.3: Schematic flow diagram of Flexi coking process (PROCESS CHEMISTRY OF PETROLEUM MACROMOLECULES by I. A. Wiehe. Copyright 2008 by TAYLOR & FRANCIS GROUP LLC - BOOKS. Reproduced with permission of TAYLOR & FRANCIS GROUP LLC - BOOKS in the format Dissertation via Copyright Clearance Center)

2.2.4 Other Coking Technologies

Beside the most common coking processes mentioned above, other coking processes have been proposed and developed to suit heavy oil processing. The concept of each of these processes is closely related to the older processes. All coking processes depend on a heat source that supplies the heat for the thermal cracking reaction. This heat source could be either a furnace or heater like the delayed coking process, or hot solids (coke or sand particles) like the case of fluid coking and flexi coking. The method of delivering and moving the solids around the system is a key difference between the processes. Some of these processes are still under development and testing in pilot scales and other processes have been discontinued after reaching certain level of development in lab, pilot or commercial scale.

2.2.4.1 Ivanhoe Heavy to Liquid (HTL) Process

The origins of the HTL process are technology initially developed by Ensyn Group in the early 1980s for biomass conversion (Veith, 2006, Koshka et al., 2008). The HTL process uses a short residence time for reaction in a continuous process. The process concept is similar to fluid coking, except that the heavy oil feed is mixed with hot circulating silica instead of coke particles. Coke is deposited on the silica particles during the thermal cracking reaction. The coke covered silica and the vapor products are separated in cyclone system, then the vapors are quenched rapidly and condensed. The condensed products either directed to a product tank for blending, or are recovered in a distillation column

for further separation. Part of the non-condensable gas is recycled to the reactor and can be used as fluidization gas.

The coke covered silica is directed to fluidized bed reheater where all of the coke is burnt to heat the silica particles, which are recycled to the reactor. The heat from coke combustion can be used to generate high pressure steam for electricity or in situ production. A pilot plant that was built by Ensyn was used to test the process for heavy oil upgrading. In 2004 a 1000 bbl/day commercial demonstration plant was initiated in the Belridge Heavy Oil Field in southern California (Veith, 2006). Commercial scale of operation is expected to be in the range of 10,000 to 15,000 bbl/day (Oilsands Review, 2007).

2.2.4.2 ETX Systems Upgrading Process

The ETX cross flow reactor was developed by Envision Technologies (Brown et al., 2006), as an improvement on the fluid coking process. In the ETX reactor, the moving hot solid particles (coke or sand) are introduced to the reactor and the feed of heavy oil is sprayed onto the particles, where the thermal cracking reactions take place. The fluidized solids move in the horizontal direction from one end of the reactor to the other. Fluidization gas is introduced from the bottom of the reactor and in the vertical direction, perpendicular to the direction of solid movement. The vapor products are swept by the fluidization gas and collected from the top of the reactor. The cross flow design of the reactor decoupled the residence times of the moving solid particles and the vapor phase. The solids will have enough time to move through the reactor for complete conversion of the liquid feed on the solids and the vapor products are collected and quenched

rapidly to stop any further cracking reaction in the vapor phase. The coke-covered solids are collected at the end of the reactor and send to the burner where the coke is combusted to reheat the solids and produce steam. The ETX process is currently operated on a one bbl/day pilot unit in the National Centre of Upgrading Technology (NCUT) (Oilsands Review, 2007 and ETX Systems, 2009).

2.2.4.3 ART Process

The ART process was developed by Engelhard Corp. (Bartholic, 1981). The main objective of the ART process was to upgrade the heavy oil feedstock to meet the fluid catalytic cracking (FCC) requirements by rejecting metals, nitrogen and carbon. The ART process used inexpensive microporous solids in a fluidized bed as a heat source and coke collection surface. Coke yield in the ART process was less than the CCR content of the feed, and most of the liquid product was in the atmospheric residue boiling range needed for FCC. The solids from the coker were burned in a burner to remove the formed coke and circulated to the reactor. Fouling was a major problem in the ART process due to unconverted feed on the solids particles and polymerization of olefins. The process was commercially operated at an Ashland Petroleum Refinery using a revamped FCC unit, but it was plagued by fouling problems and was eventually shut down (Wiehe, 2008)

2.2.4.4 Fluid Thermal Cracking (FTC) Process

The FTC process was invented by Fuji Standard Research (Miyauchi et al., 1988). In FTC the heavy feed was cracked in a fluidized bed of porous solids to produce distillate and coke and the produced coke was gasified to produce fuel gas. The feed was injected to the reactor and absorbed into the pores of the solid

particles by the capillary forces. The thermal cracking took place in the pores and the surface of the solid particles was kept dry which maintained good fluidity in the reactor (Speight, 2007). The solid particles with the formed coke were sent to the gasifier, where coke was gasified and fuel gas was produced. Fluidization gas that contained hydrogen was used in the reactor, which reduced coke formation due to the presence of hydrogen. The dilution of hydrogen by the generated light ends caused a problem in hydrogen stream recycle. The FTC process was only operated in a three bbl/day pilot (Wiehe, 2008)

2.2.4.5 Chattanooga Process

Chattanooga process was developed by Chattanooga Corp. to directly convert unconventional oil resources, such as oil sands, oil shale or in-situ bitumen, to synthetic crude oil (Chattanooga Corp, 2010). The process uses fluid bed reactor and associated fired hydrogen heater. Hydrogen, heated in the fired heater, is used as a heat carrier to the reactor, reactor fluidization gas and a reactant. The particulate solids are separated from the reactor overhead gases then the hydrocarbons are condensed and separated from the gases stream. Hydrogen and light hydrocarbons are separated from acid gases in an amine unite before being mixed with makeup hydrogen and being recycled to the fired heater. The reaction kinetics of Chattanooga process were proven in a pilot plant at the National Centre of Upgrading Technology (NCUT) in Devon, Alberta, Canada. Another pilot plant testing achieved fluidization and extracted 100% of Colorado oil shale. Pilot plant studies also demonstrated production of 28-30 ^{o}API product

from oil sands. Chattanooga Crop is preparing to design, construct and operate a demonstration facility as a next step in the commercialization of the process.

2.2.4.6 Discriminatory Destructive Distillation (3D) Process

The 3D process was invented by Bartholic (Bartholic, 1989) and became a joint venture of Bartholic and Coastal (Bar-Co) and was demonstrated over six month period at a refinery (Wiehe, 2008). 3D process used coke as a heat source. In the 3D process the feed was sprayed into a curtain of falling hot coke particles. The 3D gave a very short residence time of the vapors to minimize the secondary cracking reactions. The solids with incompletely converted feed fell off to a fluid bed with higher residence time (similar to fluid coker) to complete the cracking reactions (Bartholic, 1989). The process was eventually shut down due to some operational problems with the longest run being six weeks.

2.2.4.7 LR-Flash Coker

LR- Flash process was developed by Lurgi. In the LR-Flash, the reactor is a mechanical screw that gives good mixing and plug flow of the hot solids and heavy oil feed. Sand or coke can be used as the solid phase in the reactor. This process has short residence time of the vapor products to prevent over cracking (Wiehe, 2008). The solid with formed coke are burned to provide the heat for reaction. The LR-Flash has limitation with respect to size, its relatively small capacity limits its use with high capacity refineries. Because this process uses mechanical screw reactor to mix hot solids with feed material, it is suitable for high solid content feed, or feed with poor flow properties. This process was operated in lab, pilot and commercial scale. The commercial scale, known as

SATCON, was operated at Exxon Ingolstadt refinery in Germany and was shut down due to fouling problems.

2.3 Coke Formation and Coking Kinetics

2.3.1 Fundamentals of Residue Cracking

Cracking is a decomposition of the residue fractions to convert high molecular weight compounds to lower molecular weight products. Thermal cracking is a non-catalytic process that takes place at commercially useful rates at high temperatures of over 410^{o}C.

Cracking of high molecular weight products is achieved by breaking the chemical bonds in cracking reactions. In residue cracking, the targeted bonds are the carbon-carbon and carbon-sulfur bonds. The difficulty in breaking the chemical bonds depends on the structure of the compound. The following table gives the bond dissociation energies for different bonds in bitumen compounds.

Table 2.4: Bond Dissociation Energies (Benson, 1976)

Chemical Bond	Energy, kJ/mol	Energy, kcal/mol
C-C (aliphatic)	355.9	85
C-H (n-alkanes)	410.3	98
C-H (aromatic)	462.6	110.5
C-S	322.4	77
C-N (amines)	351.7	84
C-O (methoxy)	343.3	82

Thermal cracking is a free radical chain reaction. The thermal cracking reactions start with initiation step, where the carbon-carbon bond scission occurs to form free radicals. The free radicals react by abstracting a hydrogen atom from hydrocarbon or undergoing further cracking to produce stable product and a new free radical. Cracking usually occurs at bonds β to the carbon atom that carries the unpaired electron. The following is an example of chain reaction of n-alkane cracking (Blanchard and Gray, 1997).

Initiation $$M \rightarrow R_i^* + R_j^* \quad (2.1)$$

Hydrogen transfer $$R_1^* + M \rightarrow R_1H + M^* \quad (2.2)$$

B-scission $$M^* \rightarrow nR_2^* + Olefin \quad (2.3)$$

$$R_i^* \rightarrow nR_{i-2}^* + CH_2 = CH_2 \quad (2.4)$$

Isomerization $$R_p^* \leftrightarrow R_s^* \quad (2.5)$$

Termination $$R_i^* + R_j^* \rightarrow products \quad (2.6)$$

Where M and M^* are the parent alkane and the parent radical, R_1^* and R_1H are the methyl or ethyl radical and the corresponding alkane, R_2^* is the methyl, ethyl or higher primary alkyl radical, R_i^* is the butyl or higher radical and R_p^* and R_s^* are the primary and secondary pentyl or higher radicals.

The cleavage of the carbon-carbon bond requires a high activation energy, from the bond dissociation energy, 356 kJ/mol (85 kcal/mol) in the case of the aliphatic C-C bond (see table 2.4). On the other hand, propagation steps have

much lower energy requirement. The β-scission reaction has activation energy of 125-146 kJ/mol, while hydrogen abstraction has activation energy of 46-71 kJ/mol (Blanchard and Gray, 1997). The free radicals are presented in very low concentrations, but they participate in the chain reaction many times to give significant amounts of cracked products per mole of initiation reaction.

The activation energy for cracking of bitumen is comparable to the overall activation energy for cracking on n-alkanes. Wiehe (2008) reported activation energy values of 213.18 kJ/mol (50.9 kcal/mol) for Cold Lake short path distillation bottoms.

2.3.2 Mechanism of Coke Formation

Coke can be defined as a carbonaceous solid that is formed from the calcination of carbon-rich materials. In petroleum processing the term coke is commonly used as a solubility term to describe the toluene-insoluble material. Coke is formed as a separate phase during thermal cracking processes. In coking processes, coke formation is part of the design and is targeted increase the H/C ratio in the liquid products. On the other hand, coke formation is not desirable in the hydroconversion and hydrotreating processes.

Coke forming tendency is an important parameter for upgrading. It is measured by pyrolyzing sample of the heavy oil under controlled conditions in absence of oxygen and determined as the amount of solids formed after the pyrolysis as a fraction of the initial sample weight. The coke forming tendency is usually measured as Conradson Carbon Residue (CCR), Rambsbottom Carbon

Residue (RCR), or Micro Carbon Residue (MCR). All three methods use the same concept to determine the coke forming tendency with differences in the equipment used and the heating conditions. The Conradson method (ASTM D-189) measures carbon residue by evaporative and destructive distillation. The sample is placed and heated in a sample dish until vapor ceases to burn and no blue smoke is observed. The sample dish is weighted after cooling and the carbon reside is calculated as a percent of the original sample weight. The Ramsbottom test (ASTM D-524) uses 4 grams of the sample in a glass bulb then inserting the bulb in a heated bath for 20 minutes. The bath temperature is maintained at 553 ^{o}C. after the test the bulb is weighted and the carbon residue is determined. The micro carbon residue method (ATSM D-5430) uses an analytical instrument to measure Conradson carbon in an automated set.

Wiehe (1993 and 2008) suggested that the coke formation during the thermal cracking of heavy residue occurs by a mechanism that involves the liquid-liquid phase separation of reacted asphaltenes to form a phase that is lean in abstractable hydrogen. Wiehe observed a coke induction period before coke starts to form. During this period, the asphaltene concentration increases and reaches a maximum then decreases. The maximum occurs at the same reaction time as the end of coke induction period (Figure 2.4). The duration of the induction period depends on the feedstock and the coking temperature. At lower coking temperature the induction period is long and starts to shorten with increasing the temperature and even disappear at high temperatures. This phenomenon is used in the design and operation of the industrial coking processes to prevent formation of

coke in undesired areas, such as heaters and distillation towers. Wiehe suggested that asphaltenes reach a solubility limit in heptane soluble fraction before forming coke. Wiehe (1992) proposed a phase diagram for coke formation behavior based on hydrogen content and molecular weight, he observed that data for different solubility fractions tend to cluster into distinct zones on a plot of molecular weight versus hydrogen content (Figure 2.5)

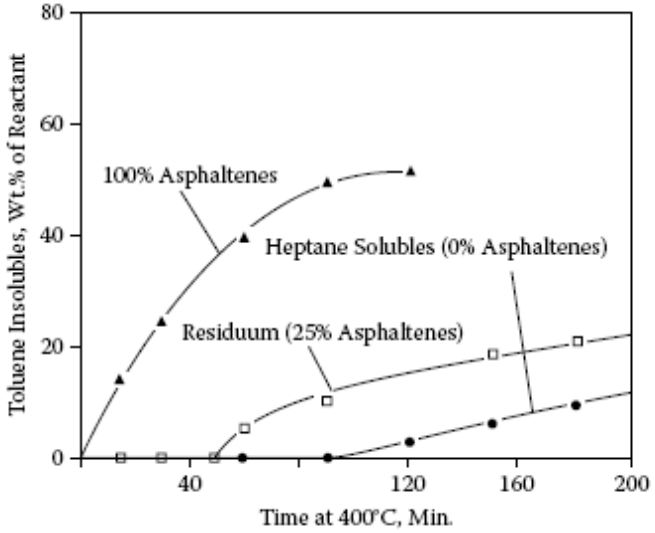

Figure 2.4: Coke formation from three reactants: asphaltenes, full resid, and heptane-soluble portion of resid for Cold Lake vacuum resid at 400°C showing different coke induction periods (PROCESS CHEMISTRY OF PETROLEUM MACROMOLECULES by I. A. Wiehe. Copyright 2008 by TAYLOR & FRANCIS GROUP LLC - BOOKS. Reproduced with permission of TAYLOR & FRANCIS GROUP LLC - BOOKS in the format Dissertation via Copyright Clearance Center)

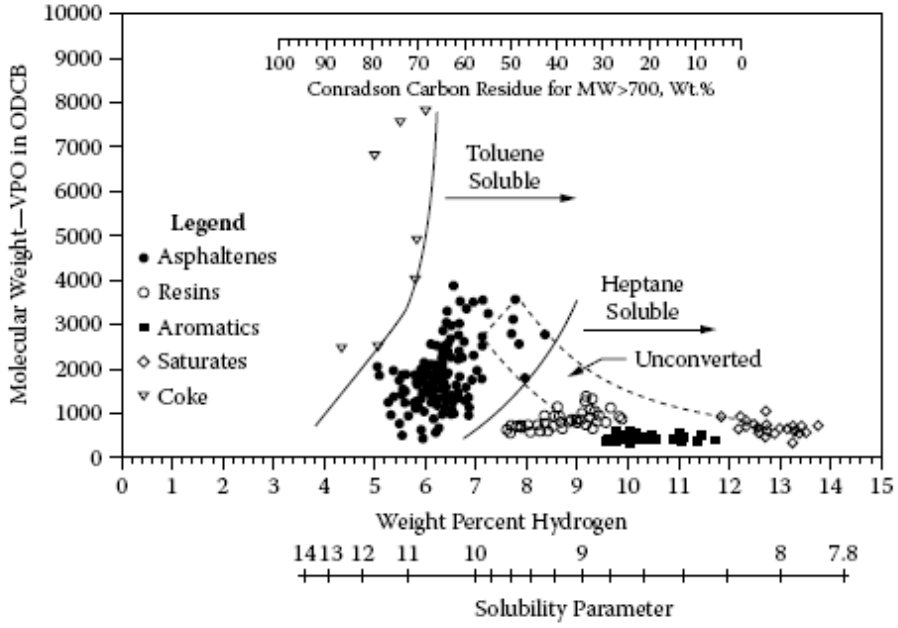

Figure 2.5: The solvent–residue phase diagram of eight different residues and their thermal reaction products displays each of the five classes in unique areas (PROCESS CHEMISTRY OF PETROLEUM MACROMOLECULES by I. A. Wiehe. Copyright 2008 by TAYLOR & FRANCIS GROUP LLC - BOOKS. Reproduced with permission of TAYLOR & FRANCIS GROUP LLC - BOOKS in the format Dissertation via Copyright Clearance Center)

Experimental observations showed that the toluene-insoluble solids that form at cracking temperatures are not the friable precipitates that are recovered at room temperature. During the heating of heavy oil, polymerization and condensation reactions process rapidly with the liquid phase until the products of the reactions remain no longer soluble and form a meso-phase that is different than the toluene-insoluble solids. The meso-phase is a liquid-crystalline state which shows the optical birefringence of disc-like nematic liquid crystals. It can be formed as intermediate phase during the thermal cracking and can be observed depending on the reactor conditions and feed properties. Wang et al. (1998) observed that the toluene-insoluble fraction formed a liquid-oil emulsion at reactor condition, consisting of toluene-insoluble sphere suspended in gas oil. This observation suggested that the toluene-insoluble material was liquid or plastic at reactor conditions, which agrees with the theory of liquid-liquid phase separation as a step in coke formation.

Wiehe (2000) divided coke formation during thermal cracking into two mechanisms: intrinsic and extrinsic. The intrinsic coke is formed from the large aromatic molecules in the feed (5 rings or more). These large organic compounds contain aromatic bonds that require very high dissociation energy in order to crack. While the aromatic core is resistant to cracking, the side chains attached to the aromatic core can be cracked to form lighter compounds, leaving the large aromatic core to form coke. Because these large organic structures are very difficult to crack, they must be rejected in order to increase the H/C ratio of the processed feed, thus, the intrinsic coke can be considered the desirable amount of

coke that is formed or rejected to improve the quality of the products. The second mechanism of coke formation is polymerization and recombination of lighter fraction to form heavier compounds and is called extrinsic coke. The extrinsic coke formation is considered undesirable because it comes on the expense of losing some of the lighter compounds in the undesired coke formation reactions. Figure 2.6 shows the different pathways of coke formation based on extrinsic and intrinsic coke mechanism.

Dutta et al. (2001) directly measured the formation of the extrinsic type of coke by labeling bitumen samples with ^{13}C isotope and tracing its appearance in the products. They found that the amount of the tracer in the coke formed increased with increasing the thickness of the reacting liquid films. The amount of the extrinsic coke increased with increasing the length of the diffusion paths, and consequently the mass transfer resistance, for the cracked products of the reaction to escape from the liquid film. The longer the diffusion path, the higher the chance for the cracked products to undergo the undesired recombination and polymerization reactions. This observation lead to further investigation of the role of mass transfer and its coupling with coking kinetics, as will be discussed later in this chapter.

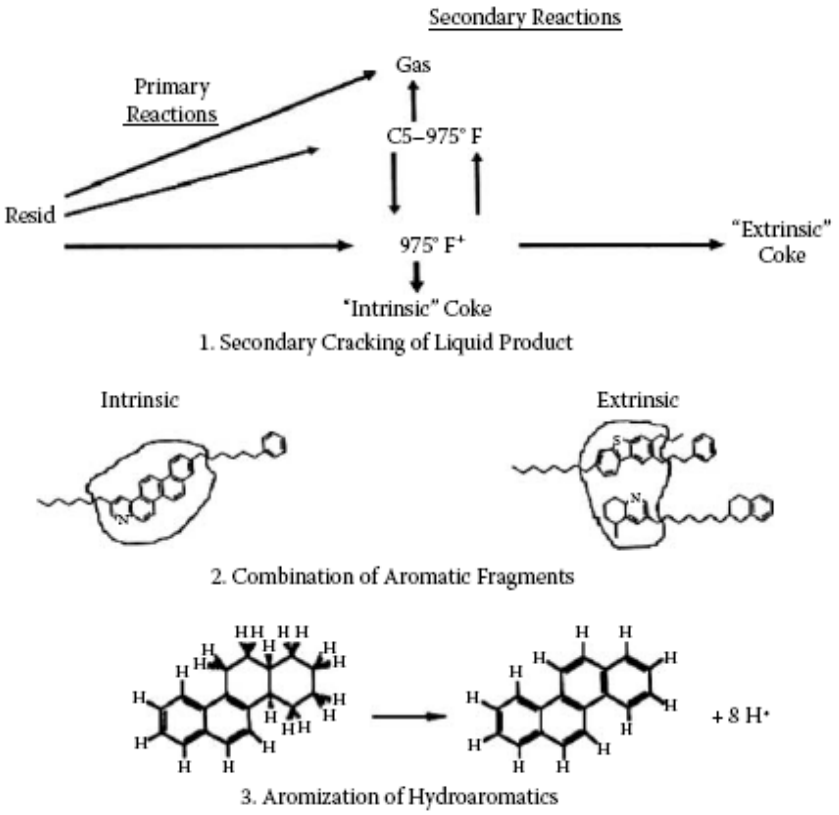

Figure 2.6: Intrinsic and extrinsic coke formation mechanism (PROCESS CHEMISTRY OF PETROLEUM MACROMOLECULES by I. A. Wiehe. Copyright 2008 by TAYLOR & FRANCIS GROUP LLC - BOOKS. Reproduced with permission of TAYLOR & FRANCIS GROUP LLC - BOOKS in the format Dissertation via Copyright Clearance Center)

2.3.3 Coking Reaction Kinetics

In case of vacuum residue processing, the reacting and product mixtures have huge numbers of components present, which complicate the reaction and kinetic modeling. Increasing the number of components in any reaction means increasing the kinetic parameters that have to be estimated and, consequently, increasing the experimental data required for parameter estimation which makes modeling the individual components in mixtures during reactions becomes nearly impossible. Besides that, the analytical methods for defining the component concentrations and chemical structure for vacuum residue are not available. In order to model the process, the oil mixtures are divided into lumps and each lump is assumed to behave as an independent entity. This lumped system would accurately describe the behavior the parent more complex system. (Wei and Kuo, 1969; Kuo and Wei, 1969; Ancheyta, 2005). Almost all the work done to date employed lumped kinetics with different approaches to seek a better fit to the experimental data and actual process.

In the kinetic model for coke formation based on phase separation, Wiehe (1993) presented the conversion of asphaltene over the whole reaction range and conversion of heptane-soluble during the coke induction period as first order reactions. The asphaltenes have maximum solubility in the heptane soluble phase, when this solubility limit is reached the insoluble product asphaltenes is converted to coke and heptane soluble byproduct.

The kinetic model proposed by Wiehe was as follows:

$$H^+ \xrightarrow{k_H} aA^* + (1-a)V \quad (2.7)$$

$$A^+ \xrightarrow{k_A} mA^* + nH^* + (1-m-n)V \quad (2.8)$$

$$A^*_{\max} = S_L\left(H^+ + H^*\right) \quad (2.9)$$

$$A^*_{ex} = A^* - A^*_{\max} \quad (2.10)$$

$$A^*_{ex} \xrightarrow{\infty} (1-y)TI + yH^* \quad (2.11)$$

Where *a*, *m* and *n* are stoichometric coefficients; A^+ is reactant asphaltenes; A^* is asphaltene cores; A^*_{max} is maximum asphaltene cores that can be held in solution; A^*_{ex} is excess asphaltene cores beyond that can be held in solution; H^+ is reactant non volatile heptane soluble; H^* is product non volatile heptane soluble; S_L is solubility limit; *TI* is toluene insoluble coke; and *V* is volatiles.

The model provided by Wiehe was shown to qualitatively describe the experimental data for Cold Lake vacuum residue at 400 ^oC. The model used the hypothesis that the phase separation occurs due to the incompatibility of the new-formed phase with the oil phase, which attributes to the coke formation. This hypothesis does not agree with the results of Gray et al. (2003), who found insignificant amount of polynuclear tracers in the toluene insoluble coke phase, which suggested that the oligomerization reactions that increase the coke phase molecular weight has a major role in coke formation.

Rahmani et al. (2002 and 2003) studied the coking kinetics of asphaltenes along with solvent interaction and chemical structure effects. They extended the phase separation model proposed by Wiehe (1993) to the case of closed batch reactor systems, as in the closed reactors the cracked products remain inside the

reactor with most of the heptane-soluble phase in the liquid phase, and to account for the solvent interaction with asphaltenes. They also used a finite rate constant for the formation of coke, k_C (Equation 2.16) instead of the infinite rate constant used by Wiehe (1993) in the TI formation reaction (Equation 2.11).

To account for the hydrogen acceptance ability of asphaltene, the phase separation model was further extended by Rahmani et al. (2002 and 2003). The asphaltene fraction was assumed to consist of unreacted asphaltenes with attached side groups *(A^+)*, and two types of aromatic cores formed by cracking of the initial asphaltenes, each with different hydrogen-accepting capability. Cores that can accept enough hydrogen to change their solubility characteristics *(A^{*A})* and cores that cannot accept hydrogen *(A^{*NA})*. The cores that accepted sufficient hydrogen from a donor were assumed to be converted to heptane-soluble material.

The modified model was as follows

$$A^+ \xrightarrow{k_A} (c-d)A^{*NA} + dA^{*A} + (1-c)(H^* + V) \qquad (2.12)$$

$$A^{*A} \xrightarrow{k'} H^* \quad \textit{in case of hydrogen donor solvent} \qquad (2.13)$$

$$A^*_{\max} = S_L (S + H^* + V) \qquad (2.14)$$

$$A^*_{ex} = A^{*NA} + A^{*A} - A^*_{\max} \qquad (2.15)$$

$$A^*_{ex} \xrightarrow{k_C} TI \qquad (2.16)$$

The two fitting parameters, asphaltene cracking rate constant (k_A) and stoichometric coefficient (c), were found to correlate with two chemical properties: sulfide content and aromaticity of the asphaltenes, respectively. The kinetic model was shown to predict coke formation, based on the chemical composition of other feed asphaltenes that were not used in model parameter estimation.

Del Bianco et al. (1993) studied the kinetics of thermal cracking for the residua at different temperatures. They assumed that the reaction pathway for coke formation could not be represented by simple first-order kinetics due to the non-linear correlation between the distillate and coke yields. They also found that coke formation showed an induction period, which decreases as temperature increases. Taking these observations into account, and instead of adopting the solubility limit idea proposed by Wiehe (1993), they proposed a reaction scheme with reaction intermediates.

$$VR' \xrightarrow{k_1} D \qquad (2.17)$$

$$VR' \xrightarrow{k_2} I \xrightarrow{k_3} C \qquad (2.18)$$

Where I is the reaction intermediate in the coke production, VR' is the fraction of vacuum residue not converted $VR=VR'+I$, D is the distillates, C is coke, and k_1, k_2 and k_3 are the rate constants.

The condensation reaction, which is responsible for the coke formation, was found to have higher activation energy; consequently, this reaction becomes relatively more important as temperature increases.

The experimental results of Del Bianco et al. (1993) showed that the disappearance of asphaltenes coincides with coke production. However, at high severity, the coke yields exceed the initial amount of asphaltenes and therefore the polymerization reactions also involve oil components. This result was confirmed

by experiments of deasphalted vacuum residue that gave 10.9% coke yield compared to 29.7% coke in case of the whole vacuum residue at the same conditions. When they examined the molecular parameters, such as H/C ratio, number of carbon per alkyl side chain, aromatic carbon and unsubstituted aromatic carbon, the results showed that the dehydrogenation of asphaltenes is a consequence of the decrease of alkyl chain length and dealkylation reactions; both processes cause the increase of aromaticity. Their explanation of the results was that all of these reactions cause the progressive insolubilization of the aromatic asphaltenes sheets and hence lead to the condensation reactions which give rise to the appearance of mesophase and therefore to coke deposition.

Other kinetic studies have been performed to study coking kinetics with different approaches and at different conditions. Wang and Anthony (2003) studied the thermal cracking behavior of asphaltenes with a three-lump model. They showed that an empirical relation of coke formation and asphaltenes conversion gave a reasonable description of the kinetic behavior at high conversion. Takatsuka et al., (1989) used the atmospheric equivalent boiling point in determining the Arrhenius parameters and to describe the effect of phase equilibrium in the reactor. Their model predicted the performance of different types of reactor by taking the residence time distribution in consideration. The residence time distribution was used to determine the average residence time in the reactors in order to achieve complete conversion. They observed the degree of reaction by the value of the softening point of pitch when pitch was the residual product. The softening point of pitch was predicted as a function of residual

components and increased with the reaction time. Banerjee et al. (1986) studied the kinetics of bitumen and its fractions (asphaltenes, soft resin, hard resin, aromatics and saturates) in the temperature range from 395 to 510 ^{o}C. They found that the rate of coke formation is higher for higher degree of aromaticity in the feedstock. They proposed a reaction scheme but did not provide information about the estimation of kinetic parameters.

2.3.4 Coupling of Mass Transfer with Reaction

Fluid coking usually has lower coke yield than the delayed coking (Nelson, 1958; Speight, 2007). One of the fundamental differences between the two modes of coking is the thickness of the reacting liquid phase. In fluid coking the reacting phase is a thin film of bitumen over the hot coke particles, unlike the delayed coking in which the reaction takes place in pool-like liquid phase. The volatile cracking products have to diffuse through the liquid film in order to reach the gas-liquid interface. In thicker films these compounds take longer time to diffuse through the liquid film. As the reaction proceeds, the viscosity of the liquid film increases (Aminu, 2004) and the diffusivity of the escaping products decreases as the liquid phase transfers into a solid-like phase. These products will be available in the liquid phase as free radicals or unsaturates for a certain period and the longer the time they stay in the liquid phase the more likely they are to recombine and to incorporate into coke.

Dutta et al. (2001) used ^{13}C labeled compound to track the pathways of potential distillate compounds during cracking of the feed. They found that the coke yield decreased with the reduction in the thickness of the liquid film. The ^{13}C analysis showed a decrease in the ^{13}C incorporation in coke fraction for both heptane-soluble and heptane-insoluble tracers as film thickness was reduced from 150 to 15 μ. McCaffrey et al. (1998) observed bubble formation and film deformation in cracking of vacuum residuum thin films. By performing the thin film cracking on horizontal and angled surface, the coke yield was found to increase with increasing the film thickness. Bubbles evolved slowly and a

formation of viscous layer on the reacting film trapped the bubble until the pressure within the bubble increased sufficiently to deform the viscous layer. Nagaishi et al (1998) compared TGA differential weight loss curves of bitumen at different pressures. They observed a formation of a peak in the TGA differential weight loss curve at atmospheric pressure. Another peak appeared at lower temperature when the pressure was lowered to 0.4 kPa. This peak shifted to lower temperatures and increased as the pressure was reduced. The shift with the low temperature peak was consistent with the removal of volatile components of the bitumen, which would distill of at lower temperatures as the pressure decreased.

Gray et al. (2001) studied the mass transfer role in reacting bitumen films of thickness from 10 to 80 μ. The total coke yield and liquid MCR content decreased with decreasing the liquid film thickness. For thick films, the final coke product in the film indicated the occurrence of bubbling during the reaction, while in thin films no evidence of bubbling was observed. They proposed a mathematical model to describe the mass transfer phenomena with reaction, which considers mass transport by diffusion and bubbling in thick films.

The mass balance equation was given by

$$D\frac{d^2C_P}{dx^2} + k_1C_R - k_PC_P - k_B(C_P - C_P^*) = 0 \quad (2.19)$$

Where C_P and C_R are the product and residue concentration, C_p^* is the critical product concentration for bubble formation, and D is the diffusivity. The rate constants are k_1 for cracking of the residue to give products, k_p for trapping of

the products in the liquid phase and k_B is for transport of the products to gas-phase bubbles.

Non-dimensionlization of the above equation gives

$$\frac{d^2\psi}{dl^2} - \theta^2\psi + \kappa'\theta^2 = 0 \quad (2.20)$$

Where ψ is C_P/C_P^* and θ is Thiele modulus for thick films and has the form

$$\theta^2 = \frac{(k_P + k_B)L^2}{D} \quad (2.21)$$

For the inner section of the film where the concentration of the gases is higher than a critical concentration of bubble nucleation limit, and κ` is the ratio between the forward and retrograde reactions considering bubble formation.

For thin films the transport by bubbling does not occur, and the last term in equation (2.19) can be dropped and the equation becomes

$$D\frac{d^2C_P}{dx^2} + k_1C_R - k_PC_P = 0 \quad (2.22)$$

And in dimensionless form

$$\frac{d^2\psi}{dl^2} - \phi^2\psi + \kappa\phi^2 = 0 \quad (2.23)$$

Where ϕ is Thiele modulus for thin films or the outer part of thick films, where the gas concentration is below the nucleation limit

$$\phi^2 = \frac{k_P L^2}{D} \quad (2.24)$$

And, κ is the ratio between the forward and retrograde reactions without bubble formation.

In case of thick films, at large values of Thiele modulus the vapor products are more likely to trapped and converted to coke, or to migrate to vapor bubbles, than in the case of thin films. Lower values of Thiele modulus mean that the liquid products will diffuse through the reacting liquid film rather than being trapped or forming vapor bubbles. In case of reacting bitumen films, as the reaction proceeds the viscosity of the liquid phase changes dramatically (Aminu et al., 2004), which in turn decreases the diffusivity of the gas products and the solution of the model equations becomes more complicated with variable Thiele modulus.

At values of κ greater than unity, the rate of the cracking is higher than the rate of trapping of the gas products in the liquid phase, and below unity the trapping is dominant to the cracking reaction.

Gray et al. (2004) proposed a lumped kinetic model that included cracking, coke formation and vaporization limited by vapor-liquid equilibrium and mass transfer (Figure 2.7). The amount of extractable materials in the liquid film did not follow first order kinetics, which also was described by the model with an initial rapid devolatilization period followed by cracking. The model suggested that the coke yield would decrease with increasing the reaction

temperature because of enhanced devolatilization. The authors suggested using data from Aminu et al. (2004) to obtain better estimates of the liquid phase mass transfer coefficient as a function of the conversion and using variable mass transfer with time to enhance the agreement with the evolution of heavy oil fraction data and to account for the insensitivity of the coke yield with temperature.

Continuing on the work of Gray et al. (2004), Radmanesh et al. (2008) revisited the kinetic model and provided a modified description of the mass transfer limitation by correlating the diffusivity of the reaction products in the reaction liquid film to the physical properties, which change greatly throughout the reaction, and adopting the intrinsic and extrinsic coke formation mechanism proposed by Wiehe (2000). The reaction scheme used by Radmanesh et al. (2008) is shown in figure 2.8.

An understanding of the role of mass transfer in the coking reactions can be employed to maximize the yield of distillate products and minimize the yield of coke in the commercial reactors, by introducing thinner reacting liquid films. In order to form a thin layer of the liquid feed over the coke particles, there must be an efficient mechanism for distributing the feed on the coke in the fluid bed. (Gray, 2002). The introduction of the liquid films to the fluidized bed can be improved by optimizing process variables such as feed atomization, design of the feed injection nozzle, the gas flow rate, and the reactor length to diameter ratio. (Gray et al., 2001)

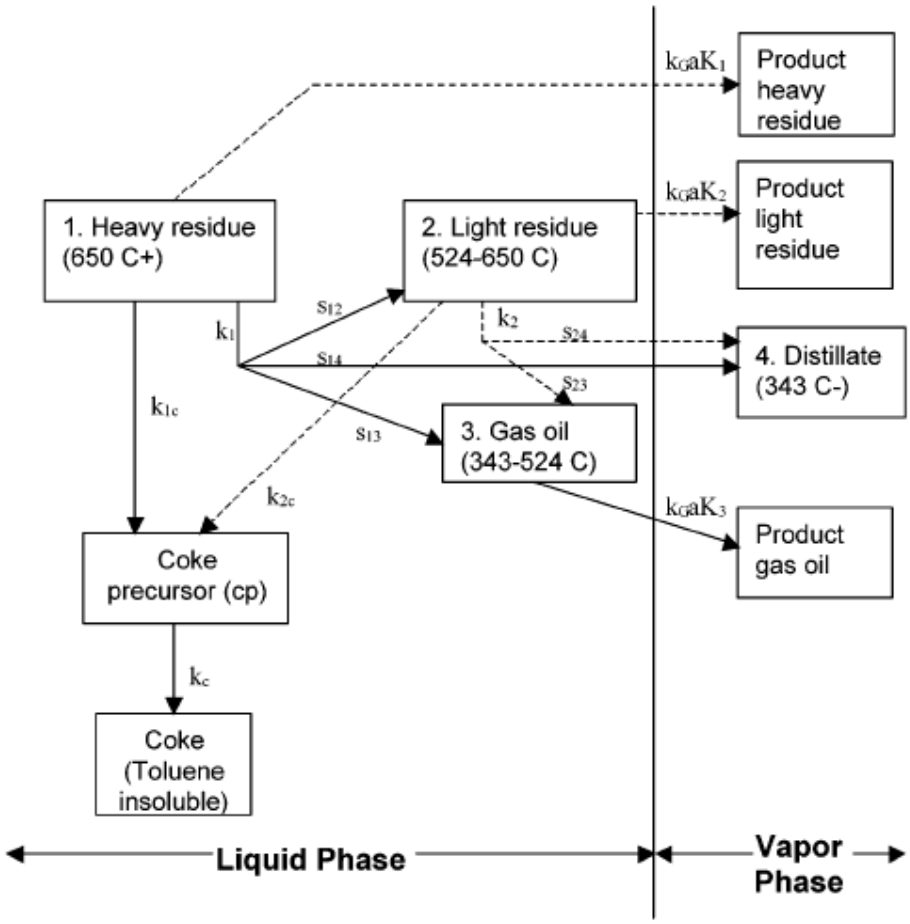

Figure 2.7: Schematic diagram of lumped reactions and volatilization during coking in a thin film. Reactions are assumed to be first order. Rate constants for reaction are k_i, stoichometric yields are s_{ij}, and the mass transfer coefficient is k_{Ga}. Equilibrium ratios are K_i (Gray et al., 2004)

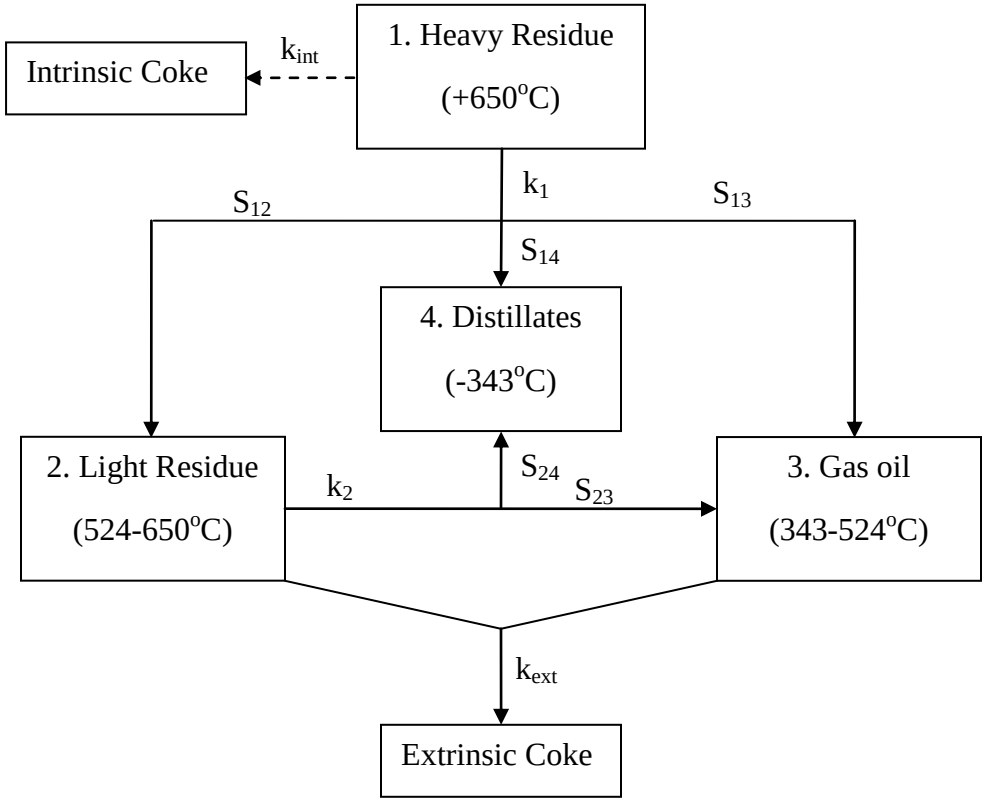

Figure 2.8: Reaction network for thermal cracking of bitumen (Radmanesh et al., 2008)

2.4 Bitumen Coke Agglomerates

2.4.1 Agglomerate Formation and Growth

Fluid coking uses finely divided coke particles as a heat carriers and reaction surface. The mean particle distribution of coke particles is usually around 150 μm. Jet attrition nozzles are usually used to grind the coke particles to control particle size and create fine seeds, and any oversized lumps are moved periodically at the bottom of the reactor (Dunlop et al, 1958). The feed is introduced to the reactor by steam-assisted spray nozzles. The droplet size of the liquid feed is much larger than the coke particle sizes. Depending on the nozzle design and the operation, the liquid feed droplet size can range from 300 μm to 3000 μm on average (Tollefson et al., 1997).

When the oil droplet enters the bed of a fluid coker, it comes into contact with many coke particles, due to the difference in their sizes. Then those coke particles accumulate with the liquid droplet and form a so called "gumball" (Gray 2002). McDougall et al. (2005) showed that viscosity and contact angle are the two important criteria in agglomerates formation in fluid beds. Pilot studies and analysis of solid particles from fluid-bed coking confirmed that the solid particles and liquid feed tend to form agglomerates in the size range of 0.1 – 2 cm within the bed of solid particles (Gray, 2002). The shear forces inside the bed due to the bed velocity can pull the particles apart, also the cracking of the liquid and devolatilization of the product can affect the strength of the gumball, specially that the liquid has low initial viscosity (ca.1 cP) at the reaction condition and good wetting ability what would give good spread of the liquid on the coke particles.

As the reaction proceeds the liquid viscosity increases very rapidly, while the surface tension is not significantly affected, (Aminu et al., 2004). The volume of liquid will decrease due to cracking and product evolution, which may lead to increasing the internal cohesive forces and allow the agglomerate to survive in the fluidized bed.

Another factor that has been studied and found to have significant effect on agglomerate formation and solid liquid mixing in fluidized bed is the liquid nozzle design. House et al. (2008) showed that improvements in the liquid-solid contact in fluidized bed can be achieved by modifying existing nozzles and developing new nozzle designs. By testing two types of nozzle designs and testing the effect of modifying the design by using pulsation or adding an attachment to the nozzle to enhance the solid entrainment, they showed the effect of nozzle types on liquid solid mixing efficiency, agglomerate formation and agglomerate size distribution. The enhanced solid entrainment (ESE) nozzle introduced by McMillan et al. (2005) and House et al. (2004) showed improvement over the free jet nozzle in solid-liquid mixing by increasing the amount of wetted solids and achieving a more uniform primary solid-liquid mixture, which helps reduce agglomeration in fluid beds.

Coke particles covered with a liquid layer, as well as the wet agglomerates, circulate in the fluidized bed and the liquid reacts on the coke surface with time. During the movement of wet coke particles and agglomerates, they transfer the unreacted liquid to reactor internals causing fouling, especially in the coke stripper section at the bottom of the fluidized reactor where

hydrocarbons are stripped using steam before coke exits the reactor (Bi et al., 2005 and House et al., 2006). Fouling is a serious problem that can greatly affect the operability of the fluid coking process. If the agglomerates keep forming and growing, "bogging" or loss of fluidity of the bed can occur, because agglomerate formation inside the bed increases the porosity of the bed, which in turn requires increasing the minimum fluidization velocity (Ennis et al. 1991). Gray (2002) showed that the required minimum fluidization velocity would increase in proportion to the logarithm of the liquid film thickness. So, thin liquid films on the coke particles in fluid coking can help reducing both the limitation of mass transfer and defluidization, which reflects the role of good feed distribution on both mass transfer and fluidization.

It has been shown that for a given collision velocity between the granules, with thick enough liquid film and with high enough liquid viscosity, rebound of the granules after collisions will be prevented and they will coalesce. Upon collision of two particles with liquid film on their surface, the formed liquid bridge helps binding the particles together. For the bridge to be stable, the kinetic energy of the colliding particles must be dissipated by the viscous flow of the liquid film. The balance between kinetic energy and viscous dissipation gives the critical conditions for the formation of an agglomerated pair of particles

$$St_v^* = \left(1+\frac{1}{e}\right)\ln\frac{L}{L_0} \quad (2.25)$$

Where e is the coefficient of restitution; L is the thickness of liquid layer; L_0 is the height of the asperities at the surface of the granule. (Ennis et al., 1991; Keningley et al., 1997; Gray, 2002).

The viscous Stokes number of the system will be given by (Ennis et al., 1991 and Keningley et al., 1997)

$$St_v = \frac{4\rho_D(2u_0)d}{9\mu} \quad (2.26)$$

Where ρ_D is the granule density; d is the granule diameter; $2u_0$ is the relative velocity; and μ is the viscosity of the liquid.

In order for the granule to grow, this Stokes number must not exceed a critical value. Collisions of particles with Stokes number higher than the critical value does not result in stable liquid bridge. Ennis et al. (1991) observed three granulation regimes based on the above two equations (2.25 and 2.26). For the particles with $St_v < St^*_v$, the rate of particles growth was independent on binder viscosity and granule kinetic energy and critically depends on the presence and distribution of binder. This is referred to as the non-inertial regime. In this regime, the operating parameters such as spray drop size and spray distribution control the growth of the granules. As granules grow, their Stokes number increases. When the largest Stokes number reaches the critical value, granules kinetic energy and binder viscosity start to play a rule. In this inertial regime, increasing binder viscosity and decreasing granules kinetic energy will increase granule coalescence. As the granule grow further and the average Stokes number reaches

the critical value, the distribution of St_v will be such that local regions where $St_v<St^*_v$, where coalescence is possible, will be balanced with other regions of disagglomeration where $St_v>St^*_v$, implying that in average granules growth is not achieved. At the final regime when the growth of the granules was ceased all the added binder coated the granules.

Minimum values for the liquid film thickness will help reduce the mass transfer limitation, trapping of the cracked products and also prevent formation and growth of agglomerate and defluidization by decreasing the value of critical Stokes number, which the Stokes number of the particle must not exceed in order to form stable liquid bridges and grow.

2.4.2 Agglomerates Disintegration and Breakage

Agglomerates can disintegrate by many mechanisms including internal stresses caused by reaction and vapor evolution, external mechanical stress caused by bed fluidization, and migration of liquid from the agglomerate to drier bed particles (Weber et al., 2006). Agglomerate breakage is undesired in many processes, but in fluid coking due to the aforementioned problems associated with agglomerate formation, less agglomerate formation may be beneficial to the coking reactions.

Agglomerates strength is affected by different factors some of them are: (Verkoeijen et al., 2002)

- The size and size distribution of the primary particles. Agglomerate strength increases with decreasing the particle size and for wider particle size distribution.
- The porosity of the agglomerate, the strength increases with decreasing porosity.
- The binder surface tension. Agglomerate strength increases with increasing the binder surface tension.

Most of the literature that investigated the agglomerate breakage and disintegration deal with the mechanical impact mechanisms of breakage, like when the agglomerates hit a stationary surface or when the agglomerate colloid, which may be of some interest in case of the fluid coking. Almost no experiments have been done to study the effect of vapor evolution on the agglomerate breakage.

Agglomerates behavior inside the bed has different aspects and depends on many variables and properties of both bed and agglomerate materials. Weber et al. (2006) found that agglomerates of 9% moisture content tend to collect bed materials and gain more weight than the lost binder weight while fluidization, while the drier agglomerate do not. The drier agglomerate on the other hand showed consistent erosion in a linear manner and that rate of erosion depended on the solid particle size and particle size distribution in the agglomerates. They found that the agglomerates that were made from hydrophobic materials did not survive the fluidized bed, which supports the liquid binder role in making the agglomerates, and those agglomerates have internal structure that restrict the

liquid mobility within the agglomerate. Agglomerates in more erosive bed materials suffered breakage and attrition more than other bed materials. They also showed that the gas velocity has a great effect on the survivability of the agglomerate, that there is an increase in the mass fraction loss rate of the agglomerate with increasing the fluidization gas velocity. In following work, Weber et al. (2008) studied the effects of some variables on the stability of agglomerates in fluidized beds, from these variables the binder concentration and binder viscosity was found to have significant effect. Their results showed that increasing the viscosity of the liquid binder to a certain level, from 1 to 3.2 cP, increased the stability of the agglomerates, and beyond that level increasing the viscosity did not have much effect. They also showed that the superficial gas velocity in fluidized bed plays an important role in stability of agglomerates. Increasing the superficial gas velocity caused fragmentation and erosion of destroyed fragments when the initial liquid binder concentration was low, while the high liquid binder content agglomerates fragmented and recruited more of the bed particles to the surface of wet agglomerate..

2.4.3 Heat Transfer and Heating Rate within Agglomerates

At the fluid coking operating temperature in the range of 500 to 540^{o}C (Nelson, 1958), the coke induction period is very short and almost insignificant (Gray et al. 2004) and the reaction takes place on the coke particle surface once the liquid comes into contact with the coke particle. However, when agglomerates are formed, the local ratio of liquid to solid is high and the liquid is not heated immediately. Gradual heating of the interior of an agglomerate will depend on its

size and density, its survival in the fluid bed, and the heat transfer from the surrounding medium. Within such an agglomerate, the reaction will depend on the local temperature, but the liquid covering the coke particles becomes trapped inside the agglomerate, with longer diffusion paths for the cracked products out of the liquid films due to the barriers imposed by the solid particles. This geometry leads to mass transfer limitations and trapping of the cracked products and enhancing the yield of coking reactions. As the agglomerate of coke and reacting liquid feed travels and circulates inside the fluidized bed, both the heat and mass transfer interactions within the agglomerate will play a role in the cracking reactions. The coupling of mass transfer with cracking reactions was discussed in section 2.3.4.

For immersed spherical particles in a fluidized bed, the heat transfer coefficient at the surface of the particle varies with the location inside the fluidized bed (Kunii and Levenspiel, 1969) with most of the heat transported (80% to 95%) by the solid particles. For submerged objects, the heat transfer in the fluid bed is a combination of different mechanisms, convection heat transfer at the times of gas bubble contact, both convection and conduction at the times of solid particles contact, and radiation heat transfer in case of high temperatures. (Yang, 1998)

In case of an agglomerate moving within the fluidized bed, the mechanisms and approach will be different than in the case of stationary object because: firstly, a moving agglomerate circulates with the bed and is subjected to different heat transfer coefficients at different locations within the bed, and

secondly in moving particles the heat transfer surface is mainly exposed to particles and less to bubbles than in the case of stationary objects. The heat transfer coefficient for mobile particles in a fluidized bed can be expressed as a combination of two components; the gas convective heat transfer and the particle convective heat transfer (Parmar and Hayhurst, 2002)

$$h = h_{gc} + h_{pc} \quad (2.27)$$

Where the gas convective component is given by

$$h_{gc} = \frac{\lambda_f}{d_s}\left\{2\frac{\lambda_e}{\lambda_f} + 0.693\left(\left[1+\mathrm{Re}_p\,\mathrm{Pr}\right]^{1/3} - 1\right)\left(\frac{C_{d\varepsilon}\,\mathrm{Re}_p}{8}\right)^{1/3}\left(\frac{q}{\varepsilon_{mf}}\right)^{2/3}\right\} \quad (2.28)$$

Where λ_f is the thermal conductivity of the fluidizing gas; d_s is the diameter of the heat transfer surface; λ_e is effective thermal conductivity of the particulate phase;

Re_p is Reynolds number of the particulate phase $\frac{\rho_f U_p d_p}{\mu}$;

Pr is Prandtl number $\frac{\mu C_f}{\lambda_f}$; $C_{d\varepsilon}$ is porosity-dependant drag coefficient for the mobile sphere; q is bed tortuosity; ε_{mf} is voidage of the particulate phase at minimum fluidization; ρ_f is the density of the fluidizing gas; U_p is gas velocity in particulate phase; d_p is the diameter of inert particles in the bed; μ is the viscosity of the fluidizing gas; λ_e, $C_{d\varepsilon}$, and q are given by other correlations in Parmar and Hayhurst (2002)

The gas convective heat transfer coefficient approximately inversely proportion to the diameter of the mobile particle (d_s), i.e. as the particle (agglomerate) continues to grow in the bed the convective heat transfer from the fluidizing gas decreases.

The convective particle heat transfer coefficient is given by (Parmar and Hayhurst, 2002)

$$\frac{1}{h_{pc}} = \left(\frac{d_p}{\Phi_t \lambda_f} + 0.5 \sqrt{\frac{\pi \tau_c}{\lambda_e \rho_p \overline{C}_p}} \right) \quad (2.29)$$

Where Φ_t is the film thickness parameter; τ_c is the contact time between the fluidized particle and heat transfer surface; C_p is the heat capacity of the fluidized particles. Parmer and Hayhurst (2002) provided the correlations for Φ and τ_c.

Inside the agglomerate, the mode of heat transfer will be different than the external heat transfer. Within the agglomerate the main heat transport mechanism will be mainly by conduction. As the reaction proceeds and the vapor products evolve and diffuse through the porous solid, they could contribute in transferring the heat within the agglomerate by convection. The heat of reaction could also affect the temperature profile inside the agglomerate. The importance of the convection heat transfer by the reaction products and the heat of reaction decreases with decreasing the amount of reacting liquid in the agglomerate and their significance on the temperature profile is difficult to estimate.

From the definition of heat transfer Biot number, the relative importance between external convective heat transfer and internal conductive heat transfer can be stated

$$Bi_h = \frac{hd}{\lambda} \quad (2.30)$$

Where h is the overall heat transfer coefficient; d is the particle diameter; λ is the agglomerate thermal conductivity.

For large Biot number internal heat transfer will be relatively slow relative to the external heat transfer, and the temperature gradient inside the agglomerate will be significant. For small Biot number the internal heat transfer will be fast enough to assume homogeneous temperature within the agglomerate. Using simple calculations to evaluate Biot number can give us an idea about the relation between the internal and external heat transfer in the agglomerate.

From fluidization literature (Parmar and Hayhurst, 2002, Rohsenow et al., 1998 and Yang, 1998) fluidized beds usually have excellent heat transfer and the heat transfer coefficient depends on many variables, such as particle type and size and on operating variables, such as fluidization velocity, temperature and pressure, and on the physical properties of the fluid and particles. An average value of 400 W/m^2K is in order of magnitude of the heat transfer coefficient in fluidized bed and can be used to calculate the agglomerate Biot number. The thermal conductivities of Syncrude coke given by Michaelian (2002) to be in the range of 0.4 to 0.9 W/mK and the thermal conductivity of Bitumen was given by Speight (2001) to be in the range from 0.11 to 0.12 W/mK. From the above

values, thermal conductivities of coke and bitumen are not far from each others, and with the fast reaction and the fast change of bitumen physical properties, the agglomerate can be approximated as a porous solid in which coke and bitumen together represent the solid phase and fluidization gas and hydrocarbons represent the fluid phase. Thermal conductivity of steam was estimated using VMGSim, and for the hydrocarbons it was estimated using the correlation given by Bahadori and Mokhatab (2008). Values for steam and hydrocarbon thermal conductivities are very close, 0.07 W/mK and 0.06 W/mK, respectively.

The effective thermal conductivity for the porous solid can be estimated by

$$\lambda_{eff} = \lambda_s(1-\varepsilon) + \lambda_f \varepsilon \qquad (2.31)$$

Where λ_{eff} is the effective thermal conductivity, λ_s is the thermal conductivity of the solid phase, λ_f is the thermal conductivity of the fluid phase and ε is the porosity of the porous solid. Using the above values of thermal conductivity and assuming that the agglomerate has 35% porosity, the effective thermal conductivity of the agglomerate is 0.44 W/mK.

Using equation 2.30 to calculate Biot number for 2 cm diameter agglomerates of a thermal conductivity of 0.44 W/mK and heat transfer coefficient of 400 W/m^{2}K, the value of Biot number was 18. Since Bi>1, the heat transfer inside the agglomerate in a fluidized bed is important and is relatively slow compared to the external heat transfer. From this analysis, a significant temperature gradient inside the agglomerate is expected.

From the Biot number analysis above, the slow internal heat transfer and the temperature profile are significant during heating of agglomerates. Due to the coupling between reaction and mass transfer, the rate at which an agglomerate is heated could be significant. In similar reactions of solids, such as pyrolysis of coal and biomass, the heating rate plays a significant role in product yields and distributions with the difference between the two systems, reacting and softening solids in case of coal pyrolysis and inert hard solids in case of agglomerate in fluid coking reaction. According to Gavalas (1982), the heating rate affects the char yield and product distribution due to the change of the solids structures and the micropore distribution in the reacting coals, which in turn affects the mass transfer limitation and lead to different products yields.

The significance of these mechanisms for the reactions in liquid-solid agglomerates is not clear. If the mass transfer limitation effects that are observed during pyrolysis of coals can be excluded for the case of coking of bitumen, then the product yields depend only on the reaction time and temperature rather than the heating rate.

3 MATERIALS AND METHODS

3.1 Materials

The heavy oil sample used throughout the experiments on agglomerates and thin films was a plant sample of Athabasca Vacuum Residue (AVR) provided by Syncrude Canada Ltd. The AVR properties are shown in Table 3.1. This sample was the bottoms stream from a commercial vacuum distillation column. Maya and Khafji vacuum residues, with the properties in Table 3.1, were used in the heating rate experiments and were provided by Idemitsu Kosan. Fluid-bed coke particles, with particle size distribution shown in Figure 3.1, were supplied by Syncrude Canada Ltd. Aluminum oxide particles with particle size of 120μm, used in preparing the AVR-alumina agglomerates for coke yield experiments in fluidized bed, were supplied by Kramer Industries Inc. (Piscataway, NJ).

Toluene solvent was obtained from Fisher Scientific (Mississauga, ON) and was used as received. Barium hydroxide was supplied by Fisher Scientific (Mississauga, ON) in the form of Barium hydroxide octahydrate crystals ($Ba(OH)_2.8H_2O$) and was used to prepare barium hydroxide solution with desired molarity by dissolving the crystals in demineralized water. Compressed nitrogen gas, used as sweeping gas in induction furnace experiments and as fluidization gas in fluidized reactor experiment, and compressed oxygen gas, used in fluidized bed experiments, supplied by Praxair. Iron-nickel alloys strips with different compositions corresponding to Curie point temperatures of 503^{o}C and 530^{o}C were obtained from Ametek Special Metals (Wallingford, CT).

Table 3.1: Properties of vacuum residues

Property	**Athabasca vacuum residue (Plant sample)**	**Athabasca vacuum residue #2**	**Khafji**	**Maya**
MCR, wt%	20.3	27.8	17.9	24.4
Boiling fractions, wt%				
524 ^{o}C -	20	10	6	5
524 - 650 +^{o}C	44	40	45	42
650+ ^{o}C	36	50	49	53

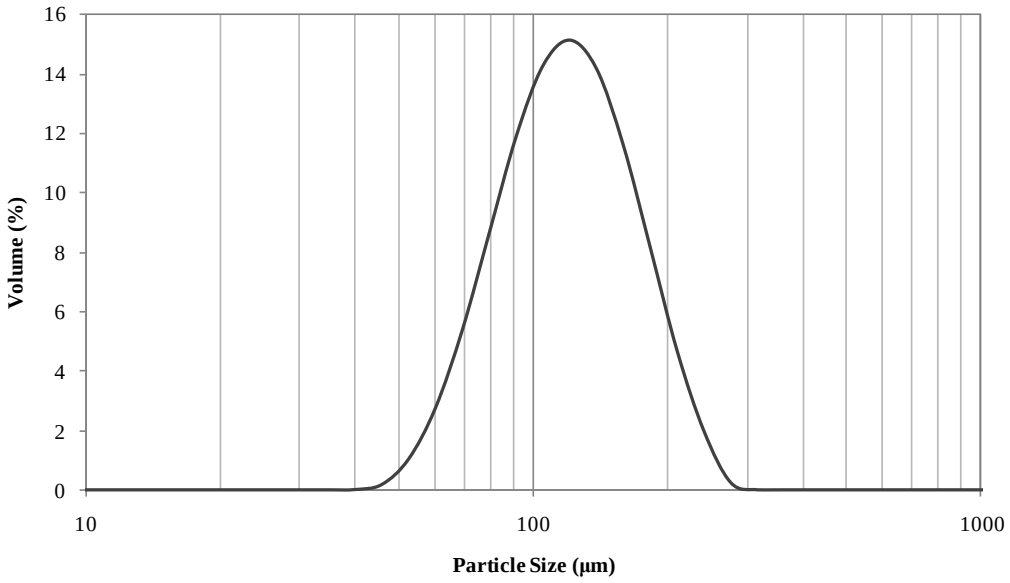

Figure 3.1: Particle size distribution of coke sample used in agglomerates experiments. Data measured using Mastersizer 2000 provided by Malvern Instrument Ltd. (Malvern, UK)

3.2 Agglomerate Preparation

Liquid-solid agglomerates were made by mixing the desired ratio of solid particles (either coke or aluminum oxide) and AVR and stirring them thoroughly over a hot plate at temperature in the range from 110^{o}C to 150^{o}C for a sufficient period of time to get a homogeneous mixture. The liquid-solid mixture was then poured into a mould with the desired agglomerate size and shape and pressed under static pressure for 10 minutes to control the agglomerate density. For the induction furnace experiments, the agglomerates were shaped into disks of 15 mm diameter and three different thicknesses, 2 mm, 3 mm, and 4 mm and in the case of fluidized reactor experiments agglomerates were pressed into 1:1 aspect ratio cylinders with sizes of 5 mm, 10 mm and 15 mm. This method was found to give good control on the agglomerate density; all the tested agglomerates had an average bulk density of approximately 1000 kg/m^3 in case of AVR-coke agglomerates and 3940 kg/m^3 in the case of AVR-alumina agglomerates. After pressing, the agglomerates were cooled in a freezer and then were taken out of the mould. Some of the agglomerates from every batch were tested for the actual concentration of AVR by dissolving the agglomerate in toluene and separating the solids by filtration. Enough replicates were performed to determine the actual AVR concentration.

The agglomerates were prepared with AVR concentrations in the range between 8% and 12.5 % AVR by weight (equivalent to 20% to 30% liquid saturation). Below that range the AVR concentration was hard to control, and the yield of coke from the AVR was too low for accurate determination. At liquid

concentrations over 12.5 wt%, the liquid flowed out of the agglomerates during heating in the induction reactor and the agglomerates lost their shape.

3.3 Induction Furnace Experiments

3.3.1 Equipment

The induction furnace was used in agglomerates reaction and thin films reaction experiments as well as in heating rate experiments and heat transfer model data collection. The experimental apparatus is illustrated in Figure 3.2, with operation following Gray et al. (2001), except that the liquid and vapor reaction products were not collected for analysis. The emphasis was on measuring the yield of coke in the agglomerates and thin films and on measuring the agglomerate temperature change with time. The reactor consisted of a Pyrex glass cylinder capped with two stainless steel flanges. The glass tube was placed within an induction coil (Ameritherm Inc., Induction Furnace model XP-30). Strips of iron-nickel alloy in this coil were heated rapidly to their Curie-point temperature. These heated metal strips were used as a heat source to supply heat to the liquid-solid agglomerate disks or the vacuum residue thin film in an inert atmosphere of flowing nitrogen.

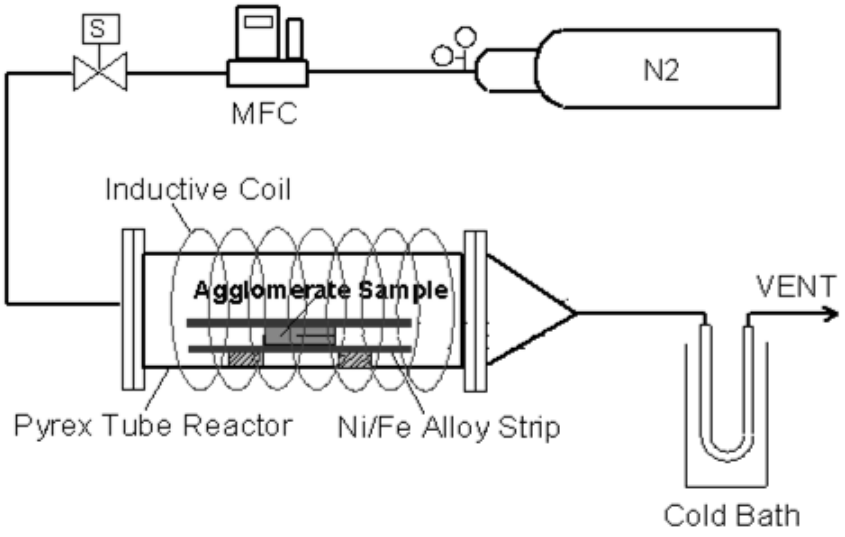

Figure 3.2: Schematic diagram of the induction furnace reactor

3.3.2 Experimental Procedure

3.3.2.1 Ultimate Coke Yield in Agglomerates

For induction furnace experiments, disk shaped AVR-coke agglomerates with 15mm diameter were prepared with thicknesses of 2 mm, 3 mm and 4 mm and with AVR concentration of 8%, 10% and 12.5% by weight. These dimensions ensured that the geometry for the evolution of products was approximated by a one-dimensional length scale.

The moisture-free weight of the agglomerates was determined by heating them in a vacuum oven at 70 ^{o}C for about one hour then weighing them in a moisture analyzer (Mettler Toledo HB43). Special care was required in storing, handling, and weighing the samples because the solid coke particles were hygroscopic. Uncontrolled moisture uptake was significant in comparison to the yield of coke, and gave biased coke yields that were too low. Agglomerates were then placed between two perforated Curie point strips (Figure 3.3). Perforation on the Curie-point alloys were 0.61 mm holes on 1.5 mm triangular pitch. Both lower and upper strips were sprayed with a thin layer of bitumen to ensure good contact with the agglomerate in both sides. The sprayed strips were then warmed up and the agglomerate placed between them and the assembly was clamped and cooled to glue the agglomerate to the strips and to ensure good contact with both strips.

The assembly of the agglomerate and the strips was placed inside the induction furnace (Figure 3.2), the reactor was sealed and purged with nitrogen for 15 minutes then the strips were heated to their Curie-point temperature by the

application of the induction field. Both the upper and lower strips heated the agglomerate by conduction and allowed vapor products to escape through the holes. The vapors were removed from the reacting agglomerates by flowing nitrogen gas at a flow rate of 12 sL/min. The agglomerates were reacted for enough time, depending on their AVR content and thickness, to ensure total conversion of the AVR in the agglomerates to toluene-insoluble coke and volatile products. The 2mm and 3mm agglomerates with AVR concentration below 12.5% were reacted for 10 minutes. The 4 mm agglomerates and 2 mm and 3 mm with 12.5% AVR were reacted for 15 minutes. Two different compositions of Curie-point alloy were used to provide two different reaction temperatures; 503^{o}C and 530^{o}C. After coking, several agglomerates were tested for any unreacted bitumen by dissolving them in toluene, but no soluble bitumen components were detected.

The weight of coke after the reaction was determined and the amount of new coke formed was calculated by difference. Coke mass was determined by using a moisture analyzer (Mettler Toledo HB43) that heats the sample up to 110 ^{o}C and determine the dry weight of coke. Coke yield was calculated as the ratio of the new coke formed over the initial amount of bitumen in the agglomerate.

$$\text{Coke Yield} = \frac{\text{Mass of final coke} - \text{mass of initial coke}}{\text{Mass of initial AVR}} \qquad (3.1)$$

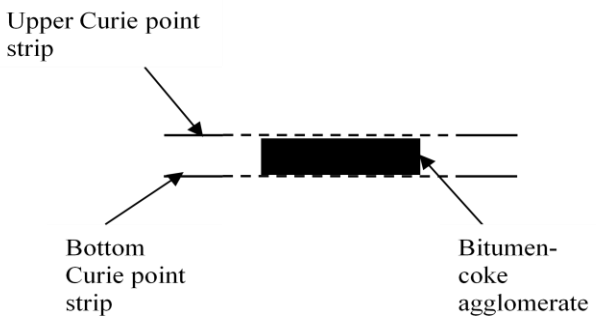

Figure 3.3: AVR-solids agglomerate between two perforated Curie-point strips

3.3.2.2 Ultimate Coke Yield in Thin Films

Thin films of AVR were reacted to determine the ultimate coke yield and to compare it to the ultimate coke yield in agglomerates. For thin film experiments, the vacuum residue material was coated onto strips of Ni/Fe alloy (25 cm x 2 cm x 0.04 cm) with Curie-point temperatures in the range of 503 °C, following Soundararajan (2001). Up to six strips were held in ceramic holders to form an annulus within a Pyrex glass cylinder capped with stainless steel flanges. Both the alloy strips and the glass tube were held within the induction coil (Ameritherm Inc., induction furnace model XP-30). Nitrogen sweep gas was introduced at one end of the glass tube through a sintered metal diffuser and exited the opposite end through a conical section. The gas flow rates used for the experiments were 12 sL/min.

Thin films of feed material are created by dissolving the feed in methylene chloride, then spraying the solution onto the strips. The strips were dried overnight and reweighed to determine the amount of vacuum residue or asphaltene deposited. Mean film thickness was in the range 20-80 μm in all experiments, calculated as volume of residue divided by the area coated.

The entire system sealed and purged with nitrogen for 15 min. The induction heater was then turned on and the strips brought to reaction temperature for 4 min to allow for complete coking to occur. At the end of this time, the alloy strips were cooled and the amount of coke on the strips after the reaction was determined by weight and the coke yield was calculated.

By adjusting the settings on the induction heater, the times for heating the strips could be adjusted between 3 s and 45 s. These heating times correspond to heating rates in the range of 14.8 K/s to 148 K/s, a difference of a factor of ten. Consequently, the equipment was able to give heating rates that varied over an order of magnitude.

3.3.3 Agglomerates Temperature Profile Measurement

For measuring the temperature profile inside the agglomerates and the temperatures of the Curie-point strips, three type-K, 24 AWG gauge thermocouples were used. Two thermocouples were spot welded to the inner side of both Curie-point strips, i.e. between the Curie-point strips and the outer surfaces of the agglomerate. The third thermocouple was inserted between two agglomerates of equal thickness to measure the centre-line temperature of the agglomerate. The Curie-point strips and agglomerate assembly with the thermocouples was then reacted in the induction furnace following the same procedure in section 3.3.2.1 and temperature data was recorded using a HP BenchLink Data Recorder. A schematic of the assembly is shown in Figure 3.4.

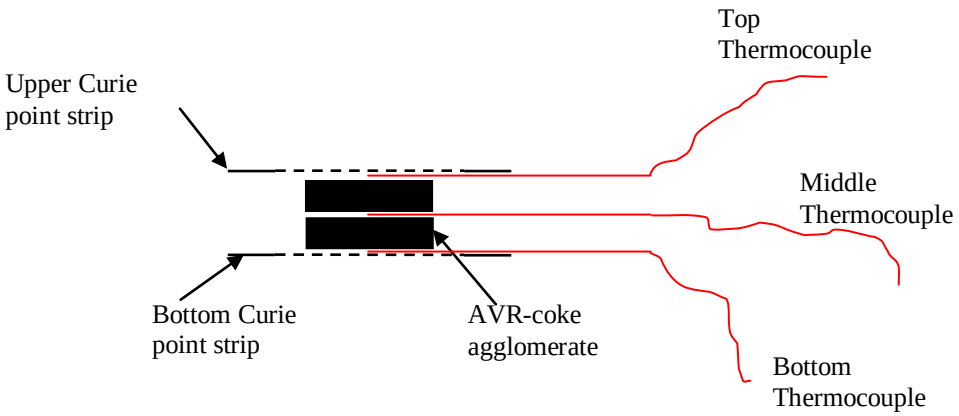

Figure 3.4: Schematic diagram of the assembly of agglomerates, strips and thermocouples. Thermocouples were used for temperature profile experiments

3.4 Fluidized Bed Reactor

3.4.1 Equipment

The fluidized bed reactor was used in determining the coke yield in AVR-solids agglomerates and in testing the agglomerate behavior under fluidized conditions. Figure 3.5 shows a schematic diagram of the reactor. The fluidized reactor section consists of a 102 mm (4-inch) diameter heated section connected to an upper free board 10-inch diameter column and a 32 mm (1.25-inch) diameter sidearm for agglomerate injection. The side arm contains a gate valve at the bottom to hold the agglomerate before the injection. A flow of nitrogen was used for aeration to avoid raise in arm temperature and to prevent agglomerates from sticking to the side arm wall or to each other. The bottom of the fluidized reactor consists of a 102 mm (4-inch) tall conical section that contains three stainless steel gas distributors. At the top of the fluidized reactor, in the 254 mm (10-inch) free board section, two internal cyclones are connected in series to remove the fine fluidization particles from the exit gas stream.

Five band heaters (114.3 mm ID × 50.8 mm wide for each heater) totaling 3350 W are employed to supply the heat to the fluidized bed. The fluidized section of the reactor is equipped with six thermocouples to measure the fluidized bed, free board and reactor body temperatures and with pressure transducers to monitor the reactor pressure.

The fluidized reactor is connected to a bottom quench section through a 102 mm (4-inch) diameter ball valve. The 204 mm (8-inch) diameter bottom

section contains a fluidized bed that can be used for rapid quenching or cooling of hot solids from the reactor bed, if needed. The gas distributor for the bottom section consists of 4 radial sparger tubes. A 204 mm (8-inch) diameter knife gate valve is used to close the bottom section of the reactor. A blind flange is used at the bottom of the 204 mm (8-inch) gate valve to give a good seal for the bottom quenching section of the reactor. Three thermocouples and a pressure transducer are used to monitor the bottom section temperature and pressure, respectively. A cooling water jacket is used at the top of the bottom section below the ball valve to prevent the heat flow by conduction from the fluidization column to the bottom section.

Fluidization gas to the reactor was heated by a sand bath heater and an electric heater in series. Fluidization gas temperature after the electric heater was monitored and controlled through the power output of the electric heater.

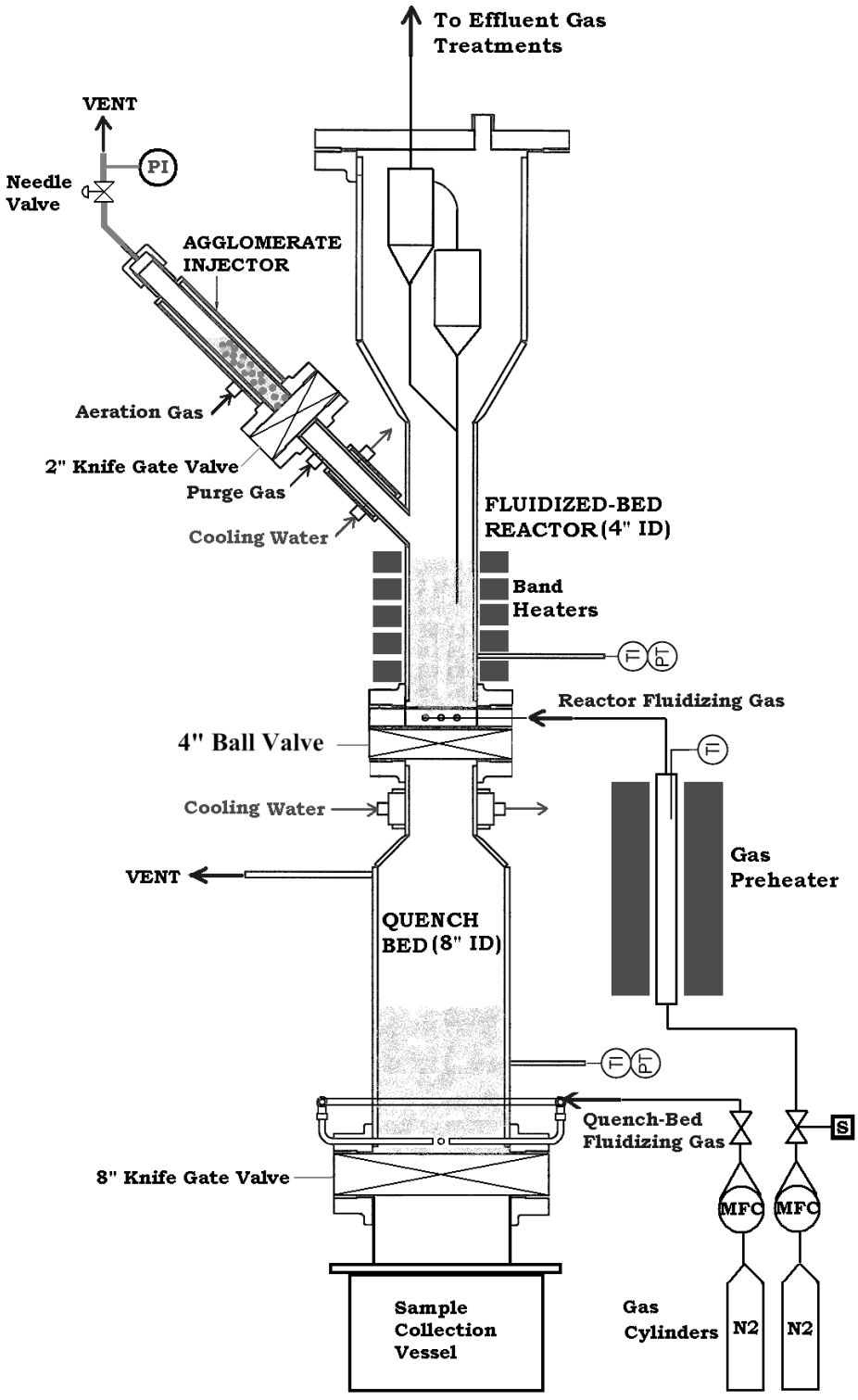

Figure 3.5: Schematic diagram of the fluidized bed reactor assembly

3.4.2 Experimental Procedure

3.4.2.1 Ultimate Coke Yield in Fluidized Bed Reactor

To determine the ultimate coke yield in reaction of AVR-solids agglomerates, cylindrical agglomerates of 1:1 aspect ratio were made out of AVR and aluminum oxide and tested in the fluidized bed reactor (Figure 3.5). AVR-alumina agglomerates were made with sizes of 5 mm, 10 mm and 15 mm and with AVR concentrations of 8%, 10% and 12.5%. 120μ Alumina particles, classified ad Type B according to Geldart Classification, was used in making agglomerates and as fluidization solids in order to be able to determine the amount of coke formed after the reaction by burning the bed charge and determining the amount of CO_2 by absorption in alkaline solution.

3.5 kg of alumina was used as fluidization solids in the reactor section. The ball valve between the reactor section and the bottom section was first closed, and the alumina was loaded through the agglomerate injection arm. After loading the alumina particles to the reactor, the 50 mm (2-inch) knife gate valve at the bottom of the agglomerate injection arm was closed. The desired amount of agglomerates for the experiments was prepared: 3 agglomerates of the 15 mm, 5 agglomerates of the 10 mm or 20 agglomerates of the 5 mm. The agglomerates were weighted and the mass was recorded, then the agglomerates were mixed with suitable amount of alumina, from 50g to 120g depending on the amount of agglomerates, to prevent the agglomerates from sticking to each other or to the walls of the loading arm before injection into to the reactor. The agglomerates and the alumina mix was then loaded into the agglomerates injection arm and the arm

was sealed and closed. Aeration nitrogen kept flowing to the agglomerate injection arm to keep the agglomerate at the room temperature and prevent them from melting or sticking together. All the reactor connections were checked for leakage and the whole reactor was purged with nitrogen for 1h.

After purging, the fluidization nitrogen was set at 10.44 sL/min during the heating up period. The preheating system (the sand bath and the electric heater) and the reactor bed band heater were switched on and the desired temperature set point was given to the temperature controllers. When the desired temperature was reached in the reactor, the nitrogen flow was switched to the high flow position at 52.4 sL/min (equivalent to 40 U/U_{mf} and bubbling regime fluidization) and the reactor was left to fluidize for 10 more minutes for the temperature to stabilize.

Before agglomerate injection, the pressure in the agglomerate injection arm was increased to 1 psi higher than the pressure in the reactor. To inject the agglomerate to the reactor bed, the 50 mm (2-inch) knife gate valve was opened, allowing the agglomerates and the mixing alumina to drop into the reactor. The agglomerates were then left to react in the fluidized bed for 30 minutes to ensure complete conversion of the feed AVR to coke.

To calculate the amount of coke formed during the reaction, the fluidization gas was switched to oxygen with flow of 10.4 sL/min to burn the coke in the bed for about from 6 to 7 hours. The carbon dioxide from the combustion of coke was absorbed in alkali solution in a system of bubbling absorber bottles and used to determine the amount of coke based on the change in

the solution electrical conductivity. Four 500-mL absorption bottles, supplied by Fisher Scientific, were used in two parallel arrangements. The gas entered the bottles through fritted glass cylinders. Barium hydroxide ($Ba(OH)_2$) was used as an absorbent for the combustion products gases, after the method used by Raymond and Winegarden (1927) to determine the CO_2 in fermenting mixtures. After each run, the absorption bottles were washed with hydrochloric acid (Fisher Scientific) to remove the deposited barium carbonate and to clean the clogged pores of the sparger tube. A calibration curve was made between the amount of coke burned in the bed and the corresponding change in the electrical conductivity of the $Ba(OH)_2$ solution by burning a known amount of coke and record the change of the electrical conductivity (Appendix A).

The amount of coke then recorded and the coke yield was calculated relative to the initial amount of AVR in the agglomerates.

$$\text{Coke Yield} = \frac{\text{Amount of coke formed in the reactor}}{\text{Initial amount of AVR}} \qquad (3.2)$$

3.4.2.2 Fragmentation of Agglomerates in Fluidized Bed Reactor

The survival and fragmentation of the AVR-alumina agglomerates were studied to link and compare the results of this study to the study of AVR-coke agglomerates done by Weber (2009).

Before loading the fluidization alumina to the reactor bed, 8kg of alumina was loaded into the bottom quench section of the reactor to help cool the reactor charge once dropped in the bottom section after reaction, and also to prevent breaking of agglomerates when dropped to the bottom section. The bottom section alumina was loaded through the agglomerates injection arm while the ball valve between the reactor section and the bottom section was open. Once the alumina was loaded to the bottom section, the ball valve was closed and the reactor loading and purging procedures were performed similarly as mentioned in the previous section. After reaction of the agglomerates for 30 minutes, the ball valve was opened allowing the agglomerates to drop to the bottom section, where fluidization and cooling nitrogen gas was introduced through the gas distributor at the bottom of the bed. When the temperature of the agglomerates dropped to about 60-70^{o}C, the bottom knife gate valve was opened and the agglomerates along with the fluidization alumina was collected. To separate the agglomerates from the fluidization alumina, the collected solids from the bed were sieved using 500 µm screen (38 mesh number). The mass of the agglomerates and fragments larger than 500 µm was then recorded and presented as a fraction of the initial mass of agglomerates before reaction.

3.5 Thermogravimetric Analysis of Agglomerate and Thin Film Coke

Samples from both thin films and agglomerate coke were prepared using the standard procedures used in determining the ultimate coke yield in thin films and agglomerates. The coke samples were then tested in a TGA to determine the amount trapped volatile materials in both cases.

TGA was performed in Thermo Cahn Thermax 300 machine. After loading the sample to the TGA, the TGA was then purged with 80 mL/min flow of argon at the room temperature. The temperature was then increased to 500^{o}C at a rate of 20^{o}C/min. when the temperature reached 500^{o}C, it was kept at this temperature for about 1 hour. After the constant temperature period was complete, the gas flow was switched to air for one more hour to burn the sample and determine the amount of coke solids in the initial sample.

4 RESULTS

4.1 Coke Yield in Agglomerates in Induction Furnace[1]

Three variables were studied to investigate their effect on the ultimate coke yield in AVR-coke agglomerates: (1) Concentrations of AVR of 8%, 10% and 12.5 wt%, corresponding to 20%, 26% and 30% of the pore volume, respectively, (2) Agglomerate thicknesses of 2 mm, 3 mm, and 4 mm, and (3) reaction temperatures of 503 ^{o}C and 530 ^{o}C. For every tested variable, enough replicate experiments were conducted to determine the mean yield of coke and the standard error. In some cases, data sets were tested for outliers or tested for statistical significance. Thin films of 20μm thickness AVR were made on the Curie-point alloys and were tested at 503^{o}C to compare the coke yield from the thin films to coke yield from liquid-solid agglomerates.

4.1.1 Coke Yield from Agglomerate versus Thin Films

Figure 4.1 shows the average coke yield from 20 μm thin films and from AVR-coke agglomerates. The average coke yield at 503^{o}C in the case of the agglomerates was found to be 23.3±1.7%. For the same AVR feed, the coke yield of reaction of thin films of 20 μm was 11.7±0.3% at the same temperature. Higher coke yield in the agglomerates supported the idea that mass transfer played a role in increasing the coke yield. The liquid films within the agglomerates would be thicker than the case of the sprayed liquid film, due to liquid bridges between particles and incomplete wettability of solids, which means the cracking products

[1] Portions of Section 4.1 were published in Ali et al. Can J Chem Eng, 2010, v 88, issue 1, 48-54

will have longer diffusion paths to exit the liquid phase and a better chance to be trapped in the liquid and undergo the undesired coke forming side reactions.

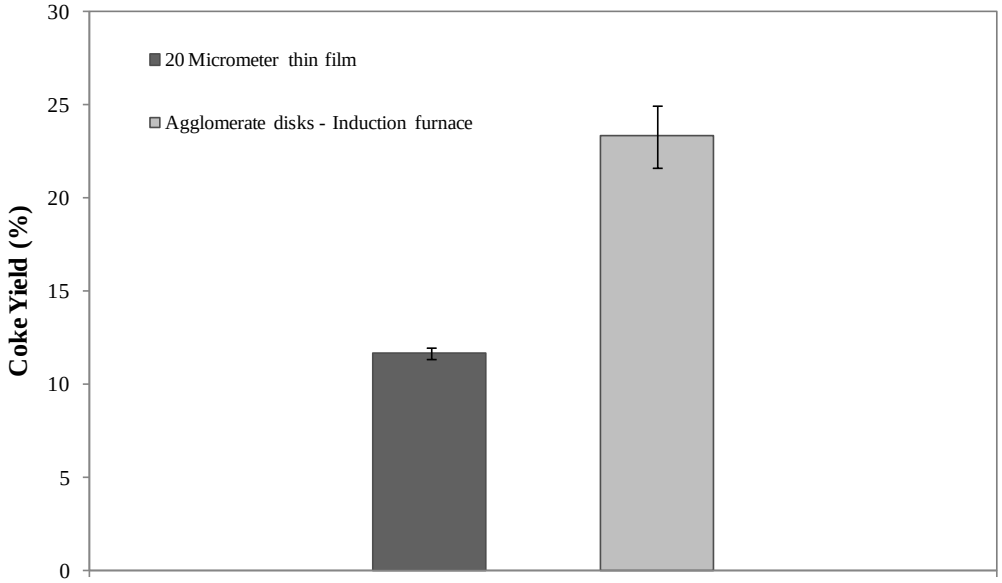

Figure 4.1: Average coke yield in 20 µm AVR films and AVR-coke agglomerates at 503^{o}C in induction furnace. The error bars represents the standard errors from replicate experiments

4.1.2 Miscroscopy of Vacuum Residue and Coke in Agglomerates

In order to visualize the environment of the vacuum residue reacting in coke agglomerates, micrographs were obtained of agglomerated material. Figure 4.2 shows a scanning electron micrograph for the AVR-coke agglomerate. The micrograph clearly show the uneven distribution of the liquid AVR over the coke particles, and the liquid bridges formed between the solid particles with lengths up to 120 μm (Figure 4.2). Polarized Light Microscopy (PLM) of the agglomerates after reaction showed that coke was formed in the thick layers and in the liquid bridges between particles (Figure 4.3). Similar coke formation in liquid bridges and particle fusion was noted in the SEM images of surviving agglomerates (peas and beans) in the industrial fluid coker (Figure 4.4). From these images, we conclude that bridges of liquid between coke particles react to form bridges of coke, and that the distances for transport of products in this bridge geometry are long in comparison to the thin films coated on flat surfaces. It is noted in the micrographs that there is a difference in color of the coke particles and the coke formed during the reaction. The difference in the coke appearance can be explained by the difference in the temperature and reaction time history that the different types of cokes have been subjected to. The particle coke (obtained from Syncrude fluid coker) passed through multiple cycles between the fluid coker and the burner and was subjected to temperatures as high as 600 ^{o}C, while the coke formed in layers and liquid bridges during the reaction was subjected only to the reaction temperature (from 503 to 530 ^{o}C) and for a single reaction path.

Figure 4.2: Electron microscopy images of AVR-coke agglomerates with 12.5% AVR by weight showing the liquid distribution over the solid particles and the formation of liquid bridges between the particles.

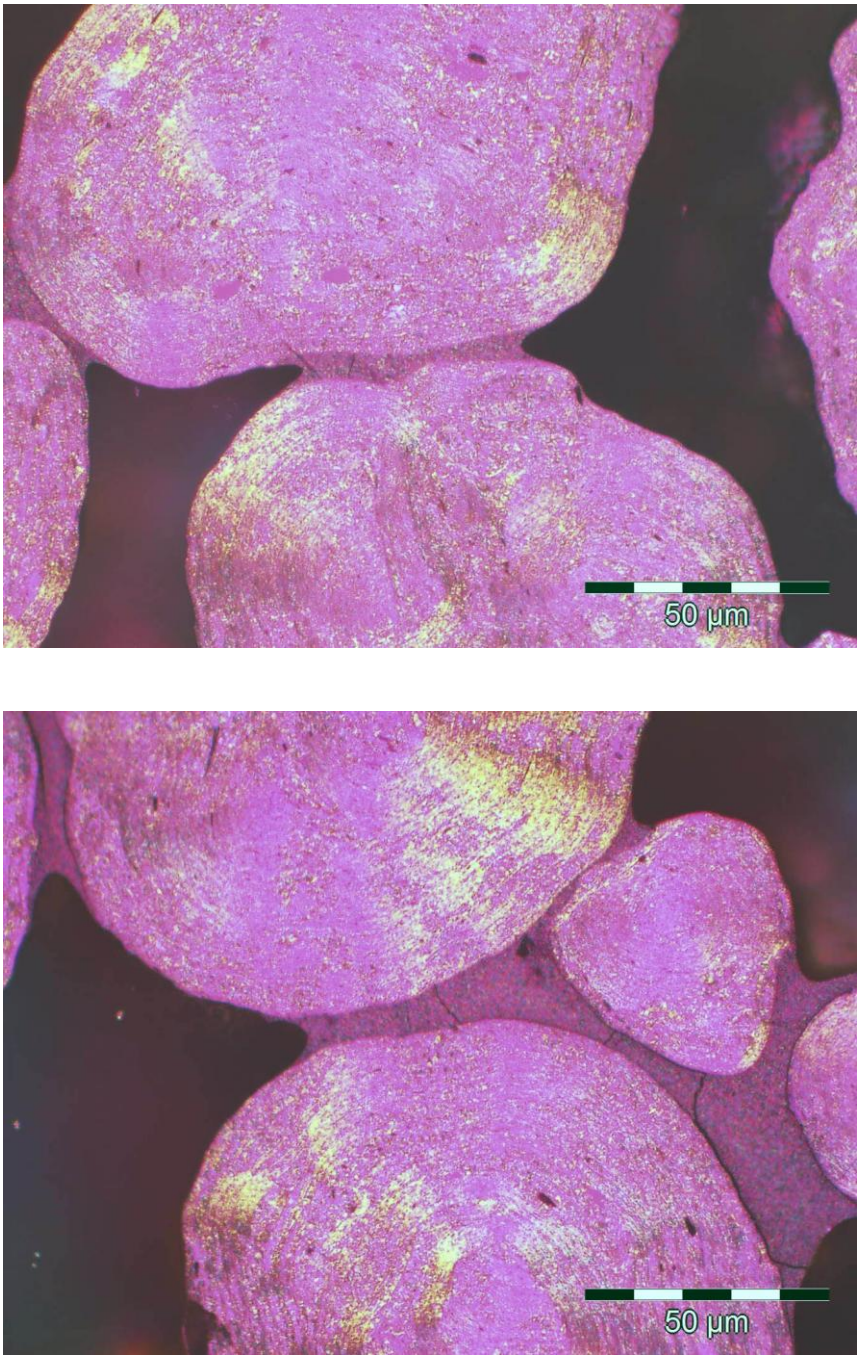

Figure 4.3: Polarized Light Microscopy images of AVR-coke agglomerates after the reaction in induction furnace showing the coke formation in the liquid bridges between solids. Images are of polished cross sections, viewed under cross polarized filters.

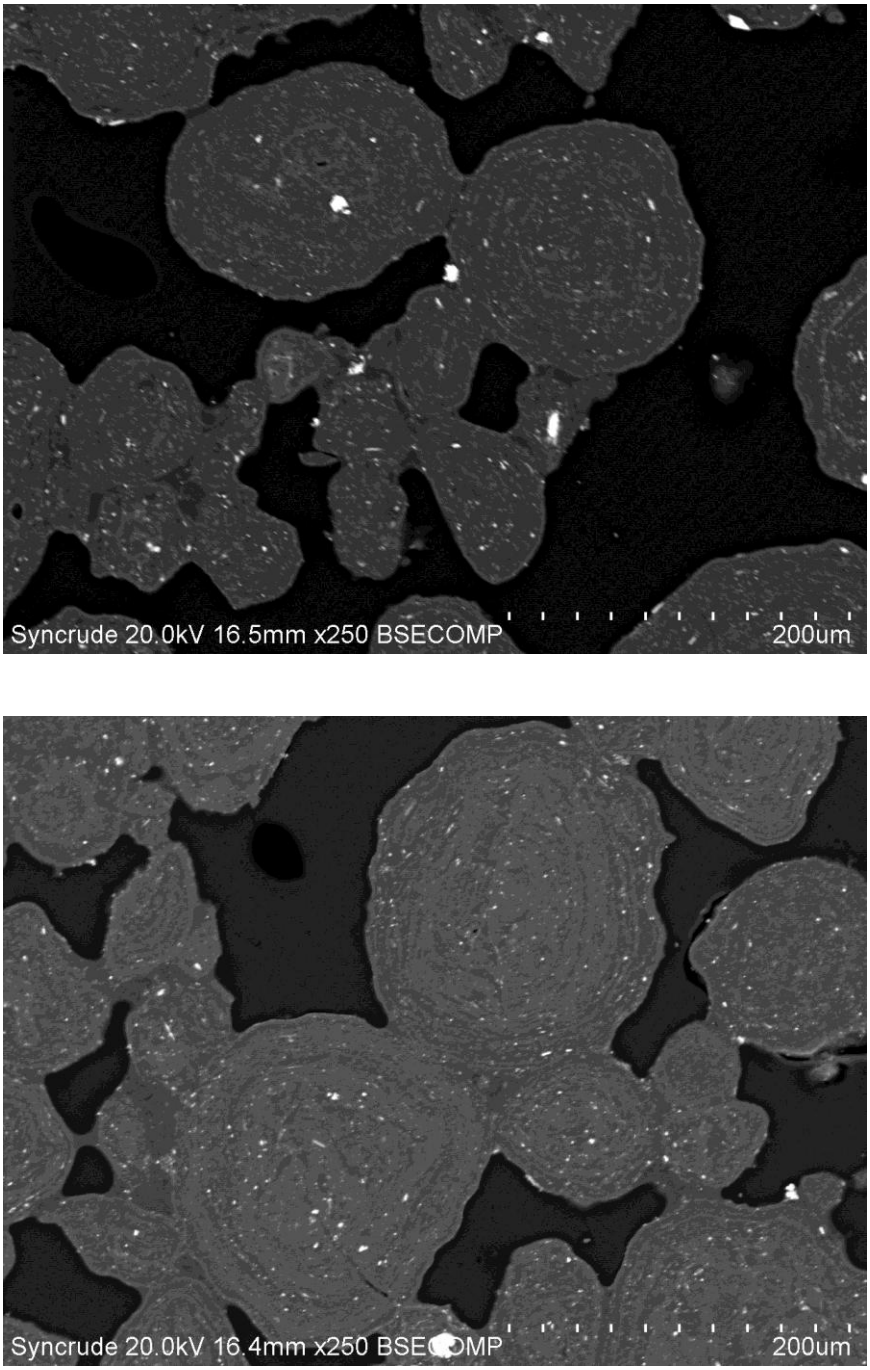

Figure 4.4: Scanning Electron Microscopy images of the surviving agglomerates (peas and beans) in the fluid cocker showing the formation of coke in the liquid bridges between coke particles. Images are of polished cross sections of agglomerated material, taken in the back-scattered mode

4.1.3 Agglomerate Thickness

The data of Figure 4.5 show the coke yield in the agglomerates as a function of the agglomerate thickness for the three different liquid concentrations at 503 ^{o}C. For each of the AVR concentrations, no significant difference in coke yield was observed. The regression parameters were estimated using the LINEST function in Microsoft Excel and the Null hypothesis H_0: slope=zero was tested by double-sided t-test with 95% significance and the values of the P-value are presented in table 4.1 (sample calculations are shown in Appendix B). This result suggests that reducing the size of agglomerate in a fluidized bed reactor down to 2 mm thickness still does not reduce the effect of mass transfer limitation in the liquid within the agglomerate. These results also show that any effect due to varying the heating rate at the center of the agglomerate, due to change in thickness, was not significant on the ultimate coke yield at long reaction time. The thicker agglomerates did react more slowly, due to the reduced rate of heating within the material, but the ultimate yield of coke was insensitive to this change.

Table 4.1: Significance testing P-values for the effect of thickness on coke yield data

Data Set	P-Value	Remarks
8% AVR	0.2039	>0.05, no significance
10% AVR	0.9540	>0.05, no significance
12.5% AVR	0.1202	>0.05, no significance

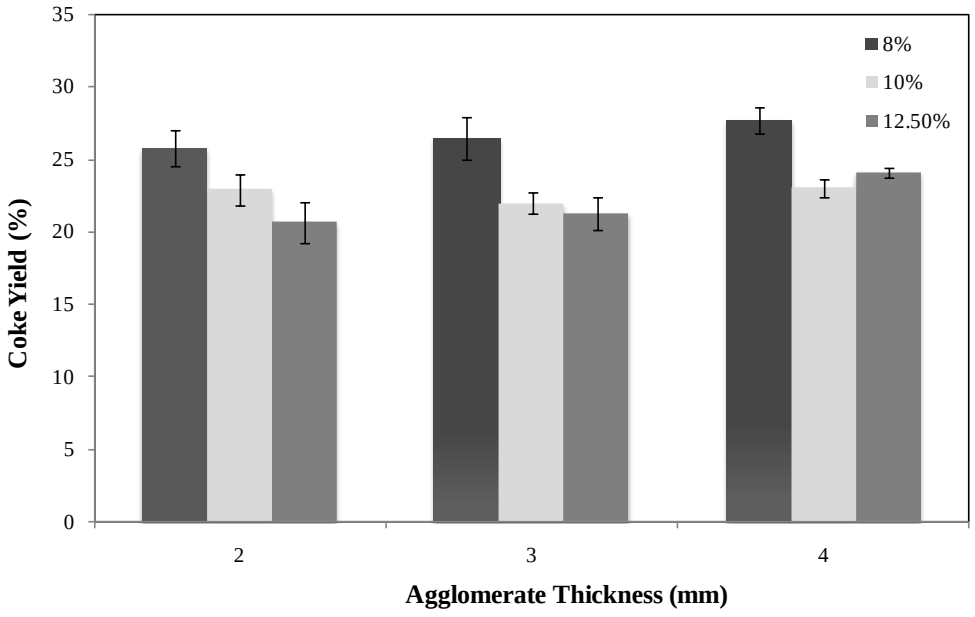

Figure 4.5: Effect of agglomerate thickness on ultimate coke yield in agglomerates of coke and Athabasca Vacuum Residue at 503 ^{o}C. The concentration of AVR in the agglomerates ranged from 8 to 12.5 wt%. Error bars represent standard error from replicate experiment

4.1.4 AVR Concentration (Liquid Saturation)

The effect of changing the AVR concentration on the ultimate coke yield for 3 mm agglomerates is showed in Figure 4.6. Every data point represents a single batch of liquid-solid mixture. The error bars in the x-axis show the standard error in determining the actual AVR concentration in the prepared agglomerates, while the error bars in the y-axis show the standard error due to the variation of the coke yield. At a given concentration of AVR, the batch-to-batch variation in both the actual AVR concentration and the corresponding coke yield can be clearly observed. This batch-to-batch variation was largest at 8 wt% of AVR and diminished as the AVR concentration was increased.

The coke yield in the case of 8 wt% bitumen agglomerates ranged from 20 % to 32%. In the case of 12.5wt% bitumen concentration, the coke yield ranged from 20% to 22%. This variability was one of the reasons that AVR concentrations below 8% could not be studied by this method. The slope of the data in Figure 4.6 did not indicate the presence of a significant correlation between the coke yield and AVR concentration in the studied range. The P-value of the hypothesis testing was 0.0764>0.05, which mean the Null hypothesis that the slope equals to zero cannot be rejected. This range of AVR concentration (from 8 to 12.5 wt% AVR by weight, corresponding to 20% to 30% liquid saturation), was below the saturation concentration of the solid-liquid matrix. Consequently, the distribution of the liquid on the solid particles would be similar, meaning no significant changes in the liquid layer thickness within the solid particles and the diffusion paths due to changes in total liquid concentration. We

would expect more liquid to give more bridges between particles, rather than changing the dimensions of the bridges themselves. Consequently, the mass transfer limitation within the liquid phase in the agglomerates would be insensitive to the initial concentration of liquid. Once the vapors exited the liquid phase, the low liquid saturation would enable easy diffusion and net flow through the pore space to exit the agglomerates.

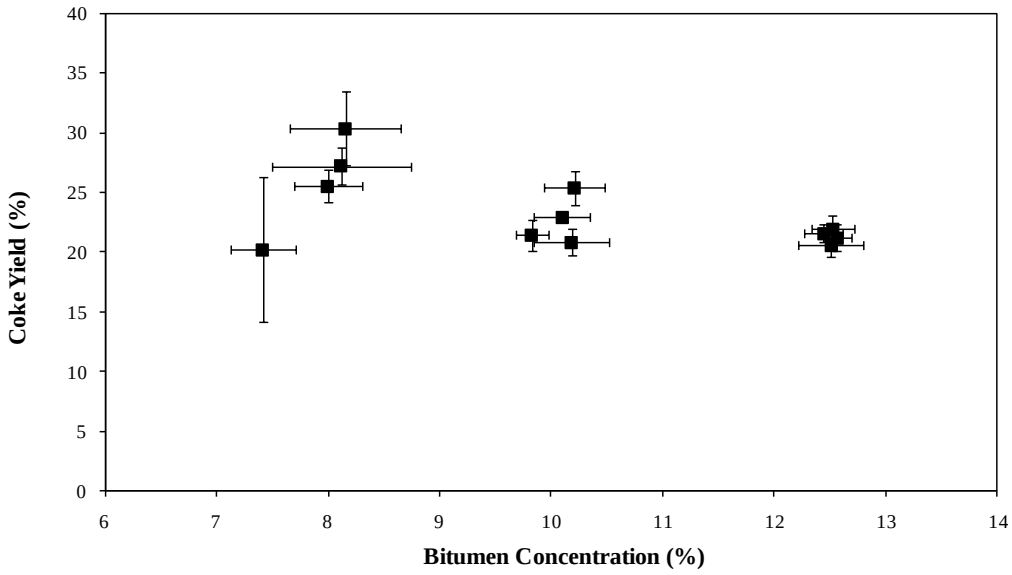

Figure 4.6: Effect of concentration of Athabasca Vacuum Residue on the yield of coke yield from 3 mm agglomerates at 503 ^{o}C. Error bars in x-axis represent the standard error in determining the actual AVR concentration in agglomerates, and in y-axis represent the standard error from replicate experiments

4.1.5 Reaction Temperature

Two different Curie-point alloys with different compositions were used in the induction furnace to provide two different reaction temperatures for agglomerates. Figure 4.7 shows the effect of bitumen concentration on the coke yield for two different reaction temperatures, 503 and 530 ^{o}C, for 3 mm agglomerates. The figure shows that changing the temperature did not have an effect on the coke yield over the tested range of liquid concentration. Similar insensitivity of the ultimate coke yield to temperature was observed by Gray et al. (2004) in coking of thin films.

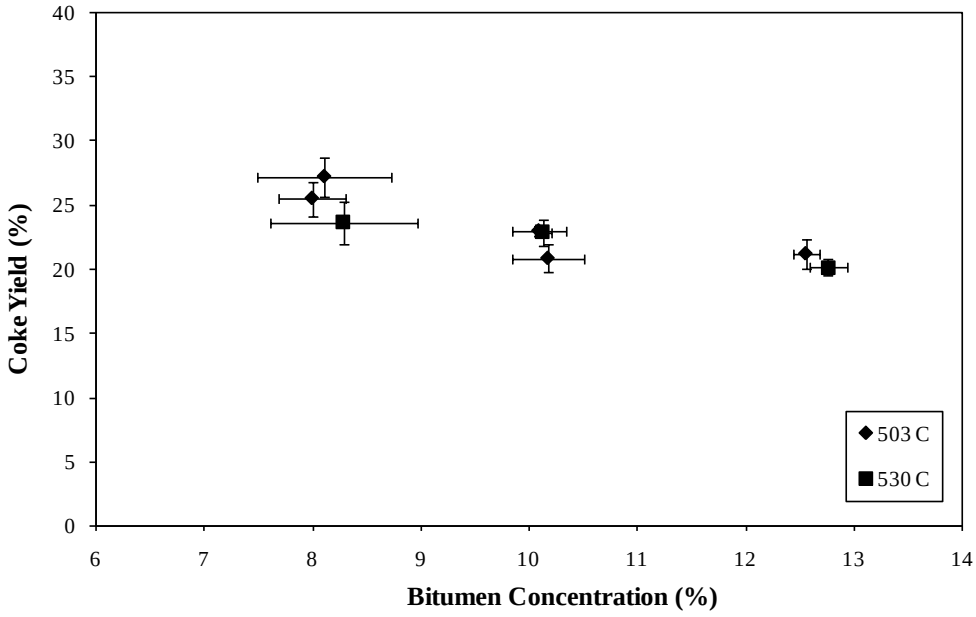

Figure 4.7: Effect on the reaction temperature on the ultimate coke yield for 3 mm thick agglomerates. Error bars in x-axis represent the standard error in determining the actual AVR concentration in agglomerates, and in y-axis represent the standard error from replicate experiments

4.1.6 Coke formation from AVR-alumina agglomerates

Before performing the fluidized bed experiments on AVR-alumina agglomerates, the AVR-alumina agglomerates were tested in the induction furnace under the same conditions as the AVR-coke agglomerates. The coke yield from the two different kinds of solids were compared to check if using different solids in agglomerates would have any effect on the ultimate coke yield.

The 3mm agglomerates were reacted at 503 ^{o}C in the induction furnace for enough time to react all the AVR. Replicate experiments were done to calculate the average coke yield and the standard error. The significance was tested using Null Hypothesis H_0: slope=zero and double sided t-test with 95% confidence. The results are shown in Figure 4.8. No significant trend in the coke yield was observed in the case of AVR-alumina agglomerates. In the cases of 10 wt% and 12.5 wt% bitumen concentrations, coke yield was almost the same in both coke and alumina agglomerates. A slight different in the coke yield was noticed in the case of 8 wt% bitumen concentration; however, the data from experiments with 8 wt% bitumen had the highest variation between batches in the case of AVR-coke agglomerates, and the lowest repeatability in experiments. Consequently, the difference was not significant between agglomerate made from coke and from alumina.

Figure 4.9 shows SEM micrographs of the AVR-alumina agglomerates, which show similar distribution of the liquid to the case of AVR-coke agglomerates (Figure 4.2), taking into account the different shapes of both solids. Uneven liquid distribution and liquid bridges also formed between the alumina

particles, leading to longer diffusion paths of the reaction products from the liquid phase to the vapor phase within the pores of the agglomerates. The PLM images of reacted AVR-alumina agglomerates showed coke formation in the liquid bridges and thick layers (Figure 4.10), similar to the coke formation in the AVR-coke agglomerates.

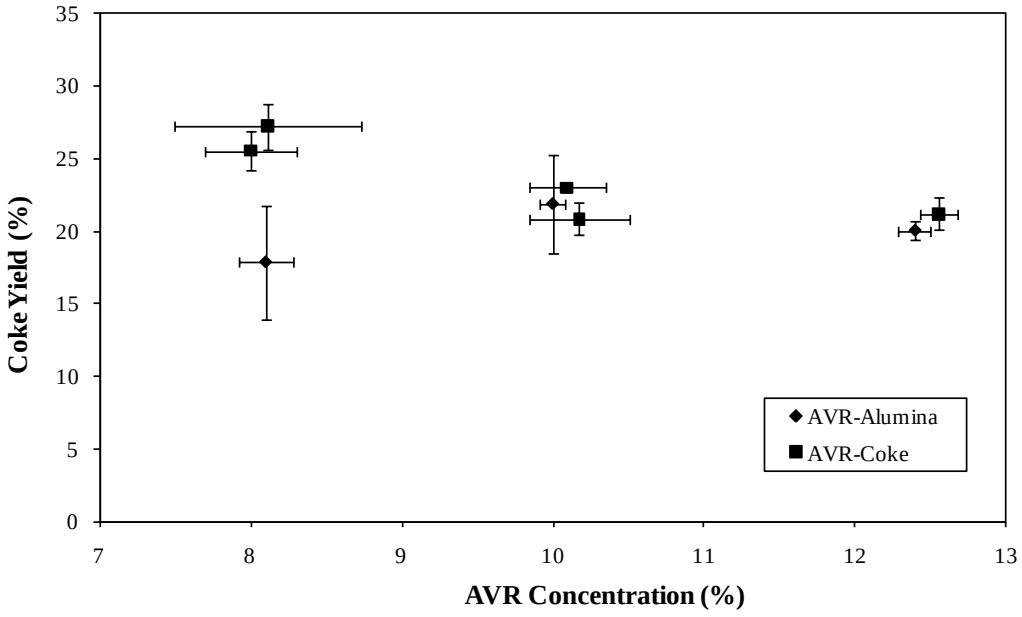

Figure 4.8: Comparison between coke yield in induction furnace in the cases of AVR-coke and AVR-alumina agglomerates at 503 ^{o}C and for 3 mm agglomerates

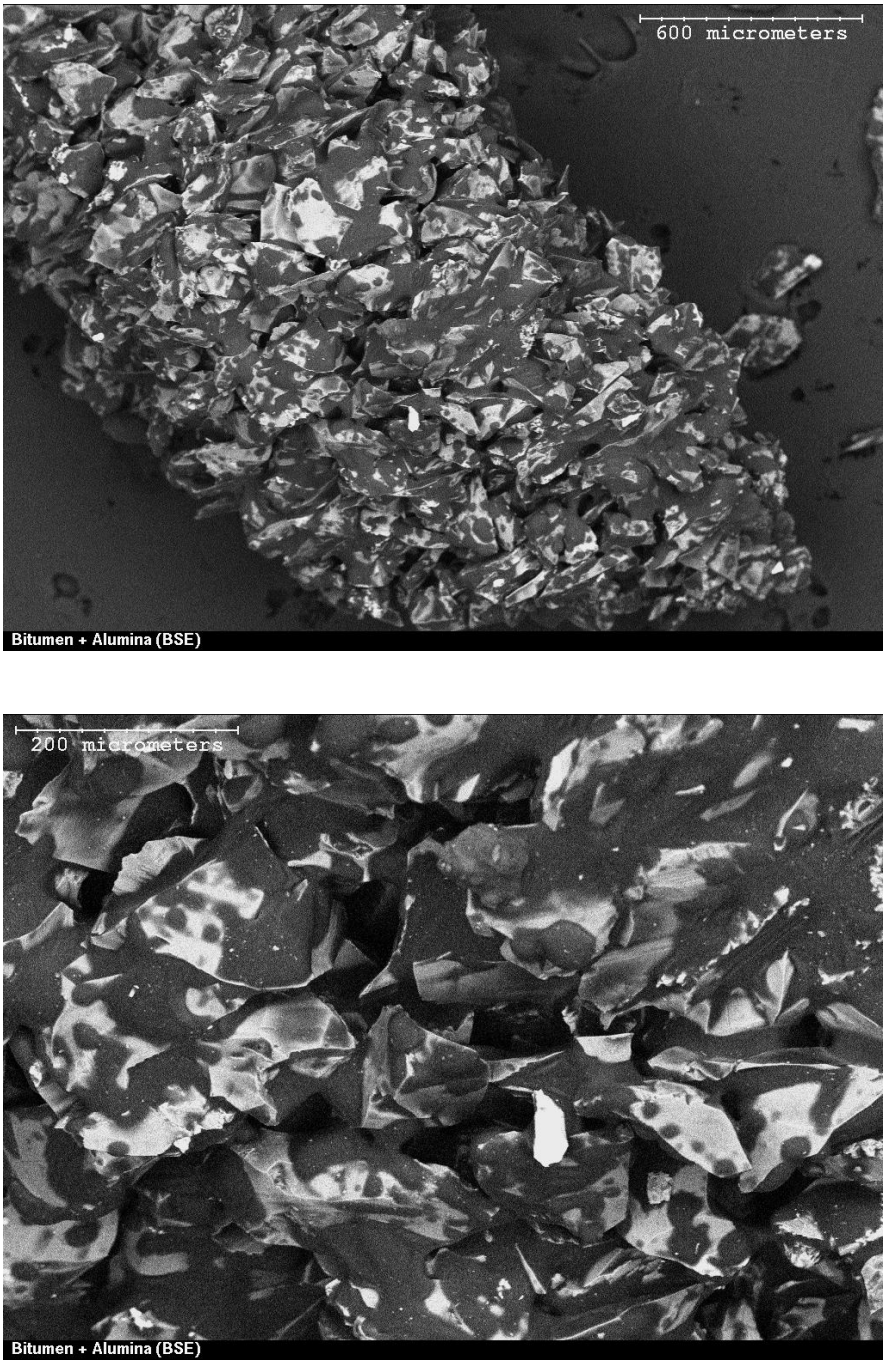

Figure 4.9: Electron microscopy images of AVR-alumina agglomerates with 12.5% AVR by weight showing the liquid distribution over the solid particles and the formation of liquid bridges between the particles

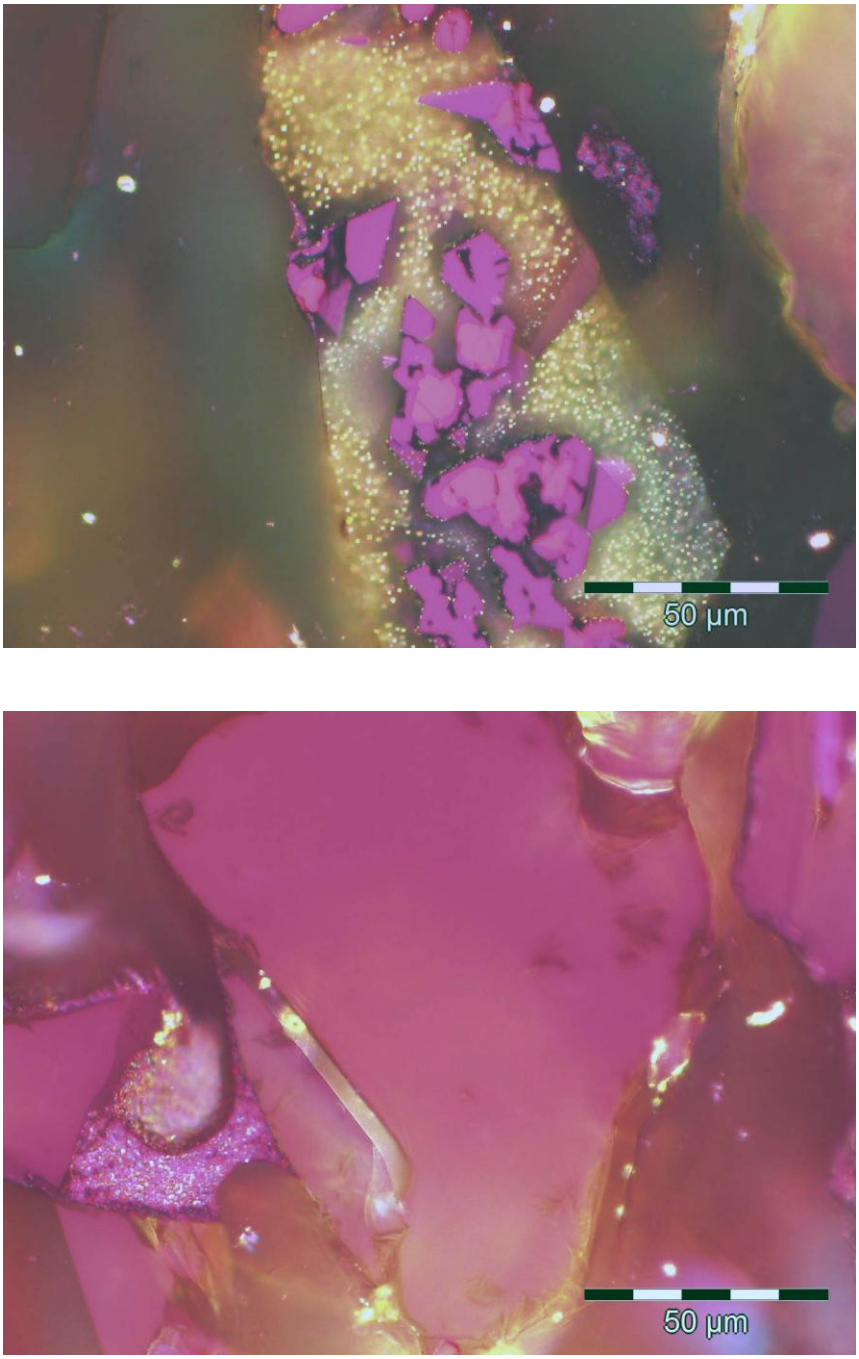

Figure 4.10: Polarized Light Microscopy of the AVR-alumina agglomerates after reaction showing the formation of coke in the thick layers and liquid bridges between alumina particles. The coke is darker than the alumina in the upper image, while the coke bridge on the lower left of the bottom image shows bright reflectance in comparison to alumina

4.2 Coke Yield in Agglomerates in Fluidized Bed

Cylindrical agglomerates of AVR and alumina were tested in the fluidized bed reactor to determine the effects of AVR concentration and agglomerate size on the ultimate coke yield. The AVR concentration tested were 8%, 10% and 12.5% by weight, equivalent to 20%, 26% and 30% of the pore volume, respectively. The agglomerate sizes were 5mm, 10mm and 15mm with 1:1 aspect ratio. The reaction temperature was 500^{o}C and the fluidization velocity was 0.3 m/sec, which gives U/U_{mf} of 40.

Average coke yield from cylindrical agglomerates was 26.4±3%. Coke yield from AVR-alumina agglomerate disks in induction furnace experiments was 22.0±3.4%. The values of coke yield in AVR-alumina agglomerates from both the induction furnace and the fluidized bed were significantly higher than the case of 20 μm film (11.7±0.3%). Figure 4.11 shows a comparison of coke yield of the two agglomerates types and thin films.

4.2.1 Effect of AVR concentration (Liquid Saturation)

Figure 4.12 shows the result of the coke yield in the agglomerates for AVR concentrations ranging from 8 wt% to 12.5 wt%. The coke yield in 5mm and 10mm agglomerates did not show any trend with changing AVR concentration. Significance testing of the slopes of the regression lines for coke yield as a function of concentration gave p-values of 0.4627 and 0.0889 for 5mm and 10mm, respectively. Although the 15mm agglomerates appeared to show a drop in the coke yield at 12.5 wt%, testing the slope of the regression line gave a P-value of 0.0737; therefore, the null hypothesis of zero slope could not be

rejected within the 95% confidence interval (sample calculations are shown in Appendix B). Table 4.2 shows the values of the p-values of the t-test of the slope of the regression line for the three agglomerate sizes. The data of 15mm agglomerates showed the widest range of coke yield, ranging from 6.4% to 42.7%, which was reflected in the large error bars. For these large agglomerates, the efficiency and capacity of the absorption system limited the number of agglomerates that could be used; only three 15mm agglomerates were allowed to be injected in each run. This limited number of agglomerates increased the variability of the results and could give significant bias. If one of the agglomerates was trapped or did not fall to the fluidized bed, then the error in the coke yield would be at least 33%. Although special care was made to ensure the complete reaction of all agglomerates, it was not feasible to ensure the complete reaction of all agglomerates after burning with oxygen to determine the coke amount. This potential bias would account for lower than expected coke yields from these large agglomerates.

Table 4.2: P-values from significance testing of the regression lines slopes of coke yield vs. the AVR concentration for 5mm, 10mm and 15mm agglomerates.

Data Set	P-Value	Remark
5mm agglomerates	0.4627	>0.05, Slope not significant
10mm agglomerates	0.0889	>0.05, Slope not significant
15mm agglomerates	0.0737	>0.05, Slope not significant

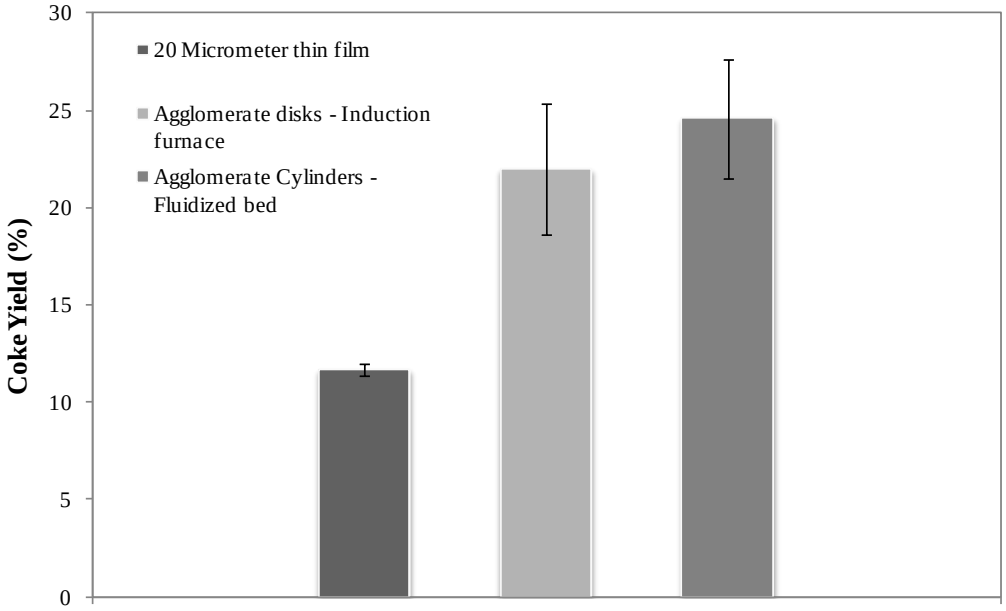

Figure 4.11: Average coke yield in 20 µm AVR films, AVR-alumina agglomerates disks and AVR-alumina cylinders at 500^{o}C. The error bars represents the standard errors from replicate experiments

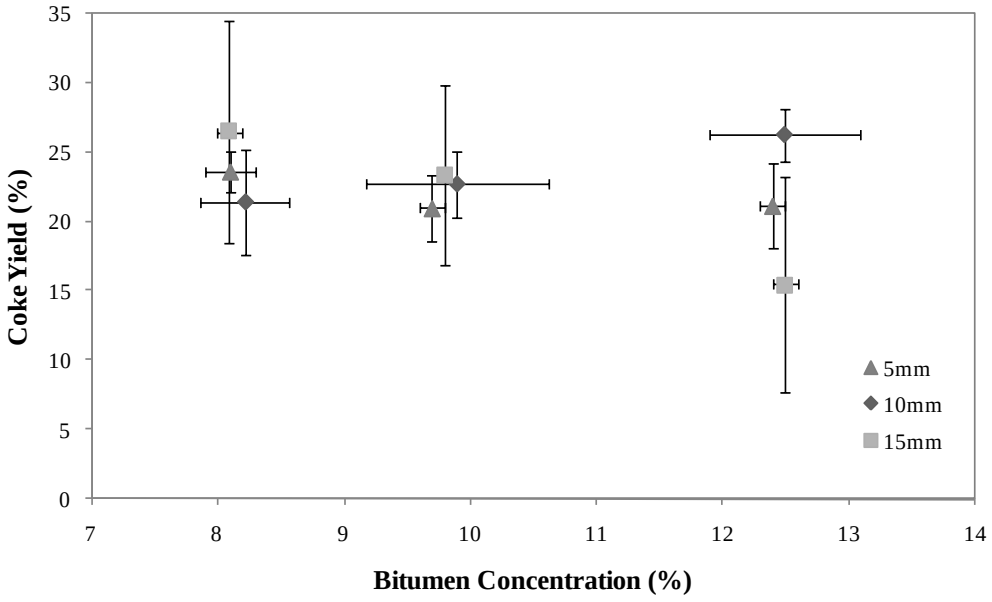

Figure 4.12: Effect of concentration of Athabasca Vacuum Residue on the yield of coke from 5 mm, 10 mm and 15 mm agglomerates of AVR and alumina at 500 ^{o}C in the fluidized bed reactor. Error bars in x-axis represent the standard error in determining the actual AVR concentration in agglomerates, and in y-axis represent the standard error from replicate experiments

4.2.2 Effect of Agglomerate Size

The effect of the agglomerate size on coke yield is shown in figure 4.13. The data shows that there was no significant change in the average coke yield with changing the agglomerate sizes at all AVR concentrations (ANOVA test worksheet is shown in Appendix B). Similar to the observation in the previous section, the 15 mm-12.5wt% agglomerates showed lower values than the rest of the data. The data for the 15 mm agglomerates also showed the widest error bars due to the high experimental error associated with injecting only three agglomerates to the reactor. The analysis of variance testing for the data group showed, with 95% confidence, that there was no significant difference between the mean values within the whole data range or within the 15 mm agglomerate data. The following table shows the results of the analysis of variance testing.

Table 4.3: Analysis of variance results for testing the means of the results for 15mm alumina agglomerates and whole data range for significance

Data Set	P-Value	Remarks
15 mm agglomerates	0.6040	>0.05, same mean values
Whole data range	0.9269	>0.05, same mean values

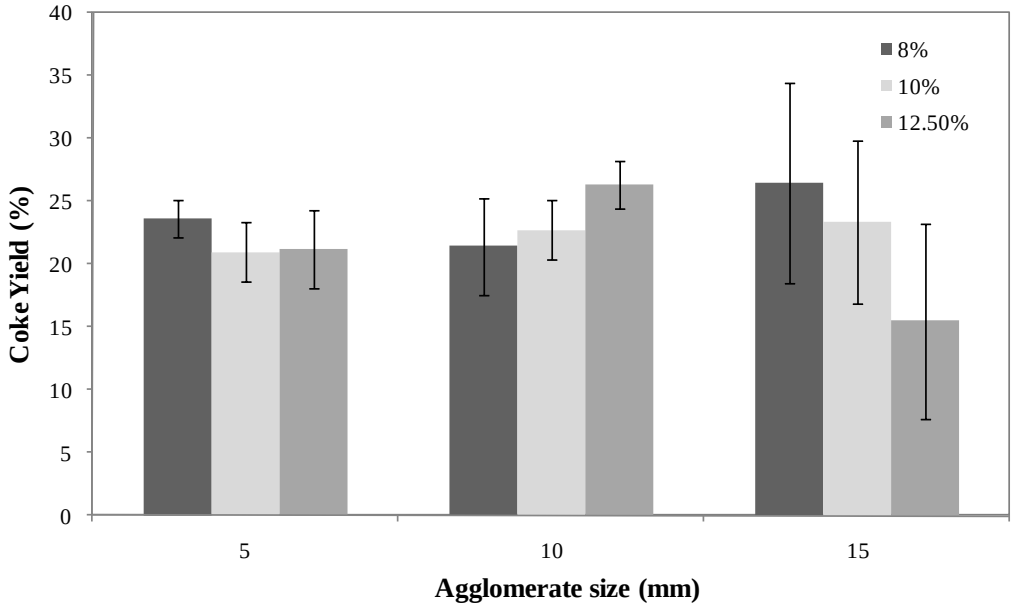

Figure 4.13: Effect of the size of alumina agglomerates on the yield of coke at 500 ^{o}C for 8%, 10% and 12.5% AVR concentrations in the fluidized bed reactor. Error bars in y-axis represent the standard error from replicate experiments

4.3 Agglomerate Survival in Fluidized Bed

AVR-alumina cylindrical agglomerates, similar to the agglomerates used in the coke yield determination in fluidized bed, were tested for survival under the reaction conditions. Agglomerates with different sizes and different liquid saturation were reacted in the fluidized for enough time for complete conversion of heavy oil. The surviving agglomerates were then separated from the fluidization silica particles to determine the survived agglomerates fractions. A 1000 μm (mesh No. 18) screen was used to separate the agglomerates and their fractions from the 120μm fluidized silica particles. The mass of the surviving agglomerates and fractions larger than 1000μm was compared to the initial agglomerates' mass and the survival was determined as a fraction from the initial mass. Three agglomerates sizes were tested: 5mm, 10mm and 15mm, over the range of bitumen concentration from 8% to 12.5% by weight at 500^{o}C and U/U_{mf} of 40. The results showed that at these conditions some disintegration and fractionation have occurred, but the average mass of the agglomerate fractions above 1000μm was in the range of 0.91 to 0.97 compared to the initial agglomerates mass (Figure 4.14). Visual inspection showed that most of the agglomerates stayed intact and survived the reacting conditions with minimum fracturing and some notable attrition to give near spherical agglomerates (Figure 4.15).

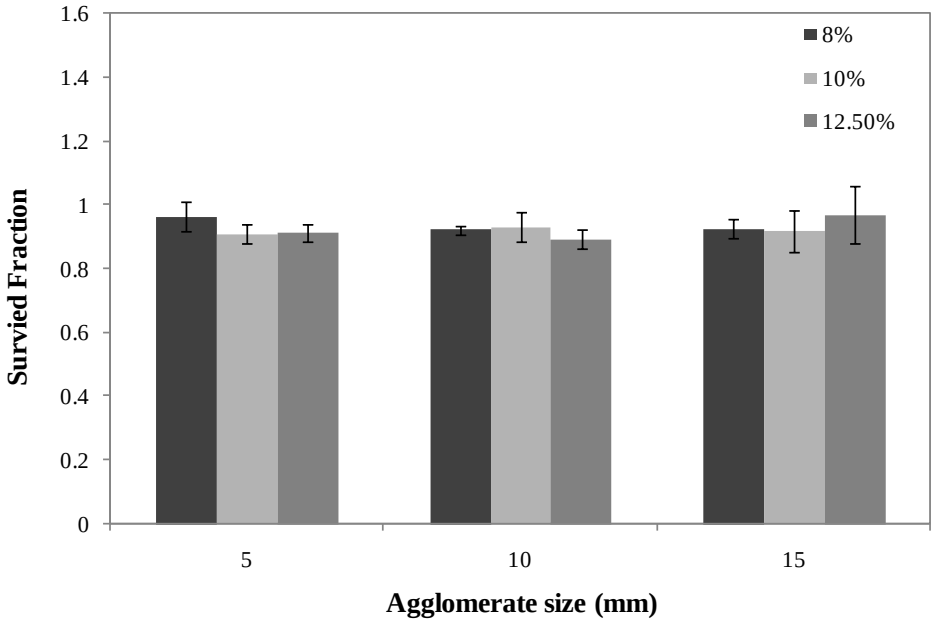

Figure 4.14: The mass ratio of survived agglomerates to initial agglomerate mass of reacting AVR-silica agglomerates at 500^{o}C and 40 U/U$_{mf}$. The AVR concentration ranged from 8% to 12.5% at agglomerate sizes of 5mm, 10mm and 15mm cylinders

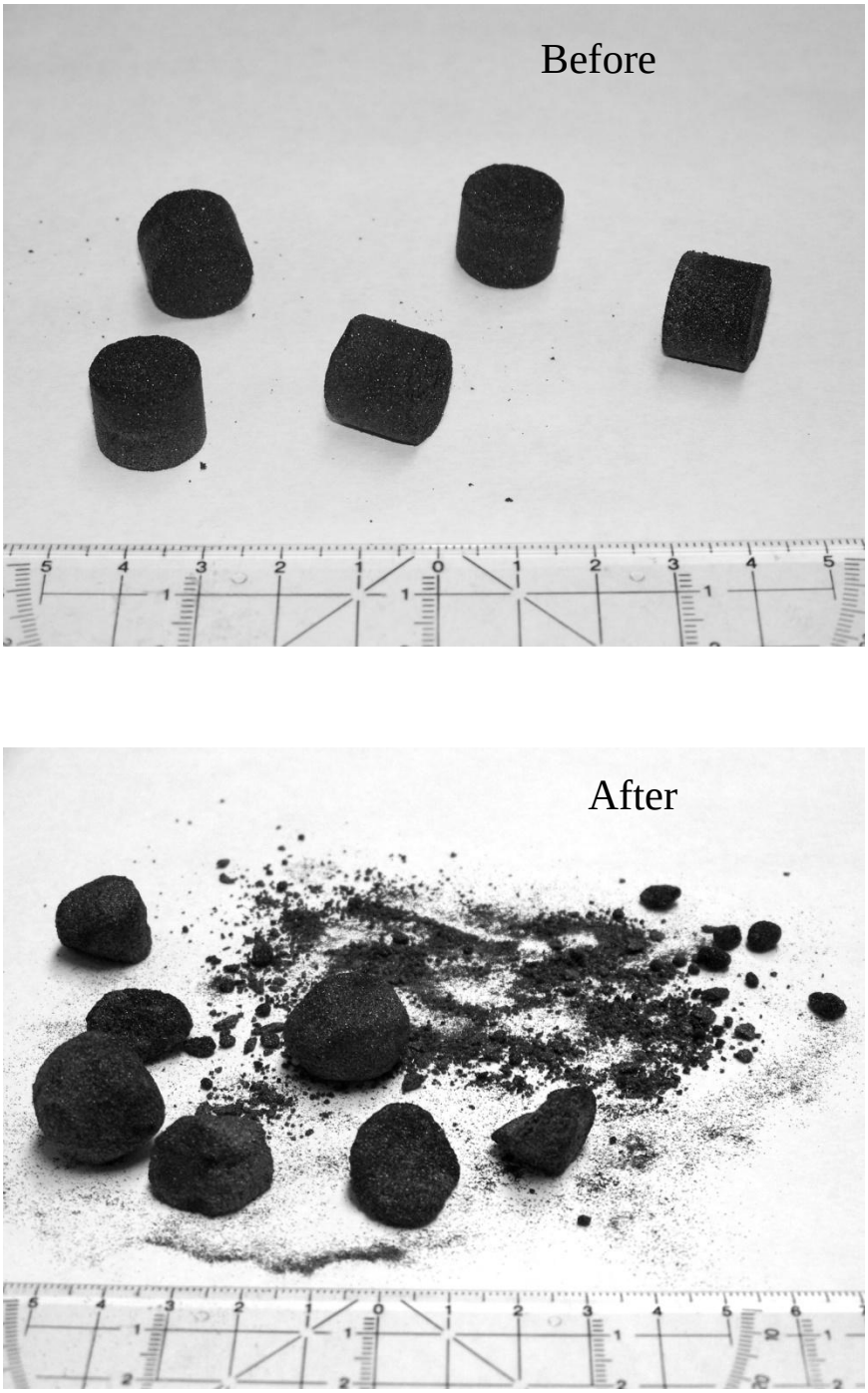

Figure 4.15: Photos of 15mm and 10% AVR concentration agglomerates before and after reaction

4.4 TGA of Agglomerates and Thin Film Coke Samples

Agglomerate coke and thin-film coke were tested by the TGA to determine and compare the amount of trapped crackable materials in each type of coke material. Agglomerate coke was prepared by reaction of AVR-alumina agglomerates of 3 mm thickness and 10% initial AVR concentration. The thin-film coke was prepared by reaction of 20 μm and 60 μm initial thickness of AVR on Curie-point strips. Each sample of the coke was loaded to the TGA apparatus (Thermo Cahn Thermax 300) and the apparatus was purged with argon at room temperature then the temperature was raised at 20^{o}C/min until it reached 500^{o}C. The sample was then heated at 500^{o}C for 1 hour. After the reaction time was ended, the gas flow was then switched to oxygen to burn the carbonaceous materials for an additional 1 hour to determine the amount of mineral solids in the initial sample weight. In the agglomerate coke the mineral solids were the alumina in the initial agglomerate. In the case of coke from thin film experiments, the mineral solids were metal fragments from scraping the Curie-point strips to remove the coke from the strip.

Figure 4-16 to 4-18 show the TGA data for the different kinds of coke. The weight loss due to of devolatilization of coke materials was calculated as the decrease of the sample weight starting at 450^{o}C till the end of the 500^{o}C reaction period. The weight at the end of the run was the weight of the initial mineral solids. The weight loss in the sample during the reaction period was then presented as a per cent of the initial sample weight, excluding the weight of mineral solids (Figure 4.19). The initial rate of devolatilization was calculated as

the slope of the weight decrease during the first stage of the reaction period under an argon atmosphere and was normalized by dividing by the initial amount of coke in the sample. Calculations of initial mass loss and initial rate of devolatiliztion are presented in Appendix C

The coke from the 20 μm film of vacuum residue showed the lowest per cent loss in weight, at 4.3%, while the per cent weight loss in the cases of 60 μm film coke and agglomerate coke were close to each other at 9.4% and 10.1%, respectively (Figure 4.19). The 20 μm film coke also gave the lowest initial rate of devolatilization compared to 60 μm film coke and agglomerate coke. The initial rate of devolatilization for the 20 μm film coke was 0.004 mg/min/mg coke, compared to 0.014 mg/min/mg coke for the 60 μm film coke and 0.030 mg/min/mg coke for the agglomerate coke (Figure 4.20).

The low per cent loss in the sample weight and low initial rate of devolatilization for the 20 μm film coke, in comparison to the two other coke samples, was consistent with the role of mass transfer limitations in the reacting film. The decreased tendency to trap volatile products of reaction within the 20 □m film, in comparison to the thicker film and the agglomerate, was consistent with the role of longer diffusion paths in trapping coke.

The agglomerates coke showed higher initial rate of devolatilization followed by the 60 μm film coke then the 20 μm film coke. These results show the higher tendency of trapping to the volatile materials in the thick liquid films and liquid bridges in the case of agglomerate coke. Lower thicknesses of the

reaction liquid films lead to lower diffusion paths and lower tendency of trapping of volatile materials (Figure 4.20).

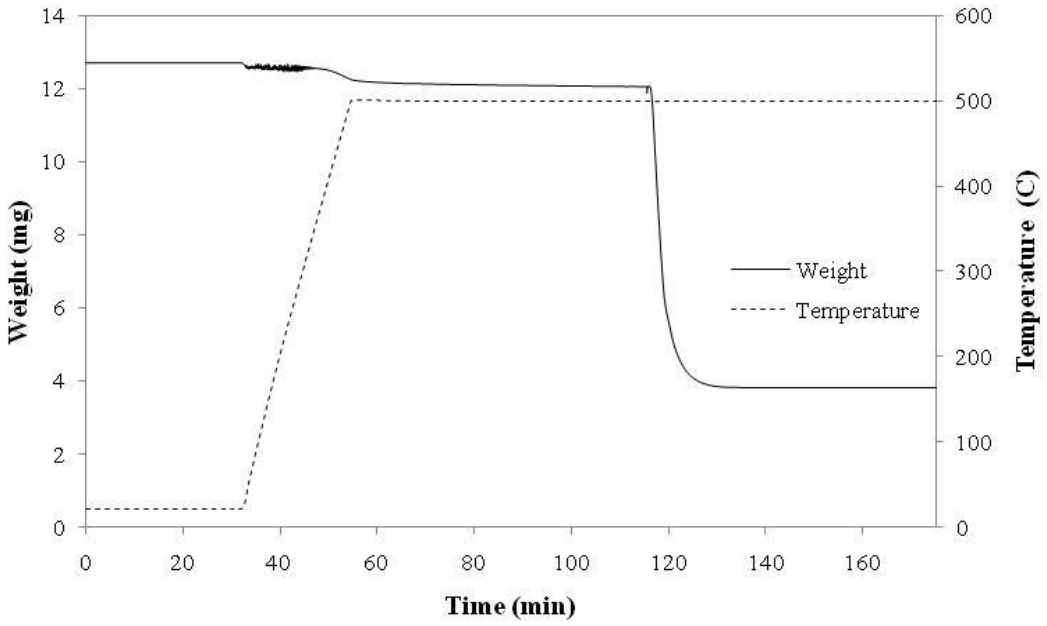

Figure 4.16: TGA results for the 20 µm film coke showing the decrease of the sample weight and the temperature data with time

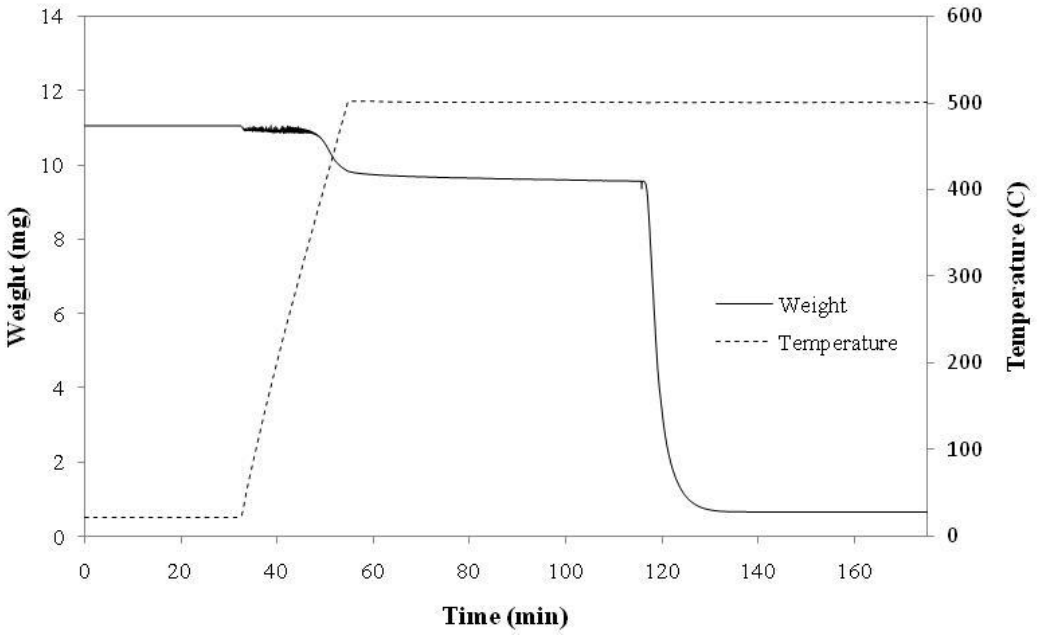

Figure 4.17: TGA results for the 60 µm film coke showing the decrease of the sample weight and the temperature data with time

.

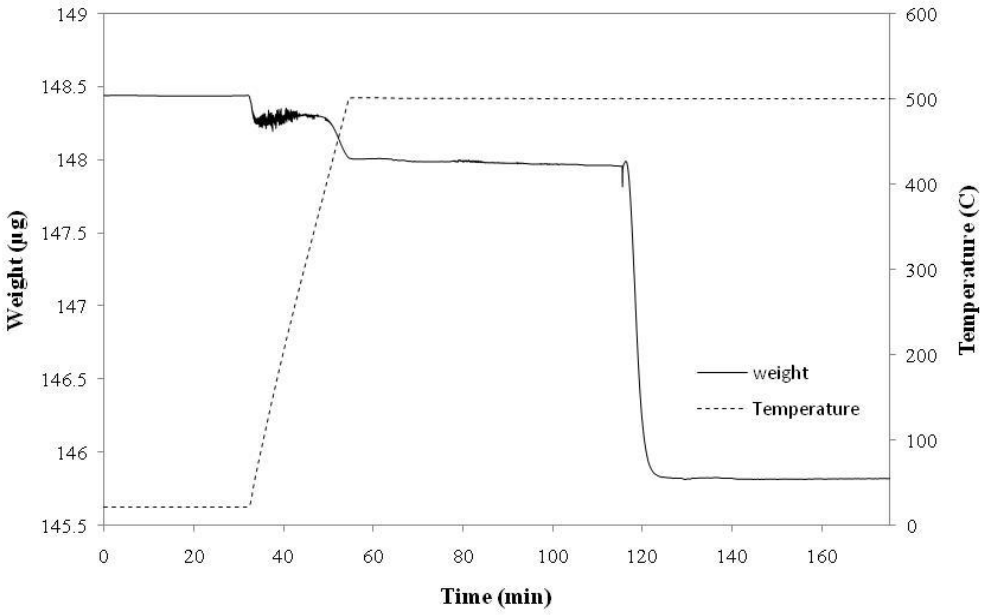

Figure 4.18: TGA results for the agglomerate coke showing the decrease of the sample weight and the temperature data with time

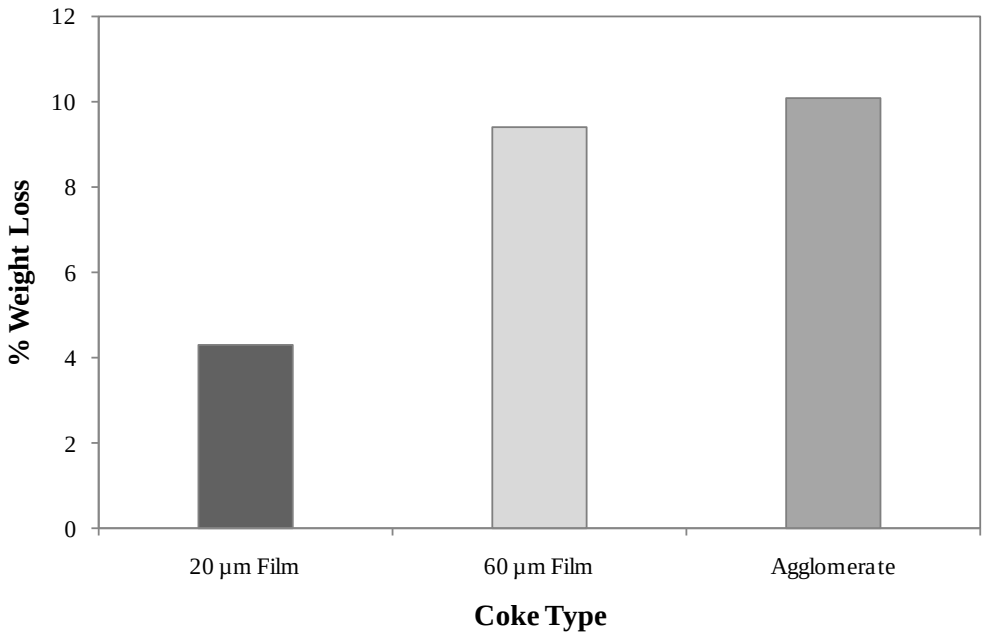

Figure 4.19: Per cent weight loss during the reaction period in the TGA for the three different types of coke

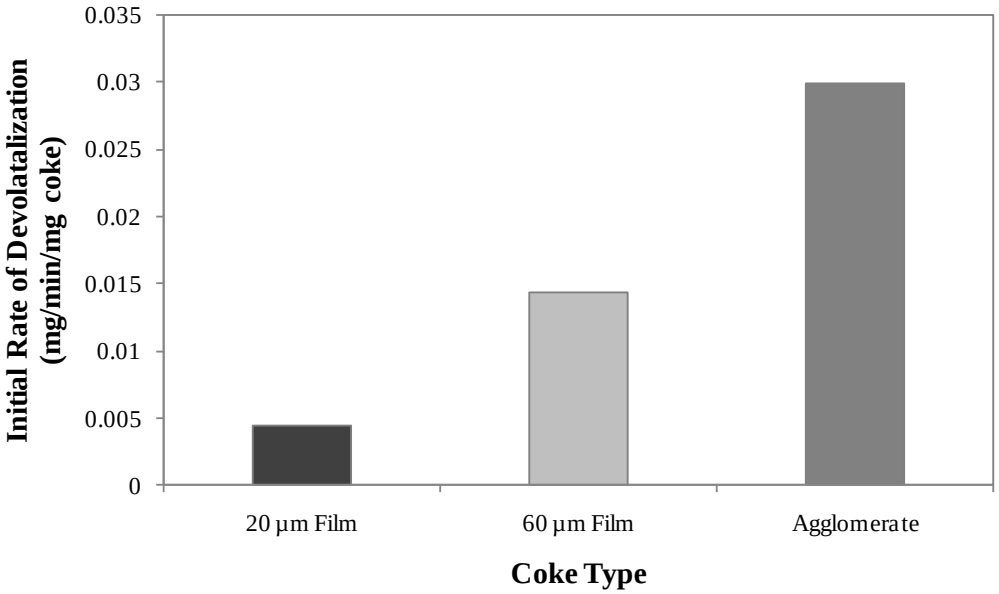

Figure 4.20: Normalized initial rate of devolatilization in the TGA for the three different types of coke

4.5 Temperature Profiles and Heat Transfer Model[2]

Unlike the reactions of thin films on Curie-point strips, the temperature within a heated agglomerate would increase with time by conduction from the heated strips to the interior of the agglomerate. The temperature profile within the reacting agglomerates was measured in the induction furnace by inserting three thermocouples as described in section 3.3.3 and in Figure 3.5. These agglomerates were then reacted according to the standard procedure. Figure 4.21 shows the temperature of the Curie point strips and the corresponding temperature at the centre of the agglomerate during heating by the induction coil. The heating rate was calculated as the slope of the linear portion of the time-temperature response. The heating rate within the agglomerate varied from 80 K/s at the Curie-point strip to 15 K/s at the center of the agglomerate.

[2] This section was published in Ali et al. Can J Chem Eng, 2010, v 88, issue 1, 48-54

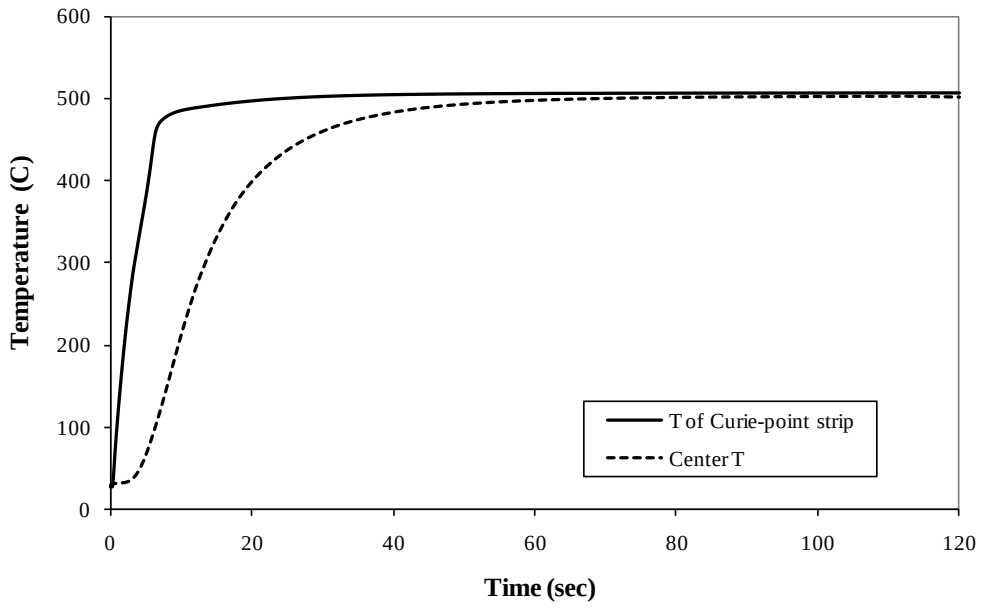

Figure 4.21: Temperatures of the Curie-point strip and at the centre of the agglomerate during heating at 503 ^{o}C. The total agglomerate thickness was 4 mm, with a thermocouple placed in the centre as illustrated in Figure 3.5

4.5.1 Heat Transfer Model

In order to model the temperature profile, a transient heat transfer model was used to describe the change of the temperature with the time and location within the agglomerates. The amount of AVR in the agglomerates was well below the saturation limit (liquid saturation was in the range of 40 to 50% AVR by weight).

The following assumptions were used in the proposed model:

- The AVR reacted rapidly to give shrinkage in volume and much higher viscosity, therefore, the AVR-solid mixture was approximated as a porous solid phase with a single effective thermal diffusivity (α_{eff}).
- The porosity of the porous solid assumed to be constant, due to low liquid loading of agglomerates
- Heats of reaction and vaporization are negligible
- The fluid phase was assumed to be nitrogen gas at the reaction conditions.
- The heat flux ($\partial T/\partial x$) at the center of the agglomerate equals to zero
- Heat transfer from the heating Curie-point strips to agglomerates is only by conduction.

The relation between the temperature T at any time (t) and distance from agglomerate centre line (x) is given as follows:

$$\frac{\partial T}{\partial t} - \alpha_{eff} \frac{\partial^2 T}{\partial x^2} = 0 \qquad (4.3)$$

The following initial and boundary conditions were used:

$$T(x,0) = T_0 \qquad (4.4)$$

$$\frac{\partial T}{\partial x}(0,t) = 0 \qquad (4.5)$$

$$T(L,t) = T_\infty(t) \qquad (4.6)$$

Where T_0 is the initial agglomerate temperature before heating, $\partial T/\partial x$ is the heat flux at the centre of the agglomerate and $T(L,t)$ is the measured temperature of the Curie-point strip as a function of time.

The effective thermal diffusivity of the agglomerate, α_{eff}, was used as the only adjustable parameter to fit the model to the experimental data. The model was solved by MATLAB (Appendix D) for a series of experiments, each with a measured boundary condition (strip temperature). The sum of squared residuals (SSR) was calculated and minimized to obtain the best value of α_{eff} to fit the data. The MATLAB code for solving the model is presented in appendix B.

$$SSR = \sum \left[T_{\exp} - T_{pred} \right]^2 \qquad (4.7)$$

The best fit value of the effective thermal diffusivity was 0.20 x 10^{-6} m^2/s with a minimum value of the sum of squared residuals (SSR) of 62660. For the case of heat transfer in a porous solid, Bejan and Kraus (2003) and Rohsenow et al. (1998) recommended the following relations to predict the effective thermal diffusivity of porous media:

$$\alpha_{eff} = \frac{\alpha_m}{\sigma} \qquad (4.8)$$

$$\alpha_m = \frac{k_m}{(\rho C_P)_{fluid}} \qquad (4.9)$$

$$k_m = \varepsilon k_{fluid} + (1-\varepsilon) k_{solid} \qquad (4.10)$$

$$\sigma = \varepsilon + (1-\varepsilon)\frac{(\rho C)_{solid}}{(\rho C_P)_{fluid}} \qquad (4.11)$$

Where α_m is the mean thermal diffusivity, k_m, k_{fluid} and k_{solid} are the mean, fluid phase and solid phase thermal conductivities respectively, $(\rho C_p)_{fluid}$ and $(\rho C_p)_{solid}$ are the heat capacities of the fluid and solid phases respectively, σ is the heat capacity ratio, and ε is the porosity of the porous solid. Using the range of physical properties of fluid coke materials measured by Michaelian et al. (2002) and agglomerate porosity of 35% in equations (4.8)-(4.11), the predicted range of the effective thermal diffusivity for the agglomerates was 0.18 x 10^{-6} m^2/s to 0.34 x 10^{-6} m^2/s.

Figures 4.22 to 4.24 show the experimental and model data of the temperature profile within the agglomerates of different thicknesses and initial AVR concentration. The model showed good agreement with the experimental data for the different agglomerate sizes and initial AVR concentrations. Figures 4.22 and 4.23 show that increasing the agglomerate thickness affected the rate of heating of the agglomerate, which was expected, but this change in the heating rate did not affect the ultimate coke yield as shown previously in the results of the effect of agglomerates thickness on coke yield. From the experimental results and

the model, the heating rates ranged from 80 K/s at the contact with the strips to 15 K/s at the centerline of the agglomerate.

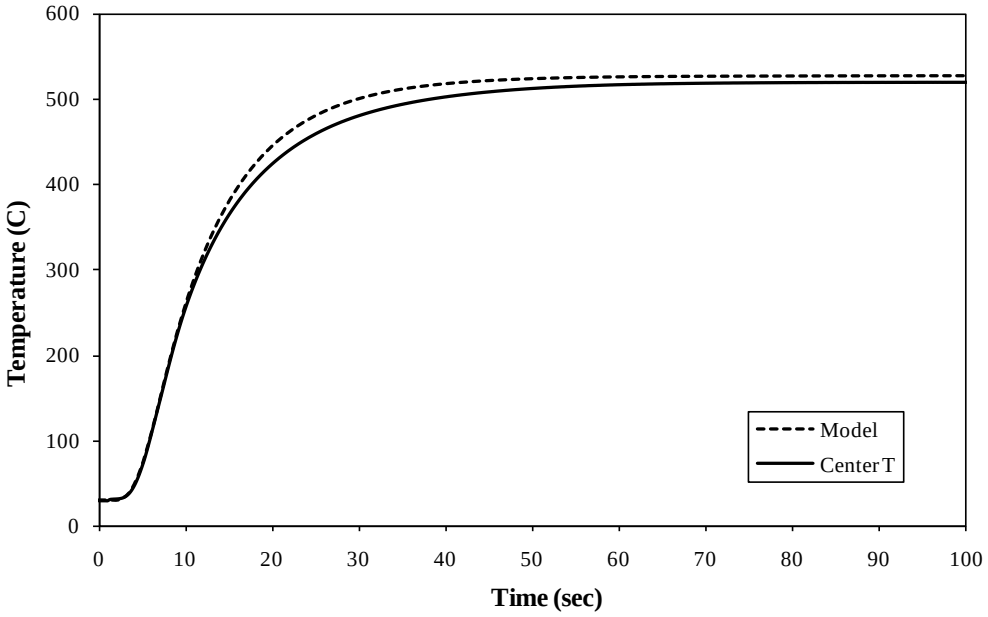

Figure 4.22: Experimental and model predicted temperature profile within an agglomerate of total thickness of 4 mm with thermocouple placed in the center and bitumen concentration of 10%

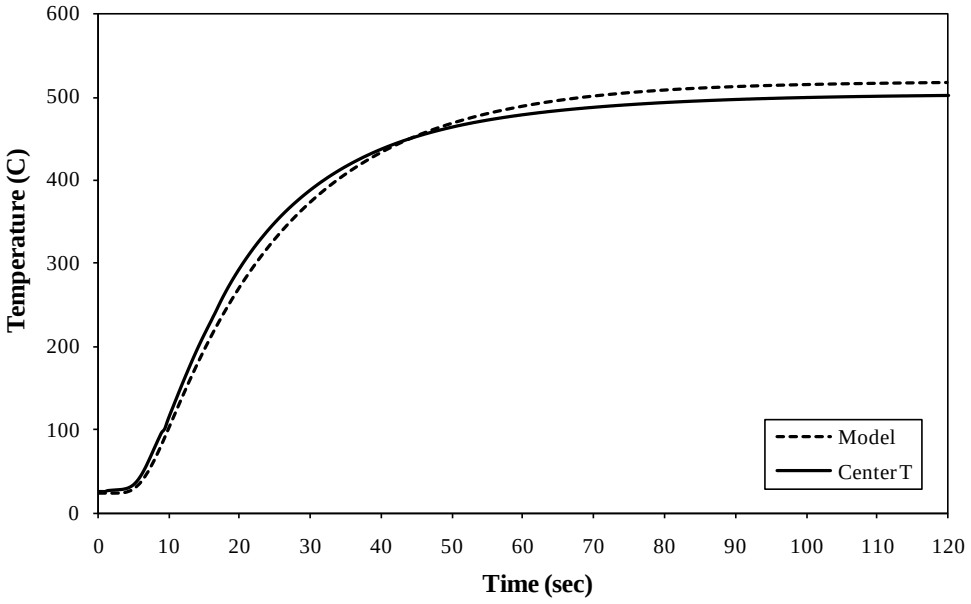

Figure 4.23: Experimental and model predicted temperature profile within an agglomerate of total thickness of 6 mm with thermocouple placed in the center and bitumen concentration of 10%

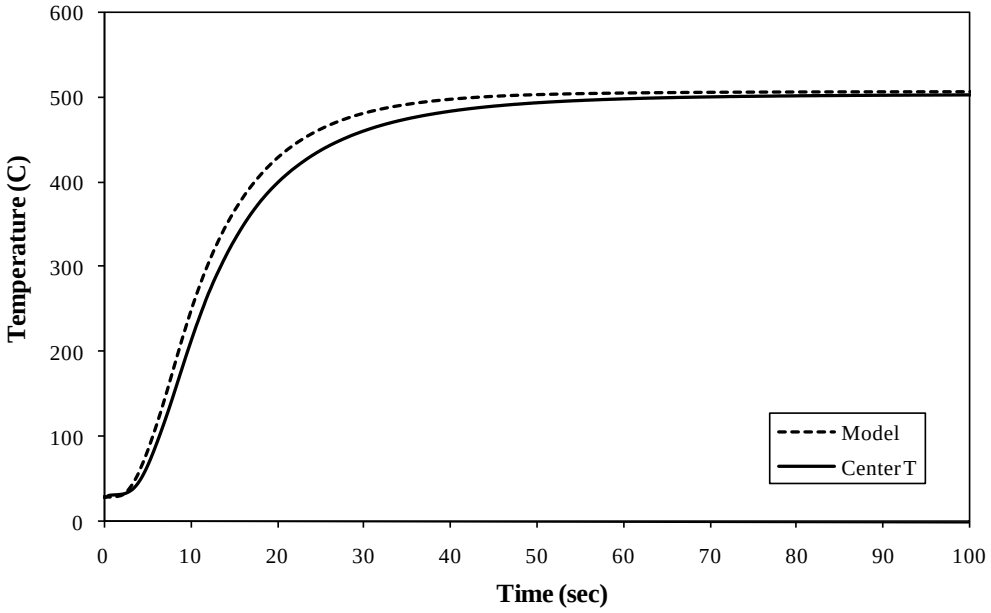

Figure 4.24: Experimental and model predicted temperature profile within an agglomerate of total thickness of 4 mm with thermocouple placed in the center and bitumen concentration of 12.5%

4.5.2 Role of Heating Rate

In pyrolysis of solids, such as coal and biomass, the yield of char is commonly observed to vary with heating rate (Wen and Lee, 1979). In order to check the role of heating rate in the coking reactions and its effect on the yield of coke from vacuum residues in agglomerates, coking of different vacuum residue materials was carried out on Curie point strips at different heating rates. Thin films of Athabasca vacuum residue (lab-prepared sample), Maya, and Khafji were reacted at low and high heating rates of 14.8 to 148 K/s. The heating rate was reduced by detuning the induction coil to give less efficient coupling of the strips with the induction field.

The data of Table 4.4 and Figure 4.25 show that the yield of coke from Athabasca vacuum residue #2 was insensitive to the heating rate. Similarly, the yield of coke form Maya and Khafji vacuum residues were insensitive to heating rates in this range. The same trends were observed for thinner films of 20 mm thickness.

The heating rate in reacting agglomerates varied from 80 K/s to 15 K/s, which lies in the same range that was used to test the heating rate role in thin films. Given the lack of dependence of the final coke yield on heating rate in film samples, we conclude that the rate of heating of vacuum residue within the agglomerates was not a significant factor. Heating rate would have a dramatic effect on the initial rates of cracking and coking, but the present comparison is on the final coke yield when the reaction is essentially complete.

Table 4.4: Coke yields from 80 µm films of vacuum residues at 503 °C

Feed	RF Setting %	Heating Rate, K/s	Coke Yield %
Athabasca VR#2	38.1	14.8	18.20
Athabasca VR#2	-5.0	148	18.80
Maya	38.1	14.8	22.85*
Maya	3.0	80	21.30
Maya	-5.0	148	21.55*
Khafji	38.1	14.8	18.00*
Khafji	3.0	80	16.50*
Khafji	-5.0	148	17.75*

* indicates mean value of two replicate experiments

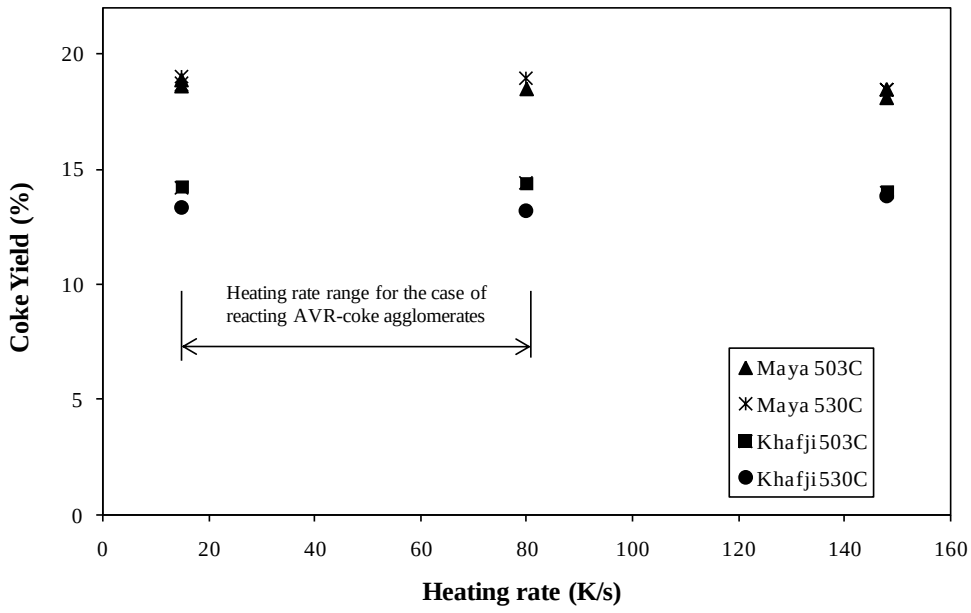

Figure 4.25: Effect of heating rate on the ultimate coke yield in reacting 20 µm thin films of Maya and Khafji feeds at 503 and 530^{o} C

5 DISCUSSION

5.1 Coke yield in agglomerates

Comparing the coke yield in AVR-coke agglomerates to coke yield from 20 μm thin films showed that the agglomerates gave higher coke yield, both from induction furnace and fluidized bed reactors, relative to the thin films for the same feed materials and same reaction temperature. At 503^{o}C, the coke yield from agglomerates from the induction furnace experiments was 23.3±1.7%, while it was 11.7±0.3% for the thin films (Figure 4.1).

The increase of coke yield in agglomerates supports the role of mass transfer in controlling the coke yield over this range of values. In agglomerates, the liquid within the solid-liquid matrix tends to form thicker layers over the solid particles due to uneven liquid distribution and the liquid bridges between particles (Figures 4.2 and 4.9). The thicker liquid films in agglomerates provide longer diffusion paths for the reaction products and higher tendency for trapping the products within the reacting liquid film and undergoing undesired condensation and polymerization reactions. The same role of mass transfer was observed in the work of Gray et al. (2001), where the coke yield was found to increase with increasing the initial liquid film of reacting heavy oils. The PLM images of cross sections of reacted AVR-coke and AVR-alumina agglomerates (Figures 4.3 and 4.10) showed that a significant amount of coke was formed in thick liquid layers and liquid bridges between the solid particles in agglomerates. A similar observation was noted in the case of coke formation in the agglomerates of the

industrial fluid coker (Figure 4.4). These agglomerates provide significant porosity for the escape of the cracked products once they escape from the liquid phase. The key distance for mass transfer is not the dimension of the agglomerates but rather the distance to diffuse out of a liquid film that is confined between solids particles.

The data for coke yield showed that decreasing the agglomerate size, down to 2 mm in the case of agglomerate disks in the induction furnace experiments and down to 5 mm for the agglomerates cylinders in the fluidized bed reactor experiments, had no significant effect on the coke yield (Figures 4.5 and 4.13). The reduction in the size of the agglomerates did not affect the thickness of reacting liquid layers on the solid particles and in liquid bridges between particles over the studied range of liquid saturation.

The concentration or saturation of liquid also did not have any effect on coke yield. In the studied AVR concentration range, from 8% to 12.5% (relative to 20% to 30% liquid saturation), the AVR concentration was below the liquid saturation concentration in the agglomerates. Below the liquid saturation, the distribution of liquid within the liquid-solid matrix was not significantly different at different liquid contents, which led to similar diffusion paths within the liquid phase and similar mass transfer limitations in that range of liquid concentration, and hence no significant effect of the AVR concentration on the coke yield was observed for both the induction furnace and fluidized bed agglomerates (Figure 4.6 and 4.12). The mass transfer resistance was only present in the liquid layers and bridges in the agglomerates. Once the reaction products reached the void

space in the agglomerates they diffused easily to the outer surface of the agglomerates with relatively no resistance to flow within the gas phase. Higher liquid saturations would be expected to significantly increase the diffusion path length to a significant fraction of the agglomerate dimension, but such high liquid saturations were not attempted in this study due to the poor mechanical properties of the agglomerates. Furthermore, in this regime the formation of vapor bubbles would have an impact both on transport of products (Gray et al., 2001) and probably on the stability and structure of the agglomerates.

Changing the reaction temperature from 503^{o}C to 530^{o}C in the induction furnace experiments did not have significant effect on the coke yield from agglomerates (Figure 4.7). Similar insensitivity of ultimate coke yield to reaction temperature was observed by Gray et al. (2004) in coking thin films. This observation indicates that although the rate of cracking and devolatilization of the products depends on temperature, the ultimate coke yield at long reaction times tends to be insensitive to temperature.

No effect of the type of solids used in making the AVR-solid agglomerates was noted when using coke and alumina (Figure 4.8) except for a slight difference in the case of 8% agglomerates. The difference in the 8% coke yield between the two different solids agglomerates was likely not significant due to the variability in the 8% agglomerates from batch to batch (see Figure 4.6) within the same solid used, due to the low AVR concentration and higher errors in actual AVR and coke yield determination. Changing the solids had no effect on the coke yield due to the similar distribution of liquid over the solid particles and in liquid bridges

and the incomplete wettability in both cases. The data in Figures 4.2 and 4.9 show that the distribution of liquid over the coke and alumina particles was similar, forming uneven liquid layers over the particles and liquid bridges between the solid particles in both cases.

5.2 Coke Yield and Agglomerate Survival Under Fluidized Bed Conditions

5.2.1 Coke Yield Under Fluidized Bed Conditions

The average coke yield of AVR-alumina agglomerates was significantly higher than the coke yield from 20 μm thin films, for both agglomerate disks and agglomerates cylinders (Figure 4.11). The average coke yield in the AVR-alumina agglomerates cylinders was 24.6±3.0%, while for the AVR-alumina agglomerates disks was 22.0±3.4 and for the 20 μm thin films was 11.7±3%.

Similar to the case of AVR-coke agglomerates, the increase in coke yield in alumina agglomerates compared to thin films supports the role of mass transfer limitation and is due to the formation of thick layers over the solid particles and thick liquid bridges between the solids (Figure 4.9), which result in longer diffusion paths, higher mass transfer resistance and higher tendency of trapping of the reaction products in the reaction liquid films

5.2.2 Survival of Agglomerates Under Fluidized Bed Condition

At the reaction conditions in the fluidized bed, 500^{o}C and U/U_{mf} of 40, the mass of agglomerates and the fraction of agglomerates that survived was in the range of 0.91 to 0.97 of the initial agglomerate mass, independent of size and liquid saturation (Figure 4.14). The visual inspection of the agglomerates after reaction (Figure 4.15) showed that some fragmentation and attrition had occurred, but the majority of the agglomerates stayed intact and survived during the reaction time in the fluidized bed. The rapid change in the AVR physical properties, especially the rapid increase in the liquid viscosity, with the reaction time tended to hold the liquid solid agglomerate together and suppress the agglomerate disintegration. The low value of U/U_{mf} was not sufficient to produce enough force in the fluidized bed to break up the agglomerates or cause significant attrition.

Weber (2009) tested AVR-coke agglomerates for stability in a fluidized bed of coke particles. The lowest fluidization velocity that was tested was U/U_{mf} = 40. At this condition, the breakup of agglomerates containing 9% AVR by weight concentration was insignificant. Disintegration of the AVR-coke agglomerates was only observed at higher fluidization velocities, corresponding to 80 and 120 U/U_{mf} (Weber, 2009). At U/U_{mf}=80, Weber (2009) observed extensive fragmentation of the AVR-coke agglomerates. Agglomerates with 9 wt%, 13 wt% and 16.7 wt% AVR showed a maximum in the mass of fragments of up to 2.2 times the initial agglomerate mass at 40 s. The increase in mass was attributed to adhesion of bed particles to the wet exterior of the agglomerates. Increasing the reaction time decreased the final relative mass of fragments to the range from 0.5

to 1.3 relative to the initial agglomerate mass, depending on initial liquid content. It should be noted that the experiments of Weber (2009) were done at much lower fluidization times compared to the fluidization times in this study, which were from 20 to 30 min. to ensure complete reaction of the AVR in agglomerates.

The lack of fragmentation of the AVR-alumina agglomerates in this study (Figure 4.14) at U/U_{mf} of 40 was qualitatively consistent with the lack of fragmentation observed by Weber (2009) for AVR-coke agglomerates at the same value of U/U_{mf}. The main difference was the lack of increase in mass of agglomerates in this study, in contrast to Weber (2009), which could be due to the long reaction times or differences in the wetting of alumina versus coke.

5.3 TGA of Agglomerates and Thin Film Coke Samples

Results from agglomerates and thin films showed that the higher thickness of liquid layers and liquid bridges in agglomerates resulted in higher coke yields compared to thin films. Thicker liquid films and liquid bridges in agglomerates result in longer diffusion paths of the reaction products, which increases the mass transfer resistance, especially with the rapid change in the AVR physical properties, specially viscosity. The longer the diffusion path and the mass transfer resistance, the higher the tendency to trap volatile products in the coke, and the higher the tendency of the reaction products to undergo undesired condensation and coke formation reactions. When cracked products are trapped in the coke, we hypothesize that the resulting material is more reactive under prolonged heating. Trapping of cracked products could occur by two mechanisms: addition reactions between the products and the coke phase, and physical trapping due to the rapid

increase in viscosity of the liquid with extent of reaction. Both mechanisms would give weight loss upon sustained heating, because the coke material would undergo prolonged cracking of side chains and saturated rings, and some physically trapped material would escape from the coke phase. Coke samples from reacted AVR-alumina agglomerates and 20 μm and 60 μm reacting films were tested in the TGA to test the hypothesis of the effect of agglomeration and increasing film thickness on trapping volatile materials.

In the TGA data for the coke in agglomerates, 20 μm films and 60 μm films, the coke from the 20 μm film showed the lowest per cent loss in weight, followed by the 60 μm film coke, then the agglomerate coke (Figure 4.19). The 20 μm film coke also showed the lowest initial rate of devolatilization compared to the two other types of coke materials (Figure 4.20). The low per cent loss in the sample weight and the low initial rate of devolatilization for the 20 μm film coke, compared to the two other coke samples, was consistent with the role of mass transfer in the diffusion of reaction products from the reacting film. The higher tendency of products to become trapped within the thicker films and agglomerates due to longer diffusion paths gave coke materials that were more reactive under sustained heating at 500^{o}C.

While the 60 μm film coke and agglomerate coke had comparable per cent loss in weight, the initial rate of devolatilization was higher in the case of agglomerate coke compared to the 60 μm film coke (Figure 4.20). The higher initial rate of devolatilization in agglomerate coke, compared to 60 μm film coke, can be explained by the uneven distribution and the incomplete wettability of the

AVR in the liquid-solid matrix in case of the agglomerates and the formation of thick liquid layers on the solids and liquid bridges between solids (Figures 4.2 and 4.9).

The coke samples were prepared at the same temperature (500^{o}C) with reaction times of 2 minutes for the 20 μm and 60 μm films and 10 minutes for agglomerates to ensure complete conversion of the AVR. These initial reaction times were relatively short compared to the TGA reaction time (1 h at 500^{o}C). The longer reaction times at the TGA allowed the coke to undergo more extensive devolatilization reactions at a low rate. All coke samples showed the highest loss in weight during the early stages of heating, which can be explained by the removal of condensed materials from the coke. The higher weight loss and initial rate of devolatilization in agglomerate coke and 60 μm film coke compared to the coke from the 20 μm film indicated that the longer diffusion paths and the greater amount of products trapped in the thicker layers produced a more reactive coke. The thin films ensured more complete evolution of the reaction products from the reaction liquid, which gave a less reactive coke material in the TGA. This less reactive coke material, with low amount of cross linked or trapped products, gave less loss of mass and less initial rate of devolatilization on extended heating at 500^{o}C.

5.4 Temperature Profiles and Heat Transfer Model and Role of Heating Rate

A transient heat transfer model was used to describe the change of the temperature with the time and location within the reacting AVR-coke agglomerates. Over the range of AVR concentrations in this study, the AVR reacted rapidly to give shrinkage in volume and much higher viscosity, therefore, the AVR-solid mixture was approximated as a porous solid phase with a single effective thermal diffusivity (α_{eff}).

The relation between the temperature T at any time (t) and distance from agglomerate centre line (x) was described by a conduction heat transfer model described in equations 4.3 to 4.6, where the effective thermal diffusivity of the agglomerate, α_{eff}, was used as the only adjustable parameter to fit the model to the experimental data. The best fit value of the effective thermal diffusivity was 0.20 x 10^{-6} m^2/s. This value of the effective thermal diffusivity for the AVR-solid agglomerates in the model was within the range of calculated thermal diffusivities of porous solids estimated using the equations from 4.8 to 4.11 given by Bejan and Kraus (2003) and Rohsenow et al. (1998) and using the physical properties data for coke materials given by Michaelian et al. (2002).

The model showed good agreement with the experimental data for the different agglomerate sizes and initial bitumen concentrations (Figures 4.22 to 4.24). Increasing the agglomerate thickness affected the rate of heating of the agglomerate in the range from 80 K/s at the contact with the heating strips to 15

K/s at the center of the agglomerate. This change in the heating rate did not affect the ultimate coke yield, as shown in the results of coke yield from the agglomerates in the induction furnace experiments.

In order to study the role of heating rate in the coking reactions and its effect on the yield of coke from vacuum residues, coking of different vacuum residue materials was carried out on Curie point strips at different heating rates of 14.8 to 148 K/s. The results shown in table 4.3 and Figure 4.25 demonstrated that the coke yields from the different heavy oils at long reaction times were insensitive to the heating rate for 20 μm and 80 μm film thicknesses.

In the case of agglomerates, the temperature measurement and heat transfer model showed that the heating rate in reacting agglomerates varied with the agglomerate thickness and within the agglomerate the heating rate varied from 80 K/s at the heating strip to 15 K/s at the center of the agglomerates. The coke yield in both cases did not show any significant effect of the heating rate on coke yield.

In the case of pyrolysis of solids, the heating rate plays a significant role in determining the yields of products and the distribution of products. According to Gavalas (1982), the effect of heating rate in materials such as coal is due to the change of the solids structure and the micropores distribution in the reacting coals, which in turn affects the mass transfer limitation and lead to different products yields. If the mass transfer limitation during pyrolysis of coals can be excluded, the products yields depend on the reaction time and temperature rather

than the heating rate. In contrast, during the coking of AVR the mass transfer limitation was in the liquid phase. In this case, the diffusion of products in the liquid phase did not involve diffusion in a porous matrix. The diffusion in the liquid phase in the case of coking was independent of the heating rate. In reaction of coal materials, the micropores in the solids matrix changed during heating. Because the porous solid is the reacting material in the coal pyrolysis, the change in the pore structure would affect the mass transfer of the products specially from the core of the reacting coal material, unlike the case of AVR-solid agglomerates, where the reaction only takes place in the liquid layer on the solid surface.

5.5 Industrial Reactor Implications

5.5.1 Effect of Agglomeration and Agglomerate Variables

Agglomeration is an important and a common problem in the industrial fluid cokers. Agglomerates tend to form when the liquid feed enters the reactor and contacts the fluidized coke particles. If agglomerates survive the forces due to the bed hydrodynamics and start to travel within the bed, they cause problems like fouling of the reactor internals, defluidization of the bed and higher coke yield and lower yields of the distillates products due to trapping of products in the reacting liquid within the agglomerates. The results in this study support the role of agglomeration in increasing the coke yield in fluid coking by providing longer diffusion paths of the products of thermal cracking, which leads to higher mass transfer resistance for the products to escape and higher tendency of trapping and undergoing the undesirable coking reactions.

Agglomerates gave higher coke yields than the case of reacting liquid films at the studied range of bitumen concentration, regardless of the shape and size of the agglomerates. Only the agglomerates formation, and the resulting higher mass transfer resistance, had significant effect on the coke yield. Other factors, like the AVR concentration, reaction temperature, heating rate and agglomerates size did not have significant effect on the coke yield in agglomerates.

5.5.2 Effect of Heat-up Time

Using the results of the heat transfer model, the time required to heat an agglomerate to the reactor temperature under the reaction conditions can be estimated using the equation given by McCabe and Smith (1993)

$$t = \frac{r_m^2}{15\alpha_{eff}} \ln\left(\frac{T_s - T_a}{T_s - T_b}\right) \qquad (5.1)$$

Where t is the time, r_m is the spherical particle radius, α_{eff} is the particle effective thermal diffusivity, T_s is the surrounding temperature, T_a is the initial temperature and T_b is the average temperature.

Solving equation 5.1 for 2 cm spherical agglomerate with initial temperature of 350^{o}C at 550^{o}C reactor, and using the effective thermal diffusivity for the AVR-coke particles of 2.0 x 10^{-6} m^2/s, indicated that the agglomerate needs 70 s to reach 500^{o}C and 200 s to reach 550^{o}C. These heating times for agglomerates are significant relative the times for solids to move within the reactor. During the heat up time, the liquid in the agglomerate is not totally

reacted and can be transferred to the reactor internals upon impact by the agglomerates, which leads to fouling.

5.5.3 Implication for Reactor Design

Defluidization and fouling in the fluidized bed reactors are directly related to the formation and persistence of agglomerates. In chapter 2, the literature on agglomerate formation showed that the agglomeration tends to increase with increasing the thickness of liquid binder on the solid particles, which also leads to higher minimum fluidization velocities to avoid defluidization (Ennis et al., 1991 and Gray, 2002). The film thickness is directly controlled by the rate of liquid feed into the fluidized bed. The results of this study also suggest that minimizing the film thickness benefits the reactor operation by reducing the mass transfer resistance in the reacting liquid film and decreasing the coke yield. Producing thinner films of the liquid feed on the solid coke particles can be achieved by optimizing the process variables such as feed atomization, positions and orientation of feed nozzles, gas flow rate, and reactor length to diameter ratio (Gray, 2002).

Tollefson et al. (1997) suggested improving the feed atomization to produce thinner liquid films in order to improve reactor operation. When the feed is atomized to a small enough liquid droplet, thin liquid films can be formed on the coke particles and the formation of gumballs can be avoided. Another strategy to improve the bed operation would be to increase the asperities on the surface of coke particles, L_0 in equation 2.25, by increasing the amount of the small coke particles (< 70 μm diameter) (Gray, 2002). Increasing the concentration of small

coke particles can be achieved by increasing the amount of steam to the attrition nozzles (Dunlop et al., 1958).

Fouling in a fluidized bed can be due to the adhesion of bed particles to the reactor internals. Formation of stable liquid bridges between the wet particle and the reactor internals is favorable if both surfaces have a liquid film. If a wet particle hits a dry surface, the formation of stable liquid bridge is unlikely because it requires that the liquid film on the solid particle flow to the dry surface (Gray, 2002). To mitigate the fouling, it is required that the flux of wet particles hitting the surface to be lower than a critical value in order to give the liquid on the surface sufficient time to dry out by reaction and to avoid formation of stable liquid bridges. A larger bed of particles for a given feed rate would tend to reduce the flux of wet particles that hit the internal reactor surface.

Optimizing the superficial gas velocity, or U/U_{mf}, can improve the performance of the reactor by avoiding agglomeration. Increasing the gas velocity by increasing the steam addition rate will increase the mixing and the shear forces on the particles and formed agglomerates, which can prevent agglomerate formation or disintegration of the formed agglomerates. It will also increase the local velocity of the particles near the reactor internals, which increases the Stokes number and prevent it from falling below the critical value to avoid forming stable liquid bridges and prevent fouling of the reactor internals. Increasing the height to diameter ratio of the reactor can also contribute to avoiding fouling by agglomerates at the bottom of the reactor by decreasing the flux of wet materials near reactor internals.

5.5.4 Benefits of Improved Feed Introduction

Improving the liquid feed nozzle design can improve the reactor operation and help in eliminate or reduce the agglomeration of the coke particles (House et al., 2004, House et al., 2008, and McMillan et al., 2005). Literature on the feed nozzle design in chapter 2 showed improvements in liquid-solid contact in fluidized bed can be achieved by modifying the feed nozzle or incorporating new nozzle designs (House et al., 2004, House et al., 2008, and McMillan et al., 2005). Improved feed introduction showed improvements on liquid solid mixing efficiency, agglomerate formation and agglomerate size distribution. Better mixing achieves more uniform primary solid-liquid mixture and reduces the local liquid to solid ratio, which makes agglomerate weaker and easily fragmented. The results from this study, however, suggested that agglomerates may not be reduced enough to increase the desired products yield. Reducing the agglomerate thickness down to 2 mm did not have significant effect on reducing the coke yield. These results suggest that agglomerates need to be eliminated in order to achieve the best possible yield of desired products.

6 CONCLUSIONS AND RECOMMENDATIONS

6.1 Conclusions

The results of this study show the significant contribution of the agglomerates formation in increasing the coke yield relative to the case of reacting thin liquid films. All agglomerates sizes tested in this study showed higher coke yield compared to the coke yield from thin liquid films. It is clearly showed that in order to eliminate the effect of higher coke yield due to agglomeration, agglomerate formation has to be eliminated rather than targeting forming smaller agglomerated.

The results of coke yield in AVR-coke agglomerates and AVR-alumina agglomerates showed that the agglomerate gave higher coke yield relative to the thin films for the same feed materials and same reaction temperature. The increase of coke yield in agglomerates supports the role of mass transfer. The liquid within the solid-liquid matrix tends to form thicker layers over the solid particles due to uneven liquid distribution and the liquid bridges between particles as shown in the micrographs (Figures 4.2 and 4.9). The thick liquid films in agglomerates provided longer diffusion paths and higher tendency for trapping of the reaction products within the liquid film and undergoing undesired condensation and polymerization reactions.

Decreasing agglomerate size, down to 2 mm in the case of agglomerate disks in the induction furnace experiments and down to 5 mm for the

agglomerates cylinders in the fluidized bed reactor experiments, had no significant effect on the coke yield. The reduction in the size of the agglomerates did not affect the thickness of reacting liquid layers on the solid particles and in liquid bridges between particles over the studied range of liquid saturation.

In the studied AVR concentration range, from 8% to 12.5% (relative to 20% to 30% liquid saturation) no significant effect of the AVR concentration on the coke yield was observed for both the induction furnace and fluidized bed agglomerates. The AVR concentration was below the liquid saturation concentration in the agglomerates and the distribution of liquid within the liquid-solid matrix was not significantly different at different liquid contents, which led to similar diffusion paths and similar mass transfer limitations. The mass transfer resistance was only present in the liquid layers and bridges in the agglomerates and once the reaction products reached the void space in the agglomerates they diffused easily to the outer surface of the agglomerates with relatively no resistance to flow within the gas phase.

Changing the reaction temperature from 503^{o}C to 530^{o}C in the induction furnace experiments, over the studied range of bitumen concentration and agglomerate thickness, did not have significant effect on the coke yield from agglomerates. This observation indicates that although the rate of cracking and devolatilization of the products depends on temperature, the ultimate coke yield at longer reaction times tends to be insensitive to temperature.

No effect of the type of solids used in making the AVR-solid agglomerates was noted when using coke and alumina. Changing the solids had no effect on the coke yield due to the similar distribution of liquid over the solid particles and in liquid bridges and the incomplete wettability in both cases as was shown in the agglomerates micrographs.

At the reaction conditions in the fluidized bed, 500^{o}C and U/U_{mf} of 40, the mass of agglomerates and the fraction of agglomerates that survived was in the range of 0.91 to 0.97 of the initial agglomerate mass, independent of size and liquid saturation. The visual inspection of the agglomerates after reaction showed that some fractionation and attrition had occurred, but the majority of the agglomerates stayed intact and survived during the reaction time in the fluidized bed.

TGA data for the coke in agglomerates, 20 μm films and 60 μm films showed that the coke from the 20 μm film had the lowest per cent loss in weight, followed by the 60 μm film coke then the agglomerate coke. The 20 μm film coke also showed the lowest initial rate of devolatilization followed by the 60 μm films then the agglomerate coke, which supports the rule of mass transfer in the diffusion of reaction products in the reacting film and the higher tendency of products trapping within the film due to thicker films and longer diffusion paths. The high initial rate of devolatilization in the case of agglomerate coke compared to the thin film coke due to the uneven distribution and the incomplete wettability of the AVR in the liquid-solid matrix in case of the agglomerates and the formation of thick liquid layers on the solids and liquid bridges between solids.

The higher weight loss and initial rate of devolatilization in agglomerate coke and 60 µm film coke compared to the coke from the 20 µm film indicated that the longer diffusion paths and the greater amount of products trapped in the thicker layers produced higher reactivity coke from the thicker film.

A transient heat transfer model was used to describe the change of the temperature with the time and location within the reacting AVR-coke agglomerates. The AVR-solid mixture was approximated as a porous solid phase with a single effective thermal diffusivity (α_{eff}). The relation between the temperature (T) at any time (t) and distance from agglomerate centre line (x) was described by a conduction heat transfer model, where the effective thermal diffusivity of the agglomerate, α_{eff}, was used as the only adjustable parameter to fit the model to the experimental data. The best fit value of the effective thermal diffusivity was 0.20×10^{-6} m^2/s. The model showed good agreement with the experimental data for the different agglomerate sizes and initial bitumen concentrations.

Increasing the agglomerate thickness affected the rate of heating of the agglomerate in the range from 80 K/s at the contact with the heating strips to 15 K/s at the center of the agglomerate. This change in the heating rate did not affect the ultimate coke yield. Coking of different vacuum residue materials at different heating rates of 14.8 to 148 K/s showed that the coke yields from the different heavy oils were insensitive to the heating rate for this range for 20 µm and 80 µm film thicknesses.

6.2 Recommendation and Future Work

The findings of this study can be used as an input for future studies to give more complete picture about the agglomerates behavior in fluid coking and to minimize the mass transfer limitation and coke yield and maximize the products yields. Some recommendations given based on the contribution on this study are:

Study the improvement of liquid feed nozzles in order to eliminate the formation of agglomerates in the fluid coking. This study clearly showed the effect that agglomerates have on mass transfer and hence on coke yield compared to liquid film. The study also showed that reduction of agglomerates size in the studied range did not have significant effect on coke yield.

More studies are needed towards the agglomerates behavior at the fluid cocking reactor conditions. One of the limitation of the current work is that the agglomerates reactions started by making the AVR-solid agglomerates at room temperature, which is not the case in the fluid coker where agglomerates are formed by the combination of hot solid particles and heated liquid feed.

BIBLIOGRAPHY

Aiba, T.; Kaji, H.; Suzuki, T.; Wakamatsu, T. "Residue Thermal-Cracking by the Eureka Process" *Chem. Eng. Prog.* **1981**, *2,* 37-44.

Aminu, M. O.; Elliott, J. A. W.; McCaffrey, W. C.; Gray, M. R. "Fluid Properties at Coking Process Conditions" *Ind. Eng. Chem. Res* **2004**, *12,* 2929-2935.

Ancheyta, J.; Sanchez, S.; Rodriguez, M. A. "Kinetic Modeling of Hydrocracking of Heavy Oil Fractions: A Review" *Catal. Today* **2005**, *1-4,* 76-92.

Ariyapadi, S.; Holdsworth, D. W.; Norley, C. J. D.; Berruti, F.; Briens, C. "Digital X-Ray Imaging Technique to Study the Horizontal Injection of Gas-Liquid Jets into Fluidized Beds" *Int. J. Chem. Reactor Eng.* **2003**, A56.

Bahadori, A.; Mokhatab, S. "Predicting Physical Properties of Hydrocarbon Compounds" *Chem. Eng.* **2008**, *8,* 46-48.

Banerjee, D. K.; Laidler, K. J.; Nandi, B. N.; Patmore, D. J. "Knetic Studies of Coke Formation in Hydrocarbon Fractions of Heavy Crudes" *Fuel* **1986**, *4,* 480-484.

Barbajosa, A. Shell, Exxon Tap Oil Sands, Gas as Reserves Dwindle. *http://www.energybulletin.net/4385.html*, **April 2010**

Bartholic, D. B. US Patent 4,859,315, **1989**.

Bartholic, D. B. US Patent 4,859,315, **1989**.

Bartholic, D. B.; Haseltine, R. P. "New crude/resid Treating Process Offers Savings" *Oil gas J.* **1981**, *79*, 242-252.

Bejan, A.; Kraus, A. D. *Heat Transfer Handbook;* John Wiley & Sons: **2003**.

Benson, S. W. *Thermochemical Kinetics;* 2nd Edition, John Wiley and Sons: **1976**.

Blanchard, C. A.; Gray, M. R. "Free Radical Chain Reactions in Thermal Hydrocracking of Residue" *Abstracts of Papers of the American Chemical Society* **1997**, 54-FUEL.

Brown, W.; Monaghan, G. V.; Pinchuk, R. J. Canada Patent 2,505,632, **2006**.

Chattanooga Corp *http://www.chattanoogaprocess.com/*, **April 2010**

Chung, K. H.; Janke, L. C. G.; Dureau, R.; Furimsky, E. "Leachability of Coke from Syncrude Stockpiles" *Env. Sci. Eng.* **1996**, 50-53.

Conradson, P. H. "Apparatus and Method for Carbon Test and Ash Residue in Petroleum Lubricating Oils" *J. Ind. Eng. Chem.* **1912**, 903-905.

Del Bianco, A.; Panariti, N.; Anelli, M.; Beltrame, P. L.; Carniti, P. "Thermal Cracking of Petroleum Residues: 1. Kinetic Analysis of the Reaction" *Fuel* **1993**, *1*, 75-80.

Department of Energy, Government of Alberta Oil Sands, http://www.energy.gov.ab.ca.login.ezproxy.library.ualberta.ca/89.asp, **April 2010**

Dunlop, D. D.; Griffin, J., L.I.; Moser, J., J.F. "Particle Size Control in Fluid Coking" *Chem. Eng. Prog.* **1958**, *8*, 39-42.

Dutta, R. P.; McCaffrey, W. C.; Gray, M. R.; Muehlenbachs, K. "Use of ^{13}C Tracers to Determine Mass-Transfer Limitations on Thermal Cracking of Thin Films of Bitumen" *Energy Fuels* **2001**, *5*, 1087-1093.

Ennis, B. J.; Tardos, G.; Pfeffer, R. "Microlevel-Based Characterization of Granulation Phenomena" *Powder Technol* **1991**, *1-3*, 257-272.

ERCB 2009 ST-98 Report "Alberta's Energy Reserves 2008 and Supply/Demand Outlook 2009-2018."

Gavalas, G. R. *Coal Pyrolysis;* Elsevier Scientific Publishing Company: Amsterdam, **1982**.

Government of Alberta Alberta's Oil Sands. http://www.oilsands.alberta.ca, **April, 2010**

Gray, M. R.; McCaffrey, W. C.; Huq, I.; Le, T. "Kinetics of Cracking and Devolatilization during Coking of Athabasca Residues" *Ind. Eng. Chem. Res.* **2004**, *43*, 5438-5445.

Gray, M. R. *Upgrading petroleum residues and heavy oils;* Marcel Dekker: New York, **1994**.

Gray, M. R.; Masliyah, J. H. *Extraction and Upgrading of Oilsands Bitumen, intensive short course;* **2004**.

Gray, M. R.; Le, T.; McCaffrey, W. C.; Berruti, F.; Soundararajan, S.; Chan, E.; Huq, I.; Thorne, C. "Coupling of Mass Transfer and Reaction in Coking of Thin Films of an Athabasca Vacuum Residue" *Ind. Eng. Chem. Res.* **2001**, *15,* 3317-3324.

Gray, M. R.; Jokuty, P.; Yeniova, H.; Nazarewycz, L.; Wanke, S. E.; Achia, U.; Krzywicki, A.; Sanford, E. C.; Sy, O. K. Y. "The Relationship between Chemical-Structure and Reactivity of Alberta Bitumens and Heavy Oils" *Can. J. Chem. Eng.* **1991**, *4,* 833-843.

Gray, M. R.; McCaffrey, W. C.; Srinivasan, N.; Chung, K. "Trapping of Aromatic Compounds during Coking of Athabasca Vacuum Residue" *Energy Fuels* **2003**, *2,* 282-284.

Gray, M. R. "Fundamentals of Bitumen Coking Processes Analogous to Granulations: A Critical Review" *Can. J. Chem. Eng.* **2002**, *3,* 393-401.

House, P. K.; Saberian, M.; Briens, C. L.; Berruti, F.; Chan, E. "Injection of a Liquid Spray into a Fluidized Bed: Particle-Liquid Mixing and Impact on Fluid Coker Yields" *Ind. Eng. Chem. Res.* **2004**, *18,* 5663-5669.

House, P. K.; Briens, C. L.; Berruti, F.; Chan, E. "Effect of Spray Nozzle Design on Liquid-Solid Contact in Fluidized Beds" *Powder Technol.* **2008**, *1,* 89-98.

Hulet, C.; Briens, C.; Berruti, F.; Chan, E. "A Review of Short Residence Time Cracking Processes" *Int. J. Chem. Reactor Eng.* Vol 3, **2005**, Review R1.

Keningley, S. T.; Knight, P. C.; Marson, A. D. "Investigation into the Effects of Binder Viscosity on Agglomeration Behaviour" *Powder Technol.* **1997**, *2,* 95-103.

Knapper, B. A.; Gray, M. R.; Chan, E. W.; Mikula, R. "Measurement of Efficiency of Distribution of Liquid Feed in a Gas-Solid Fluidized Bed Reactor" *Int. J .Chem. Reactor Eng.* **2003**.

Koshka, E.; Kuach, J.; Veith, E. "Improving Athabasca Bitumen Development Economics through Integration with HTL Upgrading" *World Heavy Oil Congress*. **2008.**

Kunii, D.; Levenspiel, O. *Fluidization Engineering;* John Wiley & Sons: USA, **1969**.

Kuo, J. C. W.; Wei, J. "Lumping Analysis in Monomolecular Reaction Systems. Analysis of Approximately Lumpable System" *Ind. Eng. Chem. Fundamentals* **1969**, *1,* 124-133.

Lorenz, A. "Building a Small Scale Upgrader" *Oilsands Review,* **2007,** 48-52.

Mattar, S.; Hatch, L. F. *Chemistry of Petrochemical Processes;* Gulf Professional Publishing: **2001**.

McCaffrey, W. C.; Cameron, R. A.; Gray, M. R. "Physical Behavior of Bitumen under Rapid Heating" *Am. Chem. Soc. Div. Pet. Chem*. **1998**; Vol. 43, pp 616-618.

McDougall, S.; Saberian, M.; Briens, C.; Berruti, F.; Chan, E. "Effect of Liquid Properties on the Agglomerating Tendency of a Wet Gas-Solid Fluidized Bed" *Powder Technol,* **2005**, *2-3,* 61-67.

McMillan, J.; Zhou, D.; Ariyapadi, S.; Briens, C.; Berruti, F.; Chan, E. "Characterization of the Contact between Liquid Spray Droplets and Particles in a Fluidized Bed" *Ind. Eng. Chem. Res.* **2005**, *14*, 4931-4939.

Michaelian, K. H.; Hall, R. H.; Bulmer, J. T. "Photoacoustic Infrared Spectroscopy and Thermophysical Properties of Syncrude Cokes" *J. Therm. Anal.* **2002**, *1*, 135-147.

Miyauchi, T.; Ikeda, Y. United States Patent 4,722,378, **1988**.

Nagaishi, H.; Ikeda, K.; Chan, E. W.; Gray, M. R. "Observation of Heavy Oil Vaporization Under Rapid Heating*" Energy Fuels* **1998**, 1174-1180.

Nelson, W. L. *Petroleum refinery engineering;* McGraw-Hill: New York, **1958**.

Parmar, M. S.; Hayhurst, A. N. “The Heat Transfer Coefficient for a Freely Moving Sphere in a Bubbling Fluidised Bed” *Chem. Eng. Sci.* **2002**, *17*, 3485-3494.

Radmanesh, R.; Chan, E.; Gray, M. R. “Modeling of Mass Transfer and Thermal Cracking during the Coking of Athabasca Residues” *Chem. Eng. Sci.* **2008**, *6*, 1683-1691.

Rahmani, S.; McCaffrey, W. C.; Dettman, H. D.; Gray, M. R. “Coking Kinetics of Asphaltenes as a Function of Chemical Structure” *Energy Fuels* **2003**, *4*, 1048-1056.

Rahmani, S.; McCaffrey, W.; Gray, M. R. “Kinetics of Solvent Interactions with Asphaltenes during Coke Formation” *Energy Fuels* **2002**, *1*, 148-154.

Rohsenow, W. M.; Hartnett, J. P.; Cho, Y. I. In *Handbook of Heat Transfer*. McGraw-Hill: **1998**.

Song, X. Q.; Bi, X. T. T.; Bolkan, Y. “Hydrodynamics of High-Density Downer Reactors using a Novel Solids Feeder” *Int. J. Chem. React. Eng.* **2005**.

Soundararajan, S. *Determination of thermal cracking kinetics of Athabasca bitumen vacuum residue*. M.Sc. Thesis, University of Saskatchewan, **2001**.

Speight, J. G. *The Chemistry and Technology of Petroleum;* CRC Press: **2007**.

Speight, J. G. *Handbook of petroleum analysis;* Wiley-Interscience: **2001**.

Takatsuka, T.; Kajiyama, R.; Hashimoto, H.; Matsuo, I.; Miwa, S. “Practical Model of Thermal Cracking of Residual Oil” *J. Chem. Eng. Japan* **1989**, *3,* 304-310.

Tollefson, E. L.; Bui, V.; Hyndman, C. L.; Chan, E. and Famulak, D. “Importance of feed droplet size in fluid coking*” 47th Canadian Chem. Eng. Conference*; **1997**.

Verkoeijen, D.; Meesters, G. M. H.; Vercoulen, P. H. W.; Scarlett, B. “Determining Granule Strength as a Function of Moisture Content” *Powder Technol* **2002**, *3,* 195-200.

Voorhies, J., A.; Martin, H. Z. “Fluid Coking of Residua” *American Petroleum Institute -- Proceedings* **1953**, *Sec 3,* 39-46.

Wang, J.; Anthony, E. J. A “Study of Thermal-Cracking Behavior of Asphaltenes” *Chem. Eng. Sci.* **2003**, *1,* 157-162.

Wang, S.; Chung, K.; Masliyah, J. H.; Gray, M. R. “Toluene-Insoluble Fraction from Thermal Cracking of Athabasca Gas Oil: Formation of a Liquid-in-Oil Emulsion that Wets Hydrophobic Dispersed Solids” *Fuel* **1998**, *14,* 1647-1653.

Weber, S. *Agglomerate Stability in Fluidized Beds*, PhD Thesis, University of Western Ontario, **2009**.

Weber, S.; Briensa, C.; Berruti, F.; Chan, E. and Gray, M. “Effect of Agglomerate Properties on Agglomerate Stability in Fluidized Beds” *Chem Eng Sci* **2008**, *63*, 5245-5256.

Weber, S.; Briens, C.; Berruti, F.; Chan, E.; Gray, M. “Agglomerate Stability in Fluidized Beds of Glass Beads and Silica Sand” *Powder Technol* **2006**, *3*, 115-127.

Wei, J.; Kuo, J. C. W. “Lumping Analysis in Monomolecular Reaction Systems. Analysis of Exactly Lumpable System” *Ind. Eng. Chem., Fundamentals* **1969**, *1*, 114-123.

Wiehe, I. A. *Process Chemistry of Petroleum Macromolecules;* CRC Press: **2008**.

Wiehe, I. A. “Enhanced Microcarbon Tester and Other Ideal Laboratory Cokers” *Abstracts of Papers of the American Chemical Society* **2000**, U142-U142.

Wiehe, I. A. “A Phase-Separation Kinetic-Model for Coke Formation” *Ind. Eng. Chem. Res.* **1993**, *11*, 2447-2454.

Wiehe, I. A. “A Solvent Resid Phase-Diagram for Tracking Resid Conversion” *Ind. Eng. Chem. Res.* **1992**, *2*, 530-536.

Worldwide Look at Reserves and Production. Special Report; *Oil Gas J.* **December 22, 2008**, *48.*

Yang, W. In *Fluidization, Solids Handling, and Processing - Industrial Applications.* William Andrew Publishing/Noyes: **1998**.

APPENDIX A

Calibration Procedure for Coke Determination in Fluidized Bed Experiments

Coke for calibration was made by reacting the AVR in 2.54 mm (1 inch) quartz tube in a molten salt bath at 530 ^{o}C. The calibration curve is shown in Figure A.1.

4 gm of AVR was placed in the quartz tube and the tube was sealed and purged with nitrogen for about 30 minutes. The tube with the sample was then dipped in the salt bath and left for about 20 minutes. After reaction the tube was left to cool and the formed coke was removed. Known amount of coke was mixed with alumina and introduced to the fluidized bed reactor. The coke-alumina bed was burned using oxygen as fluidization gas at 10.4 sL/min for 6-7 hrs. The combustion products were passed through absorption bottles with $Ba(OH)_2$ solution. The change in the $Ba(OH)_2$ conductivity was recorded corresponding to the amount of coke. This method of calibration using actual coke material accounted for any effects of incomplete combustion to form carbon monoxide, or side reactions of the sulfur products with the barium hydroxide.

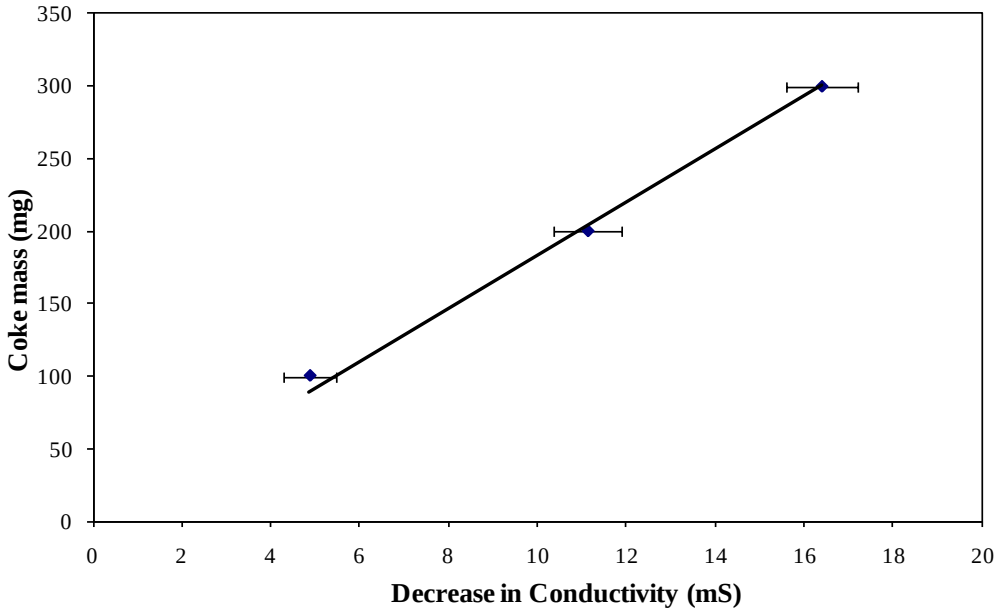

Figure A.1: Calibration curve between the amount of coke burned in the fluidized bed reactor and the change of the electrical conductivity of the $Ba(OH)_2$ solution

APPENDIX B

Sample Calculations of Significance Testing of Data

B.1.Slope Significance Testing Using LINEST function

The LINEST function in Microsoft Excel was used to determine the regression parameters and Null Hypothesis H_0: slope = zero was tested using two sided t-test with 95% confidence.

Excel worksheet for testing the slope of the line of the data between agglomerate thickness and coke yield for 8% AVR concentration agglomerates in induction furnace experiments.

Agglomerates thickness	Coke Yield
2	25.75
3	26.3975
4	28.7936
LINEST function output:	
1.5218	22.41497
0.504777	1.569417
0.900882	0.713863
9.088986	1
4.63175	0.5096
t=	3.014795
t critical=	12.7062
P=	0.203895

Excel worksheet for testing the slope of the line of the data between agglomerate thickness and coke yield for 10% AVR concentration agglomerates in induction furnace experiments.

Agglomerates thickness	Coke Yield
2	22.90625
3	21.93125
4	22.9825
LINEST function output:	
0.038125	22.49229
0.584928	1.818615
0.00423	0.827213
0.004248	1
0.002907	0.684282
t=	0.065179
t critical=	4.302653
P=	0.95396

Excel worksheet for testing the slope of the line of the data between agglomerate thickness and coke yield for 12.5% AVR concentration agglomerates in induction furnace experiments.

Agglomerates thickness	Coke Yield
2	20.6375
3	21.21625
4	24.0575
LINEST function output:	
1.71	16.84042
0.653127	2.030656
0.87269	0.923662
6.854824	1
5.8482	0.853151
t=	2.618172
t critical=	4.302653
P=	0.120151

Excel worksheet for testing the slope of the line of the data between AVR concentration and coke yield for 5mm agglomerates cylinders in fluid bed experiments.

AVR concentration	Coke Yield
8.1	23.63333
9.7	21
12.4	21.16667
LINEST function output:	
-0.50706	27.03771
0.450838	4.608413
0.558488	1.385671
1.264946	1
2.428804	1.920085
t=	1.124698
t critical=	12.7062
P=	0.46268

Excel worksheet for testing the slope of the line of the data between AVR concentration and coke yield for 10mm agglomerates cylinders in fluid bed experiments.

AVR concentration	Coke Yield
8.22	21.425
9.9	22.725
12.5	26.3
LINEST function output:	
1.15925	11.65126
0.163019	1.688458
0.980608	0.497149
50.56811	1
12.49826	0.247157
t=	7.111126
t critical=	12.7062
P=	0.088941

Excel worksheet for testing the slope of the line of the data between AVR concentration and coke yield for 15mm agglomerates cylinders in fluid bed experiments.

AVR concentration	Coke Yield
8.09	26.475
9.8	23.36
12.5	15.5
LINEST function output:	
-2.52673	47.37412
0.29372	3.02279
0.986667	0.923581
74.00316	1
63.12482	0.853002
t=	8.602509
t critical=	12.7062
P=	0.073673

B.2. Pair Testing Using the ANOVA function

Pair testing using ANOVA function in Microsoft Excel for the date of coke yield vs. AVR concentration for 5 mm, 10 mm and 15 mm agglomerates in fluid bed reactor experimetns

15mm			10mm			5mm		
12.5%	10%	8%	12.5%	10%	8%	12.5%	10%	8%
6.4	11.5	12.5	29.8	21.8	25.7	15	16.8	26
31	17.7	39.9	25.8	22.7	16.9	23.7	25.1	23.9
9.1	14.5	40.7	23.3	28.9	29.8	24.8	21.1	21
	42.7	12.8		17.5	13.3			
	30.4							

Anova: Single Factor

SUMMARY

Groups	*Count*	*Sum*	*Average*	*Variance*
Column 1	3	46.5	15.5	182.01
Column 2	5	116.8	23.36	168.698
Column 3	4	105.9	26.475	254.9625
Column 4	3	78.9	26.3	10.75
Column 5	4	90.9	22.725	22.09583
Column 6	4	85.7	21.425	58.3025
Column 7	3	63.5	21.16667	28.82333
Column 8	3	63	21	17.23
Column 9	3	70.9	23.63333	6.303333

ANOVA

Source of Variation	*SS*	*df*	*MS*	*F*	*P-value*	*F crit*
Between Groups	277.8444	8	34.73054	0.36792	0.92688	2.37481
Within Groups	2171.108	23	94.39599			
Total	2448.952	31				

Pair testing using ANOVA function in Microsoft Excel for the date of coke yield vs. AVR concentration 15 mm agglomerates in fluid bed reactor experiments

Bitumen concentration	12.5%	10%	8%
Coke yields	6.4	11.5	12.5
	31	17.7	39.9
	9.1	14.5	40.7
		42.7	12.8
		30.4	

Anova: Single Factor

SUMMARY

Groups	*Count*	*Sum*	*Average*	*Variance*
Column 1	3	46.5	15.5	182.01
Column 2	5	116.8	23.36	168.698
Column 3	4	105.9	26.475	254.9625

ANOVA

Source of Variation	*SS*	*df*	*MS*	*F*	*P-value*	*F crit*
Between Groups	213.8472	2	106.923	0.53352	0.60399	4.25649
Within Groups	1803.7	9	200.411			
Total	2017.54	11				

APPENDIX C

Calculations of Initial Mass Loss and Initial rate of Devolatilization in TGA Experiments

20 µ coke

Initial total mass	12.7145	mg
Sample mass at 450	12.4419	mg
Sample mass at 500	12.0592	mg
mass at end of O2 (non coke materials)	3.8206	mg
Initial mass of coke	8.8939	mg
mass of coke at 450	8.6213	mg
mass of cock at 500	8.2386	mg
Coke mass loss	0.3827	mg
% mass loss	4.302949	%
Initial rate of delvolatilization	-0.03924	mg/min
Normalized initial rate of devolatalization	-0.00441	mg/min/mg coke

60 µ coke

Initial total mass	11.0645	mg
Sample mass at 450	10.5485	mg
Sample mass at 500	9.5688	mg
mass at end of O2 (non coke materials)	0.6472	mg
Initial mass of coke	10.4173	mg
mass of coke at 450	9.9013	mg
mass of cock at 500	8.9216	mg
Coke mass loss	0.9797	mg
% mass loss	9.404548	%
Initial rate of devolatilization	-0.14957	mg/min
Normalized initial rate of devolatalization	-0.01436	mg/min/mg coke

Agglomerate coke

Initial total mass	148.441	mg
Sample mass at 450	148.224	mg
Sample mass at 500	147.959	mg
mass at end of O2 (non coke materials)	145.819	mg
Initial mass of coke	2.622	mg
mass of coke at 450	2.405	mg
mass of cock at 500	2.14	mg
Coke mass loss	0.265	mg
% mass loss	10.10679	%
Initial rate of devolatilization	-0.07857	mg/min
Normalized initial rate of devolatalization	-0.02997	mg/min/mg coke

APPENDIX D

MATLAB Code for the Heat Transfer Model

```
function temp_prof

m = 0;
x = linspace(0,.002,20);
t = linspace(0,120,1000);

% solution of the partial differential equation using pdepe function
sol = pdepe(m,@pdex1pde,@pdex1ic,@pdex1bc,x,t);
u = sol(:,:,1);

TChat= u(:,end);
figure
plot(t,u(:,end),'r:+')
hold on
TC = xlsread('TC210.xls');
plot(TC(:,1),TC(:,2),'.')
TS = xlsread('TS210.xls');
plot(TS(:,1),TS(:,2),'.')
hold off
xlswrite('temp_p.xls',u(:,end), 'u_sheet');
xlswrite('temp_p.xls',t, 't_sheet');
figure;
surf(x,t,u);

p = length(TChat)
q = length(TC)

Res = TC(:,2) - TChat;
SSR = Res' * Res

function [c,f,s] = pdex1pde(x,t,u,DuDx)
c = 1/.20e-6;
f = DuDx;
s = 0;

function u0 = pdex1ic(x)
u0 = 29; % initial condition

function [pl,ql,pr,qr] = pdex1bc(xl,ul,xr,ur,t)

% this part is to read the variable Curie-point strip with time and
```

```
% to calculate the varying boundary conditions at each calculation point

TS = xlsread('TS210.xls');
n = length(TS);
for k = 1:n;
   tin = t;
   if tin == TS(k,1)
      Tm = TS(k,2);
      elseif tin > TS(k,1)
      Tm = (TS(k+1,2)-TS(k,2))*(tin-TS(k,1))/(TS(k+1,1)-
TS(k,1))+TS(k,2);
   else
   end
end

Tm = Tm;

pl = ul-Tm;
ql = 0;
pr = 0;
qr = 1;
```